Theories from Molecular Thermodynamics have developed vividly over the past years and the models that are derived from applying molecular theories have proven highly useful in understanding, correlating and predicting complex mixtures.
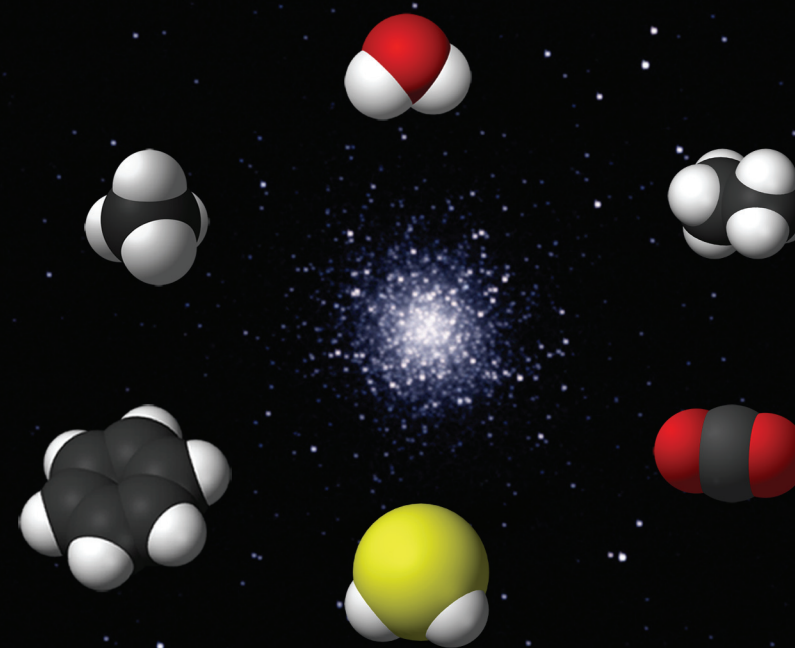
This thesis is concerned with the thermodynamic description of systems containing acid gases with hydrocarbons and water, in the presence of chemical electrolyte reactions. The technical relevance of such mixtures spans a wide range of temperature and pressure and particularly includes the region around the critical point of such mixtures.

Thermodynamic Properties
of acid gases in mixture
with natural gas and water

Xiaohua Tang

Thermodynamic Properties

of acid gases in mixture with natural gas and water

Thermodynamic Properties
of acid gases in mixture with natural gas and water

PROEFSCHRIFT

ter verkrijging van de graad van doctor
aan de Technische Universiteit Delft,
op gezag van de Rector Magnificus Prof. ir. K.C.A.M. Luyben,
voorzitter van het College voor Promoties,
in het openbaar te verdedigen op woensdag 27 april 2011 om 10.00 uur
door

Xiaohua TANG

Master of Science in Chemistry, Universiteit Leiden
geboren te Nanjing, China.

Dit proefschrift is goedgekeurd door de promotor:

Prof. dr. ir. J. Gross

Samenstelling promotiecommissie:

Rector Magnificus	Voorzitter
Prof. dr. ir. J. Gross	Technische Universiteit Delft, promotor
Prof. dr. ir. L. Vega	National Research Council of Spain
Prof. dr. ir. A. Bardow	RWTH Aachen University
Prof. dr. ir. P.J. Jansens	DSM Research
Prof. dr. ir. T. Vlugt	Technische Universiteit Delft
Dr. ir. E. Hendriks	SHELL Technology Centre Amsterdam
Dr. ir. N. A. M. Besseling	Technische Universiteit Delft
Prof. dr. ir. B. J. Boersma	Technische Universiteit Delft, reservelid

Cover design by X. Tang

Cover picture: M13 Star Cluster, Copyright © 2008 - Antonio Pascarella, http://www.pascarellas.com/m13.aspx.

To the memory of my father

Summary

The reliable removal of acid gas components, such as carbon dioxide (CO_2) and hydrogen sulfide (H_2S) from natural gas is an important technical challenge. Crude oil and hydrocarbon gas streams may contain high levels of CO_2 and/or H_2S as contaminants. It is desirable to prevent any contaminant to reach the surface, or to considerably reduce the contaminant levels reaching surface facilities. Opportunities for the disposal of the unwanted components include subsurface sequestration of the substances.

This book analyses the underlying thermodynamic properties of the involved mixtures and proposes a modelling formalism. The first Chapter gives background to the project, introduces the molecular methods that are applied in later chapters, and identifies scientific needs that are addressed with this book.

Chapter 2 proposes a physically sound model for the phase equilibrium of CO_2 and H_2S with hydrocarbons and water. The perturbed-chain polar statistical associating fluid theory (PCP-SAFT) equation of state is parameterized to correlate phase equilibria for mixtures of hydrogen sulfide and carbon dioxide with alkanes, with aromatics, and with water over wide temperature and pressure ranges. The binary mixtures of H_2S-methane and CO_2-methane are studied in detail including vapor-liquid, liquid-liquid and fluid-solid phase equilibria as well as the three phase equilibria. Very satisfying results were obtained for the binary mixtures as well as for the ternary mixture of H_2S-CO_2-methane using the (constant) interaction parameters of the binary pairs.

The mixture's critical points are relevant for conditions of natural gas reser-

voirs and the separation process for CO_2 and H_2S. Chapter 3 proposes a model for an adequate description of the critical region (as well as conditions away from the critical point) using renormalization group corrections. Classical fluid theories do not describe the long-range fluctuations that occur in the vicinity of a pure component or mixture's critical point. The perturbed-chain statistical associating fluid theory (PC-SAFT) equation of state is extended with a renormalization group theory for mixtures. The theory accounts for the long-range density fluctuations and the results reduce to the results of the classical PC-SAFT equation of state away from the critical point. Two approximation methods, the isomorphic density approximation and the individual phase-space cell approximation, are used for the renormalization group corrections of mixtures. The two variants are evaluated by comparison to experimental vapor-liquid data for systems of alkanes, carbon dioxide and hydrogen sulfide. Overall, the considered implementation of the individual phase-space cell approximation is slightly superior to the isomorphic density approximation for the mixtures investigated here. The individual phase-space cell approximation tends to overestimate the renormalization corrections for some cases but generally leads to good agreement with experimental data for binary mixtures.

The surface tension of the considered fluids are important in many technical processes, for example in separation processes using membrane contactors. Chapter 4 proposes a model for the calculation of the surface tension including the critical region. This study for the first time proposes a density functional theory (DFT) treatment that enforces the critical point through a renormalization procedure. A Helmholtz energy functional is here proposed, where the long-range density fluctuations leading to the universal critical scaling behavior are accounted for using a renormalization group theory. The appeal of the approach is its simple implementation, where the renormalization is treated in a local density approximation. The model is almost exact at the critical point. Away from the critical point, the model reduces to the perturbed chain statistical associated fluid theory (PC-SAFT) equation of state. The conventional PC-SAFT pure component parameters are supplemented with a single substance-specific renormalization parameter, which is adjusted to reproduce the bulk phase critical temperature. The surface tension is obtained with excellent agreement to experimental data for some non-polar and moderately polar substances (alkanes, ethers, acetates, aromatic substances) up to the critical point.

Chapter 5 proposes a simple, pragmatic model for the solubility of CO_2 in K_2CO_3 aqueous solutions. The solubility of carbon dioxide (CO_2) and hydrogen sulfide (H_2S) in basic aqueous electrolyte solutions is determined by a combined phase and reaction equilibrium. A cubic equation of state is applied to model the vapor-liquid equilibria of these reacting systems. The Peng-Robinson equation of state with Wong-Sandler mixing rules is combined with an extended UNIQUAC model for electrolytes where ion-specific interactions are determined from a Debye-Hückel term. The thermodynamic model is parameterized for aqueous systems containing carbon dioxide and hydrogen sulfide along with water and potassium carbonate solutions at high pressure. The UNIQUAC binary interaction parameters are estimated by minimizing deviations in the liquid phase composition of the model with respect to the experimental data. The data is taken from literature and is supplemented by own experimental work conducted as part of this study.

This study provides models for the physical properties of natural gas and crude oil mixtures, needed for a reliable calculation of separation systems. An adequate model for electrolytes which is needed for an improved modelling of a membrane contactor remains to be developed.

Samenvatting

De betrouwbare verwijdering van zure gascomponenten, zoals kooldioxide(CO_2) en waterstofsulfide (H_2S) uit aardgas is een belangrijke technische uitdaging. Ruwe olie en koolwaterstoffengassen kunnen hoge gehaltes aan CO_2 en/of H_2S bevatten als verontreinigingen. Het is wenselijk dat wordt voorkomen dat verontreinigingen het aardoppervlak bereiken, of dat er een aanzienlijke reductie van deze concentraties plaatsvindt voordat installaties aan de oppervlakte worden bereikt. Mogelijkheden voor het verwerken van de ongewenste stoffen bevatten ondergrondse opslag van deze stoffen.

Dit proefschrift analyseert de onderliggende thermodynamische eigenschappen van de betrokken mengsels en stelt een modelformalisme voor. Het eerste hoofdstuk beschrijft de achtergrond bij het project, introduceert de moleculaire methoden die worden toegepast in latere hoofdstukken, en omschrijft de wetenschappelijke behoeften waarin het proefschrift wil voorzien.

Hoofdstuk 2 legt een moleculair gebaseerd model voor voor het fase-evenwicht van CO_2 en H_2S met koolwaterstoffen en water. De geperturbeerde-keten polaire statistische associrende vloeistoftheorie (PCP-SAFT) toestandsvergelijking is geparametriseerd om fase-evenwichten te correleren voor mengsels van waterstofsulfide en kooldioxide met alkanen, met aromaten, en met water over een breed temperatuur- en drukbereik. De binaire mengsels van H_2S-methaan en CO_2-methaan zijn in detail bestudeerd met inbegrip van damp-vloeistof-, vloeistof-vloeistof- en vloeistof-vaste-stofevenwichten, alsmede de drie fase-evenwichten. Zeer bevredigende resultaten werden verkregen voor de binaire mengsels en ook

voor het ternaire mengsel van H_2S-CO_2-methaan met behulp van de (constante) interactieparameters van de binaire paren.

De kritieke punten van het mengsel zijn relevant voor de toestand in aardgas-reservoirs en het scheidingsproces voor CO_2 en H_2S. Hoofdstuk 3 stelt een model voor voor de adequate beschrijving van het kritieke gebied (en ook toestanden hierbuiten) met behulp van renormalisatiegroepcorrecties. Klassieke vloeistof-theorien beschrijven niet de grote fluctuaties die zich voordoen nabij een kri-tiek punt in een zuivere component of een mengsel. De geperturbeerde-keten statistische associerende vloeistoftheorie (PC-SAFT) toestandsvergelijking is uit-gebreid met een renormalisatiegroeptheorie voor mengsels. De theorie neemt grote dichtheidsfluctuaties in acht en de resultaten reduceren tot resultaten voor de klassieke PC-SAFT toestandsvergelijking uit de nabijheid van het kritieke punt. Twee benaderingsmethoden, de benadering van isomorfe dichtheden en fase-ruimtecelbenadering, worden gebruikt voor renormalisatiegroepcorrecties van mengsels. De twee varianten zijn gevalueerd door ze te vergelijken met ex-perimentele damp-vloeistofgegevens voor systemen van alkanen, kooldioxide en waterstofsulfide. Over het algemeen is de fase-ruimtecelbenadering licht super-ieur aan de isomorfe benadering voor de hier onderzochte mengsels. De fase-ruimtecelbenadering neigt ertoe in sommige gevallen de renormalisatiecorrecties te overschatten, maar in het algemeen is er goede overeenkomst met experimentele data voor binaire mengsels.

De oppervlaktespanningen van de beschouwde vloeistoffen zijn van belang in veel technische processen, bijvoorbeeld in scheidingsprocessen met behulp van een membraanabsorber. Hoofdstuk 4 stelt een model voor voor de berekening van de oppervlaktespanning met inbegrip van het kritieke gebied. Deze studie is de eerste die een aanpak op basis van de dichtheidsfunctionaaltheorie (DFT) biedt, waarbij het kritieke punt met een renormalisatieprocedure wordt afgedwon-gen. Een Helmholtzenergiefunctionaal wordt hier voorgesteld, waarbij de grote dichtheidsfluctuaties, die leiden tot het universeel kritisch schalingsgedrag, wor-den verwerkt met behulp van een renormalisatiegroeptheorie. Dit is aantrekkelijk vanwege de eenvoudige uitvoering, waar renormalisatie wordt behandeld in een lokale dichtheidsbenadering. Het model is bijna exact op het kritieke punt. Bui-ten het kritieke punt, reduceert het model tot de PC-SAFT toestandsvergelijking. De conventionele PC-SAFT parameters van pure componenten worden aangevuld met één enkele stofspecifieke renormalisatieparameter, die is aangepast om de kri-

tieke temperatuur in de bulkfase te reproduceren. De oppervlaktespanning die wordt verkregen heeft een uitstekende overeenkomst met experimentele gegevens voor een aantal niet-polaire en matig polaire stoffen (alkanen, ethers, acetaten, aromatische stoffen) tot aan het kritieke punt.

Hoofdstuk 5 stelt een simpel pragmatisch model voor voor de oplosbaarheid van CO_2 in K_2CO_3 oplossingen in water. De oplosbaarheid van koolstofdioxide (CO_2) en waterstofsulfide (H_2S) in basische waterige elektrolytenoplossingen wordt bepaald door een gecombineerd fase- en reactieevenwicht. Een cubische toestandsvergelijking wordt toegepast om de damp-vloeistofevenwichten van deze reagerende systemen te modeleren. De Peng-Robinson toestandsvergelijking met Wong-Sandler mengregels wordt gecombineerd met een uitgebreid UNIQUAC model voor elektrolyten, waarbij ion-specifieke interacties worden bepaald uit een Debye-Hückel term. Het thermodynamische model is geparametriseerd voor waterige systemen die zowel kooldioxide en waterstofsulfide bevatten als ook water en kaliumcarbonaatoplossingen bij hoge druk. De UNIQUAC binaire interactieparameters worden geschat door het minimaliseren van afwijkingen, vergeleken met de experimentele data, in de samenstelling van de vloeibare fase van het model. De gegevens zijn afkomstig uit de literatuur en worden aangevuld met eigen experimenteel werk verricht in het kader van deze studie.

Deze studie voorziet in het modeleren van de fysische eigenschappen van aardgasmengsels of ruwe-oliemengsels, die nodig zijn voor de betrouwbare calculatie van scheidingssystemen. Een adequaat model voor elektrolyten, wat nodig is om het modeleren van membraanabsorbers te verbeteren, moet nog worden ontwikkeld.

Contents

Chapter 1

Introduction

Theories from Molecular Thermodynamics have developed vividly over the past years and the models that are derived from applying molecular theories have proven highly useful in understanding, correlating and predicting complex mixtures. The term 'complex' is here used for mixtures

- where specific, non-isotropic molecular interactions are present, such as hydrogen-bonding, polar, and ionic interactions

- where phase and reaction equilibra have to be considered simultaneously, and in particular where the reactions involve electrolyte species

- in the vicinity of the critical point, where long-range density fluctuations need to be accounted for explicitly.

This thesis is concerned with the thermodynamic description of systems containing acid gases with hydrocarbons and water, in the presence of chemical electrolyte reactions. The technical relevance of such mixtures spans a wide range of temperature and pressure and particularly includes the region around the critical point of such mixtures. In that respect all of the above elements that reflect complexity are present in the considered systems.

An equation of state model is a mathematical equation that relates temperature, pressure, molar volume and compositions (T,p,v,x_i). If supplimented only with pure components' enthalpies (or heat capacities) in the ideal gas state, an equation of state can provide all other thermodynamic properties, such as, chemical potential (or activity), phase equilibrium, and entropy. Molecular based equations of state, however, also allow the calculation of interfacial properties.

This thesis proposes comprehensive parameterizations of a molecular-based equation of state and extends equation of state approaches in several ways: (1) for calculating phase equilibria up to the critical point of mixtures. And (2), a new equation of state (Helmholtz energy functional) is proposed to calculate the surface tension with quasi-exact behavior at the critical point.

1.1   Molecular based equation of state

Molecular-based theories yield significant improvements compared to phenomenological approaches to predict phase behavior in complex mixtures. These fluid theories take classical intermolecular potentials as a starting point. Statistical

thermodynamics provides two major routes to develop a molecular-based model of the microscopic and macroscopic behavior of the considered component or mixture. The first route is given by *integral equations* leading to the mean local arrangement of molecules to one another (the so-called pair distribution function) which in turn enables the calculation of other thermodynamic properties. The second route is given by *perturbation theories*, where the properties of a substance are obtained by expanding around the properties of an (approximately) known reference fluid. This approach is briefly described below.

Modern equations of state are developed in terms of the Helmholtz energy per molecule $f(T, \rho_1, ... \rho_K) = \frac{F(T, V, N_1, ... N_K)}{N}$ as a function of temperature T and density $\rho_i = \frac{N_i}{V}$ of component i, while all other properties of interest are determined from thermodynamic derivatives of the Helmholtz energy. The pressure, for example, is obained from $p = \rho^2 (\frac{\partial a}{\partial \rho})_{T,N}$ with the total number density $\rho = \sum_{j=1}^{K} \rho_j$ and the chemical potential is $\mu_i = (\frac{\partial F}{\partial N_i})_{T,V,N_{j \neq i}}$.

1.1.1 Ideal gas contribution

A molecular description of a fluids' ideal gas state is obtained by solving the partition function in the absence of intermolecular interactions. The ideal gas contribution to any thermodynamic quantity only comprises contributions due to the kinetic energy of the atomic fluids. For the temperature range of interest in our study, the quantized energy states can without significant error be considered so closely spaced, that the kinetic and potential energy can be considerd as continuous [1, 2]. This leads to the ideal gas Helmholtz energy contribution F^{id}, as

$$F^{id} = kT \sum N_i \left(ln[\rho_i \Lambda_i^3] - 1 \right) \tag{1.1}$$

where, $\Lambda_i(T)$ is the de Broglie wavelength, which here comprises the translational and internal degrees of freedom. Further, k denotes the Boltzmann constant and N_i is the number of molecules of component i. If the thermal equation of state is considered, then the ideal gas contribution trivializes to the well-known relation $p = \rho kT$ for the system pressure. Details of the ideal gas contribution, in particular the temperature dependence of the de Broglie wavelength, are irrelevant in this variable set. Eq. 1.1 determines properties such as the enthalpy of a substance and could be used accordingly. In practice, one usually takes a dif-

ferent approach by providing an empirical correlation for, say, the heat capacity of a substance. In the course of this study, namely in Chapter 3 and Chapter 4, however, the calculation of ideal gas contribution are needed explicitly.

1.1.2 Hard-sphere fluid

The hard sphere fluid is model fluid with a potential $\phi(r)$ along the radial distance r from one to another spherical particle as displayed in Figure 1.1. The potential is zero for all distances $r > \sigma$, so that the particles do not attractively interact. At $r = \sigma$ the potential shows an infinitely sharp repulsive behavior, much like two idealized billard balls do. The Lennard-Jones potential also shown in Figure 1.1 is another more realistic potential for simple fluids.
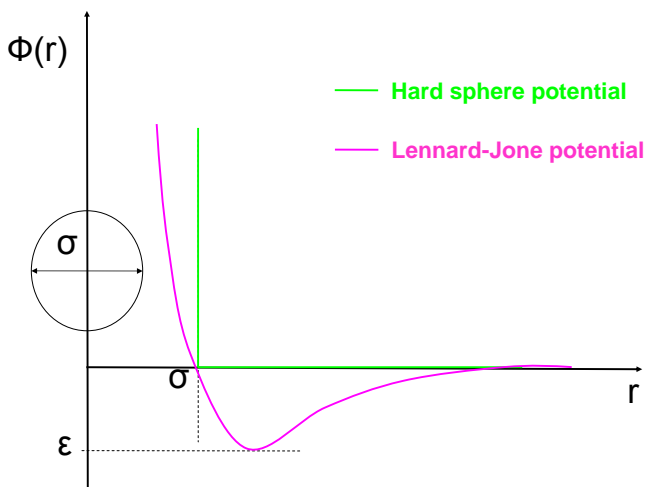
Figure 1.1: *Two different potential profiles used in the equation of state calculation*

Although the hard sphere doesn't show a vapor-liquid transition and has thermodynamic properties far from those of any real substance, it is of great theoretical and practical interest. The imporance is due to the fact that it can serve as reference fluid that already bears important features of real substances. In particular, the arrangement of spherical molecules around one another (the pair distribution function) of a hard sphere fluid is a good approximation to that of an

attractive fluid of same density. This observation is used in perturbation theories, where the properties of attractive fluids are developed by expanding the pair distribution function around the one of hard-sphere fluid. The advantages that the hard-sphere fluid offers is, first, that all properties are a function of density only (i.e. independent of temperature). Secondly, the hard sphere model doesn't show a liquid-vapor phase transition, with the involved instable regions in the entire fluid regime. As a result of both aspects, the properties of the hard-sphere fluid and those of mixtures of hard spheres are well-known. Accurate correlations of hard-sphere properties are partially empirical [1].

1.1.3   Hard-chain fluid

Both of the potentials introduced above, the hard-sphere potential and Lennard-Jones potential are for spherically symmetric fluids. The treatment of non-spherical substances can nonetheless be based on these potentials. That is when modelling a molecule such as nitrogen N_2 as two fused spherical segments, both of which interact with, say, a Lennard-Jones potential to the spherical segments of another molecule. Also complex fluids can be build up by spherical segments. In general the full geometrical details of a large molecule are difficult to deal with in fluid theories. However, it is possible to represent larger molecules more coarse-grained, i.e. as chains of tangentially bonded spherical segments. This molecular model still preserves much of the essence of a molecule: its size and a representation of its non-spherical shape. This molecular model has shown to be successful even for fully polymeric substances[3, 4, 5].

In order to describe chains of bonded spheres based on spherical fluids it is required to connect spheres to form a chain. The term 'to connect' refers to a theory, that provides the Helmholtz energy change for connecting spheres. Such a theory was developed by Wertheim[6, 7, 8, 9]. His first order perturbation theory (TPT1) was developed for specific off-center sites on a spherical core, that can interact with other off-center sites on other particles. The resulting theory provides a powerful framework for modelling specific, directed interactions, such as hydrogen bonds of fluids. If two such interactions are considered at the limit of infinite attraction, however, the theory irreversibly connects the spherical cores to chains. The theory for connecting a defined number m of spherical cores to a chain of connected spheres was worked out by Chapman et al.[10, 11], leading to

the Statistical Associating Fluid Theory (SAFT) equations of state. The stucture of the SAFT equation of state for hard chains

$$F^{hsc} = F^{hs} + F^{chain} \tag{1.2}$$

where, F^{hsc} is the Helmholtz energy of the hard-sphere chain fluid, F^{hs} the Helmholtz energy of all involved spherical segments that interact as hard spheres. Further, F^{chain} denotes the contribution of connecting the spheres to form chains. In the notation applied throughout this study, we define all Helmholtz energy contributions to be 'residual' contributions, so that the ideal gas contribution needs to be added in order to get to the Helmholtz energy.

1.1.4 Perturbation theory

Perturbation theories are based on the observation that the arrangement of molecules around one another is primarily determined by strong, short range repulsive forces, or in turn, that the structure of a fluid is only slightly modified by weak, long range attractive forces. The pair distribution function $g(r)$ captures the average arrangement of molecules towards each other. For spherically symmetric fluids, $g(r)\rho 4\pi r^2 \, \mathrm{d}r$ gives the probability of finding other molecules in the inverval of distance r and $r + \mathrm{d}r$ from a considered central molecule. Figure 1.2 illustrates this interpretation. The figure also shows a typical pair correlation function of a spherically symmetric fluid at high density. The peaks are the 'shells' of neighbors which are around a central molecule. The notation $g(r)$ is common although the pair distribution function is actually dependent on distance r, all densities ρ_i, temperature T, and for non-isotropic fluids the orientation and conformation of the two considered species.

   In perturbation theories for spherical molecules, the hard sphere fluid is usually taken as the reference and the non-directional attractive (dispersive) forces are taken as the perturbation. The idea of a perturbation theory is mathematically developed by decomposing the intermolecular potential into a harshly repulsive part $\phi_0(r)$ and an attractive branch $\phi_a(r)$, as

$$\phi_\lambda(r) = \phi_0(r) + \lambda\phi_a(r) \tag{1.3}$$

   where λ, with $0 \leq \lambda \leq 1$, is a coupling parameter that can lead to a continuous
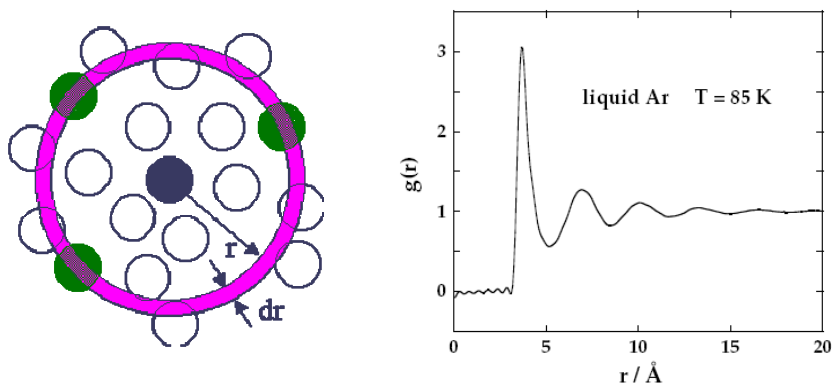
Figure 1.2: *Illustration of the pair distribution function g(r) giving the average arrangement of the molecules around a central molecule.*

transition from the reference fluid with potential $\phi_0(r)$ (with $\lambda = 0$) towards the target fluid $\phi(r) = \phi_{\lambda=1}(r)$ (with $\lambda = 1$). The perturbing potential is simply the difference between target and reference potential, $\phi_a(r) = \phi(r) - \phi_0(r)$. With this coupling parameter, the Helmholtz energy of the target fluid is

$$F = F_0 + \int_0^1 \left(\frac{\partial F}{\partial \lambda}\right) \mathrm{d}\lambda \qquad (1.4)$$

where F_0 is the Helmholtz energy of the reference fluid. When the partition function and the definition of the pair distribution function are introduced in Eq. 1.4 one can derive the relation

$$F = F_0 + \frac{1}{2}\rho N \int_0^1 \int_0^\infty g_\lambda(r)\phi_a(r)4\pi r^2 \mathrm{d}r\mathrm{d}\lambda \qquad (1.5)$$

This equation is exact for spherically symmetric fluids in homogeneous phases. Both conditions are in the course of this study relaxed: in Chapter 4 an analogous equation, but now extended to chain fluids, is formulated for inhomogeneous systems and is applied to interfaces. The direct application of Eq. 1.5, however, is hindered by the fact that the pair distribution function is now needed not only for the reference fluid, but for fluids with potentials $\phi_\lambda(r)$ for all values of λ. That is generally not available. Rather, one can now develop an expansion of $g_\lambda(r)$

around the reference fluids' pair distribution function, as

$$g_\lambda(r) = g_0(r) + \left(\frac{\partial g(r)}{\partial \lambda}\right)_0 \lambda + ...$$ (1.6)

where the subscript '0' for all terms on the right hand side of the equation is for $\lambda = 0$, i.e. for the reference fluid.

With this expansion, the Helmholtz energy is also obtained as the sum of terms, as

$$F = F_0 + F_1 + F_2 + ...$$ (1.7)

where F_0 is the Helmholtz energy of the reference fluid and F_1 and F_2 are the first and second order perturbation terms, respectively. For spherical fluids, in practice, it is often the hard-sphere fluid (superscript 'hs'), that serves as a reference fluid. The perturbation terms of first and second order are then

$$F_1 = \frac{1}{2}\rho N \int g^{hs}(r)\phi_a(r)\, 4\pi r^2 \,\mathrm{d}r$$ (1.8)

$$F_2 = \frac{1}{2}\rho N \int \left(\frac{\partial g(r)}{\partial \lambda}\right)_{\lambda=0} \phi_a(r)\, 4\pi r^2 \,\mathrm{d}r$$ (1.9)

An explicit expression can be derived for the second order term, however, the derivation as well as the final result is quite involved[12]. The application of the resulting second order term is limited by the fact that 3-body and 4-body correlation functions are required, for which simple theories are absent. Barker and Henderson have derived an approximate expression for the second order term by approximating microscopic properties as their macroscopic analogues[13, 14]. This expression involves only the pair correlation function of the reference fluid and can thus conveniently be evaluated.

The first generation of SAFT equations have assumed the hard chain fluid as a reference, but have subsequently ignored the chain formation in the attractive term[10, 11, 15, 16, 17]. More rigorously, one can take two paths to get towards a description of attractive chain fluids. The first is to apply a perturbation theory to hard spheres in order to get a theory for attractive spheres, and subsequently apply Wertheim's theory to connect these attractive spheres to attractive chains. There are several SAFT variants that have taken that path[18, 19, 20, 21, 22]. The second path is to first connect the hard spheres to a hard-sphere chain using

Wertheim's TPT1, while subsequently apply a perturbation theory to get attracting chains. This approach was taken by Gross and Sadowski, who considered a hard-chain reference fluid and reformulated the perturbation theory for chain fluids[23, 24]. This model is referred to as Perturbed-Chain Statistical Associating Fluid Theory (PC-SAFT) equation of state. Several reviews summarize recent developments of the SAFT-models[5, 4, 3].

The PC-SAFT model was later extended to explicitly account for polar interactions, as a result of a molecules' dipole moment or quadrupole moment. A perturbation approach was also applied to derive a Helmholtz energy contribution due to polar moments. This lead to the Perturbed-Chain Polar Statistical Associating Fluid Theory (PCP-SAFT) equation of state, which is applied in Chapter 2, and is modified in Chapter 3 and in Chapter 4. In summary, the PCP-SAFT equation of state has the form

$$F = F^{id} + F^{hsc} + F^{disp} + F^{assoc} + F^{polar} \qquad (1.10)$$

where F^{hsc} is the Helmholtz enery contribution of hard sphere chains, $F^{disp} = F_1 + F_2$ (analogous to Eq. 1.8 and 1.9, but for chain molecules) is the dispersion term describing the attraction of chain molecules, F^{assoc} is the association term based on Wertheim's TPT1 describing the H-bonding interactions[25, 26, 27, 10, 11, 15], F^{polar} is the polar term describing the interactions due to dipolar and quadrupolar moments[28, 29, 30] and possibly accouting for the effect of electrostatic polarizibility[31].

1.2 Phase equilibrium

Thermodynamics is usually subdivided into a theory dealing with equilibrium and into one concerned with irreversible processes. The equilibrium condition that the entropy is maximal for a closed system of defined internal energy, volume and composition, can be recast into three equilibrium conditions. For the phase equilibrium betwee two coexisting phases (1) and (2) these conditions are: $T^{(1)} = T^{(2)}$ for thermal equilibrium, $p^{(1)} = p^{(2)}$ for mechanical equilibrium, and $\mu_i^{(1)} = \mu_i^{(2)}$ for all components i as the chemical equilibrium condition.

Thermodynamic models are needed to determine the chemical potentials. The condition of same chemical potentials in all coexisting phases is used for calcula-

ting the phase equilibria from these models. In this thesis, we use analytic equation of state models for the chemical potential of all phases, so that the condition of same chemical potentials is equivalent to the condition of same fugacities f_i. For two phases, it is

$$f_i^{(1)} = f_i^{(2)} \tag{1.11}$$

In many engineering applications, the chemical potentials of two phases are evaluated with different models. This is done for example for vapor-liquid equilibria using Gibbs excess energy models[32]. While this is limited to a range of temperatures and pressures and requires the mixtures to be far from their critical points, we use the same equation of state for all phases so that phase equilibrium correlations or predictions can be made over a wide range of temperature and pressure, including near the critical region.

Equations of state developed for fluid phases are almost unanimously incapable of describing the liquid solid phase transition. It is nonetheless possible to calculate solid-fluid equilibria using such models. That is accomplished by expressing the chemical potential of a compound i for a solid phase based on the chemical potential of a hypothetical fluid, as

$$\mu_i^{solid} = \mu_i^{\text{hypothetical fluid}} + \left(\mu_i^{\text{solid}} - \mu_i^{\text{hypothetical fluid}} \right) \tag{1.12}$$

The equation of state model is then applied to estimate the properties of component i in the hypothetical state of a liquid. The bracketed term on the right hand side of Eq. 1.12 can conveniently be expressed in terms of a pure component phase transiton enthalpy of the considered species. The details of this approach are given in Chapter 2.

1.3   Identifying physical property needs - separation of acid gases as an example

This subchapter illustrates the need for physical properties of complex mixtures involving acid gases by analysing a novel separation process, namely a membrane contactor, as an example. This study was conducted as part of the Integrated System Approach Petroleum Production (ISAPP) program (see Appendix A) which is a joint initiative by TNO, Shell and Delft University of Technology targeting

at research in upstream oil and gas production technology. As part of the ISAPP initiative the author proposed an absorption process, which could be realized underground, i.e. within the bore well. A membrane contactor is promising to address the challenges of an underground separation process. Considering this process as an example here, allows us to deduce and motivate physical-property needs for describing such processes.

Natural gases may contain light non-hydrocarbon compounds, such as carbon dioxide and hydrogen sulfide. These acid gases must be removed to sweeten the gas phase, and an accurate knowledge of the underlying phase behavior of H_2S and CO_2 with hydrocarbons and with water is important for these industrial processes. The presence of non-hydrocarbon molecules increases the complexity of natural gas mixtures, because these compounds exhibit specific intermolecular interactions.

Different *sorts of solvents* are used in absorption/desorption processes applied in industry for the separation of acid gas from gas streams (see Appendix A). *Chemical solvents* such as aqueous solutions of alkanolamines or aqueous $NaOH$-solutions are commonly used for the absorption of H_2S/CO_2 at low pressure conditions. While these solvents have a high capacity to absorb acid gases also at high pressures, the regeneration processes are in practice prohibitivly expensive. *Physical solvents*, such as alcohols, glycols, sulfolanes and mixed organic solvents are usually considered for elevated pressure conditions.

With the application of a separation process operating within the bore well in mind, one can exclude several solvent-choices: substances like methanol, ethanol and acetone give significantly higher solubilities for CO_2 at 80-90 bars than pure water, but these solvents have a fairly high vapor pressure so that solvent-loss is a technical challenge. Glycols show high CO_2-solubilities and their vapor pressure is relatively low. But glycols are fully miscible with water, which for an application in the bore-well means, the solvent would continuously be diluted with the water in the course of the process. Due to these arguments, mildly basic aqueous electrolyte solutions are suitable for the conditions at hand. The vapor pressure of water is thereby not an issue, since any loss of water can easily be compensated. Moreover, natural gases are often pre-saturated with water. We propose aqueous potassium carbonate (K_2CO_3) solution, which is considered in this example. The chemically active ionic components don't have a tendency to evaporate. The chemical reactions to hydrogen carbonate is sufficiently weak to

warrant an energetically easy desorption process.

A separation process in the bore well is challenging because the fluid dynamic conditions are strongly fluctuating with time. A membrane contactor is a fluid dynamically robust device for bringing the gaseous mixture in contact with the liquid absorbent. The membrane in a membrane contactor is not necessarily selective. The pores are meso- or macropores and the purpose of the membrane is to establish a defined interface between the gas and liquid phase. The distribution of a solute between the two phases is not determined by the membrane (material) but is due to the underlying vapor-liquid equilibrium. The advantages of membrane contactors have gained considerable attention[33, 34, 35, 36, 37, 38, 39, 40]. An important criterion for an efficient membrane contactor process is, that the pores of the membrane material are gas-filled (non-wetted), as shown in Figure 1.3.
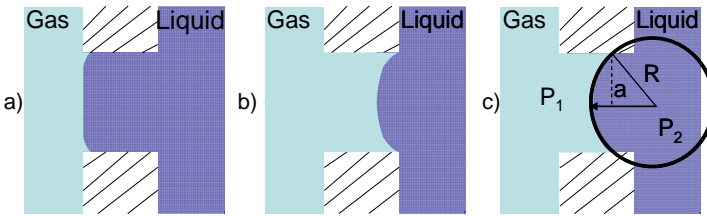
Figure 1.3: *Membrane absorption contactors: Amplification for interface of gas and liquid. Inserted: a). Completely wetted mode; b). Non wetted mode; c) Partially wetted mode.*

Membrane contactors with completely wetted pores[39, 37], with partially wetted pores[39], and with non-wetted pores[40, 41, 38, 42, 43] were considered in several studies. In some investigations[37, 40, 39, 41, 43], the results of transport models (diffusion and chemical reaction rates) are compared to experimental observations and generally good agreement was found. The wetted mode of operation[37] was found to offer considerably higher resistance to mass transfer when compared to the nonwetted mode of operation. The non-wetted working modes are concluded to be critically important for an efficient process. The mass transport in liquid filled pores is greatly reduced compared to non-wetted pores, because typical diffusion coefficients are three orders of magnitude lower for a stagnant pore-liquid compared to those for a gas-filled pore.
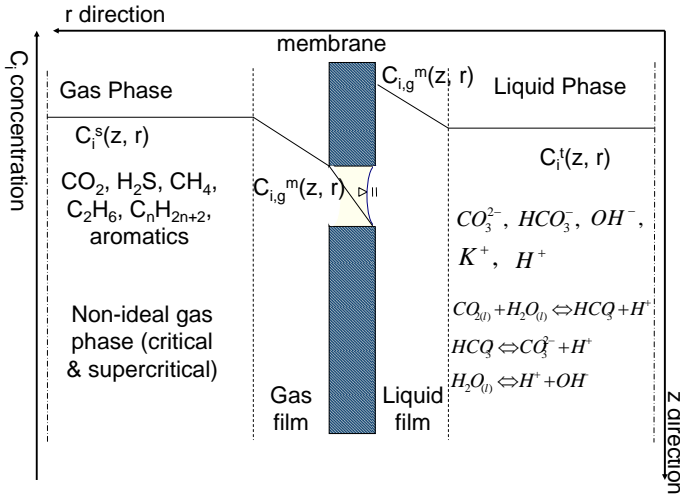
Figure 1.4: *Schematic of compositional profiles for membrane contactor. Here, $C_i^s(z,r)$ and $C_i^t(z,r)$ are the concentration in the bulk gas phase (shell side) and the bulk liquid phase (tube side), respectively. Further, $C_{i,g}^m(z,r)$ and $C_{i,l}^m(z,r)$ are the (equilibrium) concentrations of gas and liquid at the interface, respectively.*

Basic elements of the separation problem introduced in this subchaper are illustrated in Figure 1.4. It is shown that in the gas phase, not only methane exists, but also higher alkanes, aromatics and acid gases, such as CO_2 and H_2S. The system is complex in several ways. At elevated pressure these mixtures are in the vicinity of the mixture's critical points, which calls for a sound thermodynamic model for the gas phase. On the other hand, one has to consider the simultaneous reaction and *phase equilibria*, where equilibria of vapor, (two) liquid phase(s), and solid phase have to be regarded. Lastly, the liquid phase is demanding also in terms of the molecular interactions, where strongly hydrogen-bonding substances, and polar fluids as well as different ions with reactions, such as CO_3^{2-}, HCO_3^-, OH^-, K^+ and H^+ require a sound description.

A detailed *thermodynamic model* is also needed for studying the kinetics in the system. Mass transport in our system can only be described properly and with some robustness towards extrapolations in state space, when the right driving forces are considered as well as the coupling between driving forces. The appro-

priate thermodynamic driving forces are gradients in *chemical potentials*. The concentration gradients and a non-coupled transport relation as in Fick's law is insufficient. The simplest model that suffices the thermodynamic requirements is the Maxwell-Stefan approach, that relates component fluxes J_i of a K-component mixture with driving forces in chemical potential $-\nabla \mu_{i,T}$ according to diffusion coefficients D_{ij}, as

$$- x_i \frac{\nabla \mu_{i,T}}{RT} = \sum_{i \neq j}^{K} \frac{1}{cD_{ij}} \left(x_j J_i - x_i J_j \right) \tag{1.13}$$

which confirms the need for a sound thermodynamic model that provides gradients in chemical potentials. A more elaborate coupling to heat transport and basics to reaction kinetics derived from non-equilibrium thermodynamics were recently published in a textbook by Kjelstrup et al.[44].

1.4   Fluid properties study in this thesis

To accurately represent the complex mixtures introduced above, an appropriate model for the phase equilibria (and chemical potentials) is needed - one that includes details on the interactions between polar compounds and water and accounts for the hydrogen bonding character of the aqueous mixtures, see Figure 1.5. **Chapter 2** describes the perturbed-chain polar statistical associating fluid theory (PCP-SAFT) equation of state as a suitable model and proposes a parameterization for the phase equilibria of CO_2 and H_2S with hydrocarbons and with water. Wide ranges of temperature and pressure are covered and equilibria of vapor, liquid and solid phases are considered. Higher hydrocarbons that appear in real natural gas and oil mixtures are also accounted for. A reliable description of the phase behavior of these mixtures with good robustness towards extrapolations in state conditions is of importance for the acid gas purification.

A precise thermodynanmic model is needed for a wide range of pressure and temperature including the critical region. The fluid behavior in the vicinity of the critical point is influenced by fluctuations of component densities. That leads to a universal behavior of all fluids that is captured by so-called scaling laws. Classical equations of state are often based on a purely repulsive reference fluid (such as hard spheres) where long-range fluctuations are absent. As a consequence, classical models cannot describe the critical region correctly, as illustrated with
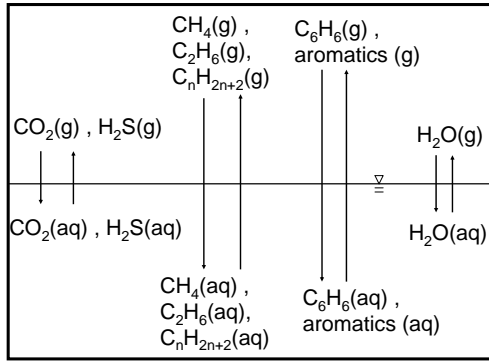
Figure 1.5: *Vapor liquid equilibria of the system containing natural gas and acid gases*

Figure 1.6 and Figure 1.7 as exmaples for pure fluids and mixtures at critical region. The temperature and pressure of critical points is usually described at too high values and the scaling law behavior around the critical point is not captured by classical equations of state. In view of the technical relevance of the critical region for the mixtures at hand, in **Chapter 3** an equation of state is proposed that accounts for the fluctuations leading to the universal scaling laws at the critical point. A renormalization group correction for binary mixtures is developed for the PC-SAFT equation of state. The renormalization group theory proposed by Wilson[45, 46] and White [47, 48] provides a framework to successively account for density fluctuations of increasing wavelength.

For a membrane contactor to be an effective separation unit, one has to ensure gas-filled, non-wetted pores. High pressure operating conditions are more severe in this respect, since the increasing gas phase density lowers the surface tension towards the liquid at a given temperature. For a given liquid absorbent, the minimum pressure (breakthrough pressure) to be applied on the liquid phase to enter the membrane pore can be estimated by the Young-Laplace equation [49, 50], as

$$\Delta p = \frac{2\gamma}{R} \tag{1.14}$$

where γ is the surface tension of liquids against the gas phase mixture. The limiting breakthorugh pressure depends on the surface tension of the liquids against
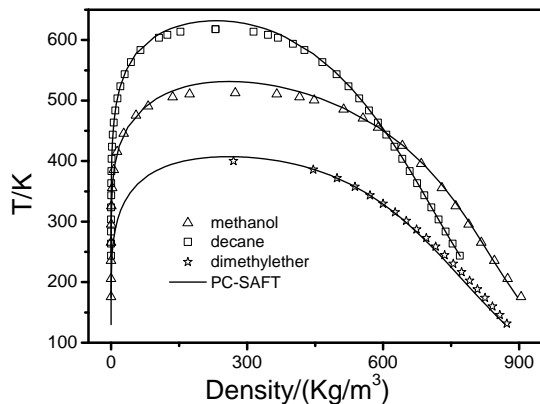
Figure 1.6: *Coexisting vapor and liquid densities of methanol, n-decane and dimethyl ether*
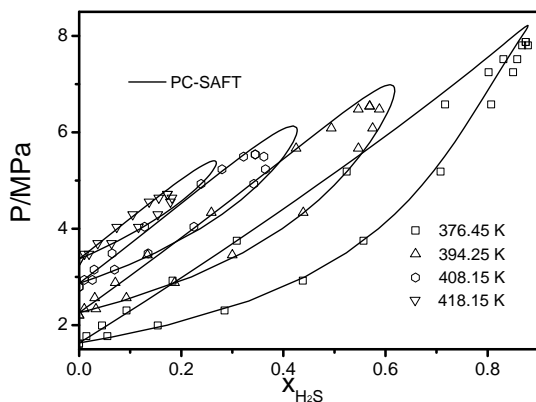
Figure 1.7: *Vapor-liquid equilibrium of H_2S-butane at four temperatures. Comparison of PC-SAFT (dashed lines) and experimental data(symbols)*

gas phase. In **Chapter 4** the density functional theory is applied with the PC-SAFT equation of state to predict the surface tension of pure substances. The calculation of the surface tension, from the density functional theory suffers from the overestimation of the critical temperature[51] of all classical Helmholtz energy functionals. Here, a new Helmholtz energy functional proposed that, for the first

time, is almost exact at the critical point. The long-range density fluctuations leading to the universal critical scaling behavior are accounted for using a renormalization group theory (similar to that of the previous Chapter 3). The appeal of the approach is its relatively simple implementation, where the renormalization is treated in a local density approximation.

Lastly, aqueous K_2CO_3-solutions were suggested as absorption liquids for the absorption of carbon dioxide and developing a model for the underlying phase equilibria is central for any engineering of the separation unit. In **Chapter 5** a simple thermodynamic model is developed for CO_2 and aqueous electrolyte solutions with and without reactions. The solubility of carbon dioxide (CO_2) and hydrogen sulfide (H_2S) in basic aqueous electrolyte solutions is determined by solving and parameterizing the combined phase and reaction equilibrium. A cubic equation of state is here applied to model the vapor-liquid equilibria of these reacting systems. The Peng-Robinson equation of state with Wong-Sandler mixing rules is combined with an extended UNIQUAC model for electrolytes where ion-specific interactions are determined from a Debye-Hückel term. The thermodynamic model is parameterized for aqueous systems containing carbon dioxide and hydrogen sulfide along with water and potassium carbonate solutions at high pressure.

REFERENCES

[1] J.-P. Hansen and I. MacDonald, editors. *Theory of Simple Liquids*. Academic Press, 3 edition, 2006.

[2] D. A. McQuarrie. *Statistical Mechanics*. Harper and Row, New York, 1976.

[3] S. P. Tan, H. Adidharma, and M. Radosz. Recent advances and applications of statistical associating fluid theory. *Ind. Eng. Chem. Res.*, 47(21):8063–8082, 2008.

[4] I. G. Economou. Statistical associating fluid theory: A successful model for the calculation of thermodynamic and phase equilibrium properties of complex fluid mixtures. *Ind. Eng. Chem. Res.*, 41(5):953–962, 2002.

[5] E. A. Muller and K. E. Gubbins. Molecular-based equations of state for associating fluids: A review of saft and related approaches. *Ind. Eng. Chem. Res.*, 40(10):2193–2211, 2001.

[6] M. S. Wertheim. Fluids with highly directional attractive forces. I. statistical thermodynamics. *J. Stat. Phys.*, 35:19–34, 1984.

[7] M. S. Wertheim. Fluids with highly directional attractive forces. II. thermo-dynamic perturbation theory and integral equations. *J. Stat. Phys.*, 35:35–47, 1984.

[8] M. S. Wertheim. Fluids with highly directional attractive forces. III. multiple attraction sites. *J. Stat. Phys.*, 42:459–476, 1986.

[9] M. S. Wertheim. Fluids with highly directional attractive forces. IV. equili-brium polymerization. *J. Stat. Phys.*, 42:477–492, 1986.

[10] W. G. Chapman, G. Jackson, and K. E. Gubbins. Phase equilibria of as-sociating fluids. Chain molecules with multiple bonding sites. *Mol. Phys.*, 65:1057–1079, 1988.

[11] W. G. Chapman, K. E. Gubbins, G. Jackson, and M. Radosz. SAFT-equation of state solution model for associating fluids. *Fluid Phase Equilib.*, 52:31–38, 1989.

[12] D. Henderson and J.A. Barker. *Physical Chemistry: An Advanced Treatise*, volume VIIIA. Academic Press, New York, 1971.

[13] J. A. Barker and D. Henderson. Perturbation theory and equation of state for fluids: the square-well potential. *J. Chem. Phys.*, 47(8):2856–2861, 1967.

[14] J. A. Barker and D. Henderson. Perturbation theory and equation of state for fluids. II. A successful theory of liquids. *J. Chem. Phys.*, 47:4714–4721, 1967.

[15] W. G. Chapman, K. E. Gubbins, G. Jackson, and M. Radosz. New reference equation of state for associating liquids. *Ind. Eng. Chem. Res.*, 29:1709–1721, 1990.

[16] S. H. Huang and M. Radosz. Equation of state for small, large, polydisperse and associating molecules. *Ind. Eng. Chem. Res.*, 29:2284–2294, 1990.

[17] S. H. Huang and M. Radosz. Equation of state for small, large, polydisperse, and associating molecules: extensions to fluid mixtures. *Ind. Eng. Chem. Res.*, 30:1994–2005, 1991.

[18] A. Gil-Villegas, A. Galindo, P. J. Whitehead, S. J. Mills, G. Jackson, and A. N. Burgess. Statistical associating fluid theory for chain molecules with attractive potentials of variable range. *J. Chem. Phys.*, 106:4168–4186, 1997.

[19] F. J. Blas and L. F. Vega. Thermodynamic behaviour of homonuclear and heteronuclear lennard-jones chains with association sites from simulation and theory. *Mol. Phys.*, 1:135–150, 1997.

[20] A. Galindo, L. A. Davies, A. Gil-Villegas, and G. Jackson. The thermo-dynamics of mixtures and the corresponding mixing rules in the SAFT-VR approach for potentials of variable range. *Mol. Phys.*, 93(2):241–252, 1998.

[21] F. J. Blas and L. F. Vega. Prediction of binary and ternary diagrams using the statistical associating fluid theory (SAFT) equation of state. *Ind. Eng. Chem. Res.*, 37:660–674, 1998.

[22] J. C. Pámies and L. F. Vega. Vapor-liquid equilibria and critical behavior of heavy n-alkanes using transferable parameters from the soft-SAFT equation of state. *Ind. Eng. Chem. Res.*, 40:2532–2543, 2001.

[23] J. Gross and G. Sadowski. Application of perturbation theory to a hard-chain reference fluid: an equation of state for squarewell chains. *Fluid Phase Equilib.*, 168:183–199, 2000.

[24] J. Gross and G. Sadowski. Perturbed-chain SAFT: an equation of state based on a perturbation theory for chain molecules. *Ind. Eng. Chem. Res.*, 40:1244–1260, 2001.

[25] W. G. Chapman, K. E. Gubbins, C. G. Joslin, and C. G. Gray. Theory and simulation of associating liquid-mixtures. *Fluid Phase Equilib.*, 29:337–346, 1986.

[26] C. G. Joslin, C. G. Gray, and W. G. Chapman. Theory and simulation of associating liquid mixtures. II. *Mol. Phys.*, 62:843–860, 1987.

[27] G. Jackson, W. G. Chapman, and K. E. Gubbins. Phase equilibria of asso-ciating fluids - spherical molecules with multiple bonding sites. *Mol. Phys.*, 65:1–31, 1988.

[28] J. Gross. An equation of state contribution for polar components: quadru-polar molecules. *AIChE*, 51(9):2556–2568, 2005.

[29] J. Gross and J. Vrabec. An equation of state contribution for polar compo-nenets: dipolar molecules. *AIChE*, 52(3):1194–1204, 2006.

[30] J. Vrabec and J. Gross. Vapor-liquid equilibria simulation and an equation of state contribution for dipole-quadrupole interactions. *J. Phys. Chem. B*, 112:51–60, 2008.

[31] M. Kleiner and J. Gross. An equation of state contribution for polar compo-nents: polarizable dipoles. *AIChE*, 52(5):1951–1961, 2006.

[32] J. M. Smith, H. C. Van Ness, and M. M. Abbott, editors. *Hansen Solubility Parameters: a user's handbook*. McGraw-Hill Education, 7 edition, 2005.

[33] E. N. Sieder and G. E. Tate. Heat transfer and pressure drop of liquids in tubes. *Industrial and Engineering Chemistry*, 28:1429–1435, 1936.

[34] Q. Zhang and E. L. Cussler. Microporous hollow fibers for gas absorption: I. Mass transfer in the liquid. *J. Membr. Sci.*, 23(3):321–332, 1985.

[35] M. C. Yang and E. L. Cussler. Designing hollow-fiber contactors. *AIChE*, 32(11):1910–1916, 1986.

[36] K. L. Wang and E. L. Cussler. Baffled membrane modules made with hollow-fiber fabric. *J. Membr. Sci.*, 85(3):265–278, 1993.

[37] S. Karoor and K. K. Sirkar. Gas-absorption studies in microporous hollow fiber membrane modules. *Ind. Eng. Chem. Res.*, 32(4):674–684, 1993.

[38] Y. Lee, R. D. Noble, B.-Y. Yeom, Y.-I. Park, and K.-H. Lee. Analysis of CO_2 removal by hollow fiber membrane contactors. *J. Membr. Sci.*, 194(1):57–67, 2001.

[39] M. H. Al-Marzouqi, M. H. El-Naas, S. A. M. Marzouk, M. A. Al-Zarooni, N. Abdullatif, and R. Faiz. Modeling of CO_2 absorption in membrane contactors. *Sep. Purif. Technol.*, 59(3):286–293, 2008.

[40] S. Shirazian, A. Moghadassi, and S. Moradi. Numerical simulation of mass transfer in gas-liquid hollow fiber membrane contactors for laminar flow conditions. *Simul. Modell. Pract. Theory*, 17(4):708–718, 2009.

[41] H. Y. Zhang, R. Wang, D. T. Liang, and J. H. Tay. Modeling and experimental study of CO_2 absorption in a hollow fiber membrane contactor. *J. Membr. Sci.*, 279(1-2):301–310, 2006.

[42] S. Atchariyawut, R. Jiraratananon, and R. Wang. Separation of CO_2 from CH_4 by using gas-liquid membrane contacting process. *J. Membr. Sci.*, 304(1-2):163–172, 2007.

[43] Y. S. Kim and S. M. Yang. Absorption of carbon dioxide through hollow fiber membranes using various aqueous absorbents. *Sep. Purif. Technol.*, 21(1-2):101–109, 2000.

[44] S. Kjelstrup, D. Bedeaux, E. Johannessen, and J. Gross. *Non-equilibrium Thermodynamics for Engineers*. World Scientific, 2010.

[45] K. G. Wilson. Renormalization group and critical phenomena. 1. Renormalization group and the kadanoff scaling picture. *Phys. Rev. B: Condens. Matter*, 4(9):3174–3183, 1971.

[46] K. G. Wilson. Renormalization group and critical phenomena. 2. Phase-space cell analysis of critical behavior. *Phys. Rev. B*, 4(9):3184–3205, 1971.

[47] J. A. White. Contribution of fluctuations to thermal properties of fluids with attractive forces of limited range: theory compared with $P\rho T$ and C_v data for argon. *Fluid Phase Equilib.*, 75:53–64, 1992.

[48] J. A. White and S. Zhang. Renormalization group theory for fluids. *J. Chem. Phys.*, 99:2012–2019, 1993.

[49] P. S. Kumar, J. A. Hogendoorn, P. H. M. Feron, and G. F. Versteeg. New absorption liquids for the removal of CO_2 from dilute gas streams using membrane contactors. *Chem. Eng. Sci.*, 57(9):1639–1651, 2002.

[50] A. C. M. Franken, J. A. M. Nolten, M. H. V. Mulder, D. Bargeman, and C. A. Smolders. Wetting criteria for the applicability of membrane distillation. *J. Membr. Sci.*, 33(3):315–328, 1987.

[51] J. Gross. A density functional theory for vapor-liquid interfaces using the PCP-SAFT equation of state. *J. Chem. Phys.*, 131:204705, 2009.

Modeling the phase equilibria of hydrogen sulfide and carbon dioxide in mixture with hydrocarbons and water using PCP-SAFT equation of state

Abstract

The perturbed-chain polar statistical associating fluid theory (PCP-SAFT) equation of state is applied to correlate phase equilibria for mixtures of hydrogen sulfide (H_2S) and carbon dioxide (CO_2) with alkanes, with aromatics, and with water over wide temperature and pressure ranges. The binary mixtures of H_2S-methane and CO_2-methane are studied in detail including vapor-liquid, liquid-liquid and fluid-solid phase equilibria. Very satisfying results were obtained for the binary mixtures as well as for the ternary mixture of H_2S-CO_2-methane using the (constant) interaction parameters of the binary pairs.

25

2.1   Introduction

Natural gases may contain light non-hydrocarbon compounds, such as carbon dioxide and hydrogen sulfide. These acid gases must be removed to sweeten the gas phase, and an accurate knowledge of the underlying phase behavior of H_2S and CO_2 with hydrocarbons and with water is important for these industrial processes. The presence of non-hydrocarbon molecules increases the complexity of natural gas mixtures, because these compounds exhibit specific intermolecular interactions. Carbon dioxide is a prototype quadruple compound, while hydrogen sulfide is an associating (hydrogen bonding) component with dipolar and quadruple moments. Explicitly accounting for these polar interactions leads to models that are more predictive or more robust to extrapolations outside the (T, p, x)-conditions where the equation of state was parameterized.

Molecular-based models yield significant improvements compared to phenomenological approaches for correlating the phase behavior in complex and macromolecular systems. Many recent thermodynamic models are derived from statistical mechanical fluid theories. The Statistical Associating Fluid Theory (SAFT) proposed by Chapman et al.[1, 2] based on Wertheim's thermodynamic perturbation theory of first order[3, 4, 5, 6] (TPT1) is one of the most successful frameworks for theoretically-based equations of state. Several modifications were suggested over the years[7, 8, 9, 10, 11, 12, 13, 14], with widespread applications[15].

The effect of polar interactions such as dipolar and quadrupolar intermolecular forces has received more attention in recent years. Zhao and McCabe[16] used an integral-equation approach in combination with the SAFT with variable attractive potential range (SAFT-VR) equation of state[9]. Equation-of-state contributions that are based on perturbation theories[17, 18] for spherical fluids have been applied in combination with several SAFT-type models[19, 20, 21, 22, 23, 24, 25, 26]. Expressions that account for the non-spherical shape of polar fluids have recently been proposed in Ref. [27, 28, 29]. Further, Kleiner and Gross[30] accounted for the polarizability of fluids and for the appropriate induction effects of dipoles in applying a renormalization scheme proposed by Wertheim[31, 32].

Hydrogen + n-alkane systems were studied experimentally and with the soft-SAFT equation of state by Florusse et al.[33]. Carbon dioxide + n-alkane systems were studied by Garcia et al.[34] using the PC-SAFT equation of state. Carbon dioxide + n-alkane systems were studied by Llovell et al.[35] using the soft-SAFT

equation of state. Thi et al.[36] compared PC-SAFT and VR-SAFT for phase equilibria of H_2 + n-alkane and CO_2 + n-alkane binary mixtures. The phase behavior of CO_2, N_2 and H_2S binary mixtures with n-alkanes ($C1 - C5$) were studied by Aparicio-Martinez and Hall[37] using the PC-SAFT equation of state. The SAFT-VR equation with a dipolar term proposed by Zhao and McCabe[16] was applied to H_2S + n-alkane binary mixtures at high pressure[38]. A Group-Contribution SAFT (GC-SAFT) approach based on London's theory[39, 40] has been developed for binary mixtures containing CO_2, N_2, H_2S, alkanes, and aromatics. Valtz et al.[41] used the SAFT-VR model (and also considered two cubic equation of state approaches) to represent VLE data of the CO_2-water mixture. The CO_2-water system was also studied by dos Ramos et al.[42, 43] using the same model. Ji et al.[44] modeled the mixture CO_2-water and proceeded to correlate mixtures of CO_2-NaCl aqueous solutions were the restricted primitive mean spherical approximation was adopted for the ion-ion contribution[45].

In this work, we apply the perturbed-chain polar statistical associating fluid theory (PCP-SAFT) equation of state (EOS) to describe phase equilibria for mixtures such as H_2S-hydrocarbons and CO_2-hydrocarbons. Vapor-liquid, liquid-liquid, solid-liquid, solid-liquid-vapor equilibrium were correlated by the PCP-SAFT equation of state for important binary mixtures, like H_2S-methane and CO_2-methane. Systems of H_2S-water and CO_2-water are studied in a wide temperature and pressure range.

2.2   Equation of state

The PCP-SAFT equation of state is based on a coarse-grained molecular model, where molecules are assumed to be chains of spherical segments exhibiting various attractive interactions. The complete perturbed-chain polar statistical associating fluid (PCP-SAFT) equation of state is given as the sum of the ideal gas contribution (id), a hard-sphere contribution (hs), a chain term (chain) connecting the spherical segments, a contribution for the dispersive attraction (disp), a term for associating interactions (assoc), and contributions of polar interactions. The whole equation of state written in terms of Helmholtz energy is

$$F = F^{id} + F^{hs} + F^{hc} + F^{disp} + F^{assoc} + F^{polar} \qquad (2.1)$$

The polar contribution consists of terms for the quadrupole-quadrupole, the dipole-dipole, and the dipole-quadrupole interactions, according to

$$F^{polar} = F^{QQ} + F^{DD} + F^{DQ} \tag{2.2}$$

These equation of state contributions were developed[27, 28, 29] by adjusting model constants of a third-order perturbation theory to comprehensive molecular simulation data of polar two-center Lennard-Jones fluids. The 2CLJ molecular model assumes point-quadrupolar moments and point-dipolar moments and it accounts for the non-spherical shape of molecules.

For non-polar components the last two terms in Eq.(2.1) vanish and a non-polar substance i is then represented by only three pure component parameters: a segment size parameter σ_i, the number of segments m_i, and the segment energy parameter ϵ_i/k. Associating substances require two additional pure component parameters, the association energy $\epsilon^{A_i B_i}/k$ between association site A and site B, and the effective association volume $\kappa^{A_i B_i}$. The most important electrostatic interactions of (neutral) polar compounds are due to dipolar and quadrupolar moments. It was shown, however, that the two appropriate pure component parameters, the dipole moment μ_i and the quadrupole moment Q_i can be taken from independent sources (experiment or quantum chemical calculations). Mixtures are described with regular Berthelot-Lorentz combination rules, where a binary interaction parameter, k_{ij}, is introduced correcting the cross-dispersive energy parameter according to $\epsilon_{ij}/k = (\epsilon_i/k \cdot \epsilon_j/k)^{0.5}(1 - k_{ij})$. For details on the PCP-SAFT equation of state we refer to the original literature.

2.3   Solid-fluid equilibria

Those equilibria involving solid phases can also be calculated using an equation of state for the fluid phases. A prerequisite is, that the involved solid phases have a known composition; in many cases a pure solid phase. The approach then requires caloric data of the pure substances, while the nonideality of the fluid phases is described by the equation of state. The assumption of a pure solid phase (or more generally of a solid phase with defined and known composition) is justified for many practical crystallization processes. The phase equilibrium relation can for such cases be written as[46]:

$$x_i^F = \frac{\phi_{0i}^{L^*}(T,p)}{\phi_i^F(T,p)} \exp \left\{ -\frac{\nu_{0i}^S - \nu_{0i}^{L^*}}{RT}\left(p^+ - p\right) - \frac{\Delta h_{0i}^{SL}}{RT}\left(1 - \frac{T}{T_{0i}^{SL}}\right) \right.$$
$$\left. + \frac{\Delta c_{p,0i}^{SL^*}}{RT}\left(T_{0i}^{SL} - T\right) - \frac{\Delta c_{p,0i}^{SL^*}}{R}\ln\left(\frac{T_{0i}^{SL}}{T}\right) \right\} \tag{2.3}$$

where the subscript '0' indicates pure component quantities, p^+ is the reference pressure (often times $p^+= 1$ bar), at which the pure component melting temperature T_{0i}^{SL} and the melting enthalpy Δh_{0i}^{SL} are given. The superscript $F \in \{L, V\}$ is for a fluid phase; it can be a vapor phase V or a liquid phase L. The index L^* refers to the hypothetical liquid phase. The hypothetical liquid is in a subcooled liquid state and the properties can often fairly reliably be extrapolated from regular data of a liquid phase. Further, $\nu_{0i}^{L^*}$ and ν_{0i}^S denote the specific liquid and solid volume, respectively, and $\Delta c_{p,0i}^{SL^*}$ is the difference of the specific, isobaric heat capacities between the hypothetical, subcooled melt and the solid. ϕ is the fugacity coefficient which is here calculated from the PCP-SAFT equation.

2.4   Results and discussion

2.4.1   Pure component parameters

Hydrogen sulfide is a self-associating component with dipolar and quadruple moments. A scalar quadruple moment was estimated from the quadruple tensor, as suggested by Singh et al.[47] by $\theta_i^2 = \frac{2}{3}(\theta_{i_{xx}}^2 + \theta_{i_{yy}}^2 + \theta_{i_{zz}}^2)$, with values of the quadruple moment tensors taken from Russell and Sparkman[48]. The TPT1 that underlies the association term does not consider angles and the resulting network structure of association bonds. It is in that respect a coarse-grained model for association. We have therefore adopted two, three, and four association sites for hydrogen sulfide and evaluated all mixtures. The result for the mixtures of all three parameterizations is practically identical and we report the mixture-parameter values only of the 2-site model. The association volume $\kappa^{A_i B_i}$ is generally strongly correlated to the association energy parameter $\epsilon^{A_i B_i}/k$ and we have prescribed a fixed value of $\kappa^{A_i B_i}=0.001$. Table 2.1 summarizes the pure component parameters of H_2S simultaneously adjusted to vapor pressure data and to liquid and supercritical density data. A second parameter set of the PC-SAFT equation of state, where the dipole moment and quadrupole moment are assumed to be zero is also displayed. The deviations of the equations of state to

vapor pressure data (about 0.1 %AAD) and to liquid and supercritical density data (about 0.8 %AAD) presented in Table 2.1 are very small for both parameterizations. Figure 2.1 gives a graphical comparison of the PCP-SAFT equation of state to experimental data of the vapor-liquid equilibrium and the equation of state is thereby seen to be in good agreement with experimental data.

Table 2.1: *PCP-SAFT and PC-SAFT Parameters for H_2S*

	PCP-SAFT (2B)	PC-SAFT (2B)	PCP-SAFT (4B)
Segment energy, (ϵ/k) / K	234.25	229.84	235.54
Segment size, σ / Å	3.309	3.055	3.332
Segment number, m	1.355	1.649	1.333
Association energy, (ϵ^{AB}/k) / K	780.8	536.6	566.3
Association volume, κ^{AB}	0.001	0.001	0.001
Dipole moment, μ / D [a]	0.978	-	0.978
Quadruple moment, Q / DÅ	2.938	-	2.938
%AAD p^{sat} $(187.7 - 371.7K)$ [c]	0.12	0.10	0.12
%AAD ρ $(187.7 - 600K)$ [c]	0.78	0.76	0.79
N (vapor pressure p^{sat})[b]	182	182	182
N (liq. & supercrit. density ρ)[b]	93	93	93

[a] reference[49];

[b] quasi-experimental data from reference[50], with N as the number of considered points.

[c] $\%AAD(x) = (100/N) \sum_{i=1}^{N} |x_i^{exp} - x_i^{cal}|$.

2.4.2   Binary mixtures of H_2S - alkanes

Mixtures of H_2S with alkanes are important for natural gas and oil production systems. Due to the prominent role of the mixture H_2S-methane we will first investigate the phase behavior of this binary system from the vapor-liquid coexistence region at higher temperature to the solid-liquid equilibria at low temperature. The vapor-liquid phase behavior of higher alkanes in mixture with H_2S is subsequently discussed.

The mixture H_2S-methane shows a phase behavior of Type III according to the classification of Van Konynenburg and Scott[51, 52]. Figure 2.2 gives a comparison of correlation results of the PCP-SAFT equation of state to some of the experimental data[53, 54] in a $p - T$ diagram. The system exhibits a liquid-liquid
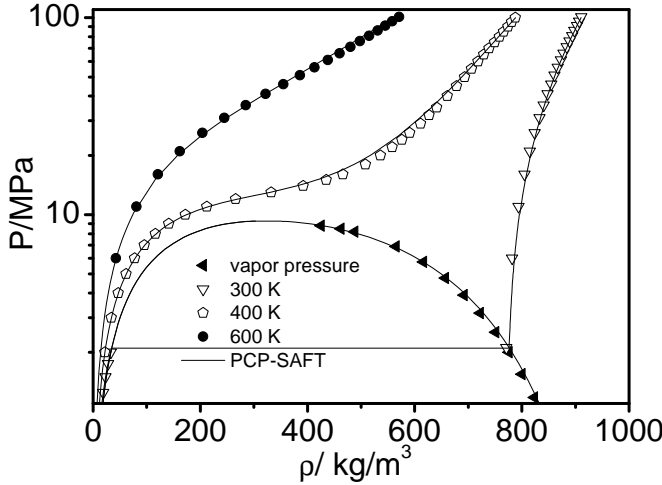
Figure 2.1: *Densities at saturation, subcritical, and supercritical conditions for H_2S: symbols-Experimental data and lines-PCP-SAFT.*

demixing with the two liquid phases labeled as L_1 and L_2. The pure component parametes of methane are taken from a previous study[14]. The k_{ij} parameter was determined by correlating experimental vapor-liquid equilibrium data[54] at $(277K < T < 344K)$ excluding the critical region of the mixtures. Deviations appear therefore in the mixture critical pressures. The upper critical end point (UCEP) of the L_1L_2V line (insert (B) of Figure 2.2) is the connecting point of the VL_2 line and L_1L_2V line. The temperature at the UCEP is over-estimated by 3.96 K with respect to the experimental value (open sphere in insert of Figure 2.2). Results of the PC-SAFT equation of state are shown with a dashed line for comparison; the over-estimation is then somewhat more pronounced, with 7.69 K. The connecting point of the SL_1L_2 line, the SL_2V line and the L_1L_2V line is a 4-phase point (SL_1L_2V). The deviation of PCP-SAFT with respect to the experimental temperature of the 4-phase point is slightly larger than the one observed for PC-SAFT. With these k_{ij} parameters, both models however over-estimate the critical pressure of the vapor-liquid demixing. Figure 2.3 shows experimental data[53] of constant composition (isopleths) for the same system in comparison to the two equations of state. The models are in very good agreement to experimen-

tal data. While PCP-SAFT more conspicuously over-estimates the vapor-liquid
critical points of the mixtures, it leads to a better agreement for isopleths, in
particular of 11.01 mole% and 24.8 mole% H_2S.

Figure 2.2: $p - T$ *diagram of H_2S-methane mixtures. Comparison of PCP-SAFT
($k_{ij} = 0.0152$), PC-SAFT ($k_{ij} = 0.0425$) to experimental data (symbols). Insert: a)
rescaled view of $S L_1 L_2 V$ four phase point; b) rescaled view of UCEP (Upper Critical
End Point).*

Figure 2.4 and Figure 2.5 show $T - x$ diagrams of H_2S-methane mixture at
2.068 MPa and 3.447 MPa, respectively, comparing smoothed experimental data
points[53] and the PCP-SAFT model. PCP-SAFT describes vapor-liquid equi-
librium, liquid-solid equilibrium, liquid-liquid demixing, solid-vapor equilibrium
as well as the three-phase liquid-solid-vapor equilibrium in satisfying agreement
with experimental data points. A constant k_{ij} parameter is applied for the wide
range of conditions covered by the data.

In Figure 2.2 it was observed that PCP-SAFT overestimates the critical pres-
sure of the vapor-liquid equilibria more pronounced as compared to PC-SAFT.
The reason might be that methane has an octapolar moment, which is not ex-
plicitly considered in PCP-SAFT, but which leads to cross-interactions to the
dipolar and quadrupolar H_2S. Figure 2.6 further illustrates this point in giving
a comparison of experimental data[54] for the vapor-liquid region and calculated
results in a $p - x$ diagram. At a temperature of $344.25K$, the difference between

Figure 2.3: *Isopleths in $p-T$ diagram of H_2S-methane mixture. Comparison of PCP-SAFT ($k_{ij} = 0.0152$), PC-SAFT ($k_{ij} = 0.0425$) to experimental data (symbols).*
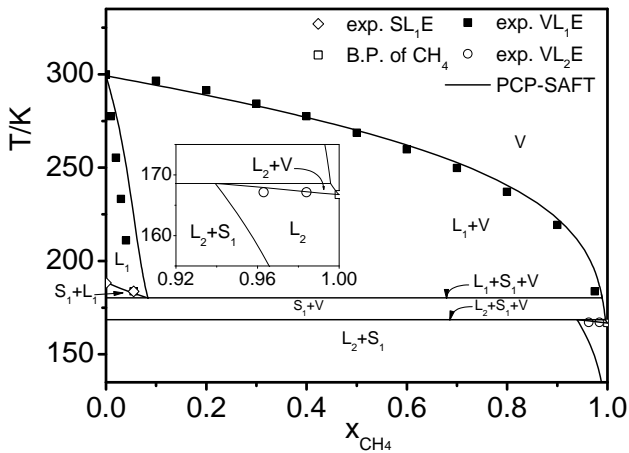
Figure 2.4: *$T-x$ diagram of H_2S-methane mixture at a pressure of 2.068 MPa. Comparison of PCP-SAFT ($k_{ij} = 0.0152$) to smoothed experimental data (symbols). Insert: rescaled view of VL_2E.*

Figure 2.5: $T - x$ *diagram of H_2S-methane mixture at a pressure of 3.447 MPa. Comparison of PCP-SAFT ($k_{ij} = 0.0152$) to smoothed experimental data (symbols). Insert: rescaled view of VL_2E.*
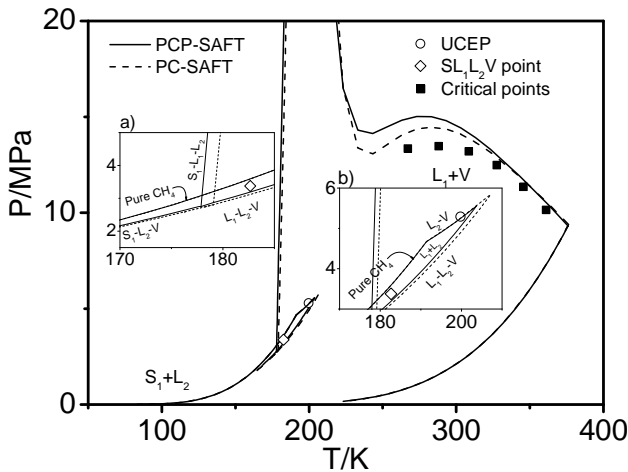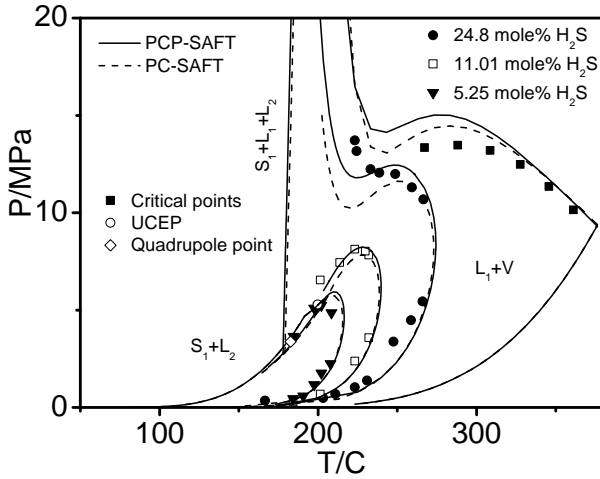

Figure 2.6: *Vapor-liquid equilibrium of H_2S-methane mixtures. Comparison of PCP-SAFT ($k_{ij} = 0.0152$), PC-SAFT ($k_{ij} = 0.0425$) to experimental data (symbols) for various temperatures.*
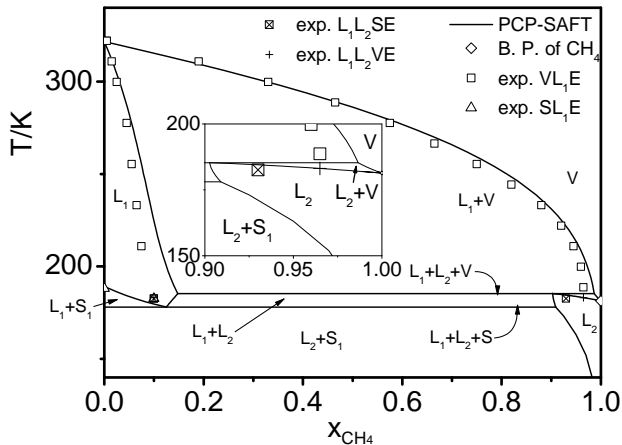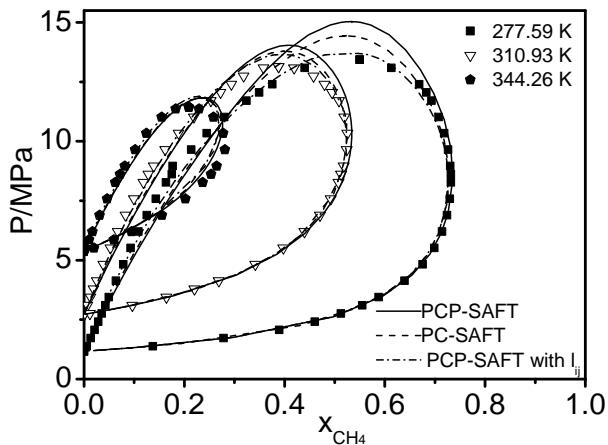
PCP-SAFT and PC-SAFT is rather small. At $T = 277.59K$ and $310.93K$, howe-
ver, PC-SAFT better correlates the phase equilibrium of H_2S-methane, especially
in the vicinity of the critical point, as compared to PCP-SAFT. We have introdu-
ced a second asymmetric binary interaction parameter for the dispersive energy,
l_{ij} with PCP-SAFT. Very good agreement is then found (dashed-dotted line in
Figure 2.6) with parameters $k_{ij} = 0.0120$, $l_{ij} = -l_{ji} = 0.0298$ (when $i = H_2S$ and
$j =$methane); the deviations are $AAD\%(x) = 0.554$ for liquid phase concentration
and $AAD\%(y) = 0.702$ for vapor phase concentration. The second binary inter-
action parameter especially improves the description around the mixtures' critical
points at lower temperatures. Appendix B gives details of the binary interaction
parameter l_{ij}.

Table 2.2: *Correlation Results for Binary Vapor-Liquid Equilibria with PCP-SAFT
and PC-SAFT H_2S – alkanes*

H_2S +	PCP-SAFT			PC-SAFT				
	k_{ij}	%AAD		k_{ij}	%AAD			
		x	y		x	y	N[a]	Ref.
ethane	0.038	1.19	1.70	0.072	2.68	2.19	28	[55]
propane	0.034	0.73	1.39	0.069	1.13	1.49	19	[56]
n-butane	0.034	0.88	1.32	0.067	1.09	1.39	35	[57]
n-pentane	0.038	1.09	1.21	0.073	0.98	1.30	48	[58]
n-hexane	0.037	0.66	0.40	0.073	0.94	0.43	25	[59]
n-heptane	0.043	1.20	0.75	0.078	1.50	0.74	47	[60]
n-nonane	0.040	0.34	0.90	0.086	0.24	0.88	15	[61]
n-decane	0.037	0.80	0.11	0.077	1.22	0.11	43	[62]
n-pentadecane	0.036	0.31	0.05	0.074	0.61	0.04	8	[59]
n-eicosane	0.033	1.16	-	0.077	1.41	-	28	[63]
isobutane	0.025	1.11	1.37	0.060	1.32	1.28	63	[57]
isopentane	0.043	1.54	1.19	0.076	1.61	1.15	29	[64]
neopentane	0.040	1.70	1.28	0.076	1.85	1.33	24	[64]
cyclohexane	0.047	2.00	0.41	0.082	2.26	0.40	24	[59]
methyl cyclohexane	0.041	1.17	1.07	0.078	1.74	1.00	29	[65]
ethyl cyclohexane	0.046	0.76	0.33	0.085	1.43	0.29	27	[66]
propyl cyclohexane	0.032	1.01	0.21	0.071	1.88	0.27	34	[66]
average %AAD		1.08	0.86		1.44	0.94	526	

[a] N is the number of experimental data points.

Table 2.2 compares the results of PCP-SAFT equation of state and the PC-
SAFT model for 17 H_2S-alkane mixtures. Listed are the k_{ij} values and the

deviations of the models to experimental liquid phase (x) and vapor phase (y) mole fractions. The PCP-SAFT model shows a small but systematic improvement compared to PC-SAFT. For most of the cases, PCP-SAFT describes the systems with k_{ij} parameters of about half the (absolute) values observed for PC-SAFT and with lower deviations from experimental data. This suggests that the equation of state is more predictive when the polar moment is accounted for. The values of the binary interaction parameter k_{ij} for H_2S with all investigated alkanes excluding methane reported in Table 2.2 fluctuate around a value of about $k_{ij} = 0.038$. We found good results for the binary mixtures using this average value for H_2S with all investigated alkane species (results not shown).

H_2S-ethane and H_2S-propane systems exhibit azeotropic behavior because ethane and propane have a similar vapor-pressure compared with H_2S[67]. The mixture phase diagram of H_2S-ethane is presented in Figure 2.7, comparing the PCP-SAFT model to experimental data. The improvement of PCP-SAFT over PC-SAFT is due to a better description of the H_2S-rich composition region. Figure 2.8 confirms that both models describe the azeotropic H_2S-propane system well. The observation that PCP-SAFT results in a better representation also of the lower temperature suggests that the enthalpy of mixing is better described by PCP-SAFT than by PC-SAFT. Figure 2.9 and Figure 2.10 present mixtures H_2S-butane and H_2S-heptane respectively, where pure H_2S is for some isotherms above the critical temperature. The PCP-SAFT model is seen in satisfying agreement to the experimental data even in the vicinity of the critical points.

2.4.3   Binary mixtures of H_2S - aromatics

Aromatics are often contained in crude oil. Table 2.3 lists optimal k_{ij} parameters for three representative mixtures along with average deviations obtained for these mixtures. As an example for these mixtures, Figure 2.11 illustrates the correlation result for the mixture H_2S with toluene. The equation of state is seen to be well suited for such mixtures.

2.4.4   Binary mixtures of CO_2 - alkanes

In view of the importance of the binary mixture methane and carbon dioxide, we will first and in some detail be concerned with this system. The results also include solid fluid equilibria of this mixture. Subsequently higher hydrocarbons

Figure 2.7: *Vapor-liquid equilibrium of H_2S-ethane mixture. Comparison of PCP-SAFT ($k_{ij} = 0.0383$), PC-SAFT ($k_{ij} = 0.0722$) to experimental data (symbols) for various temperatures.*
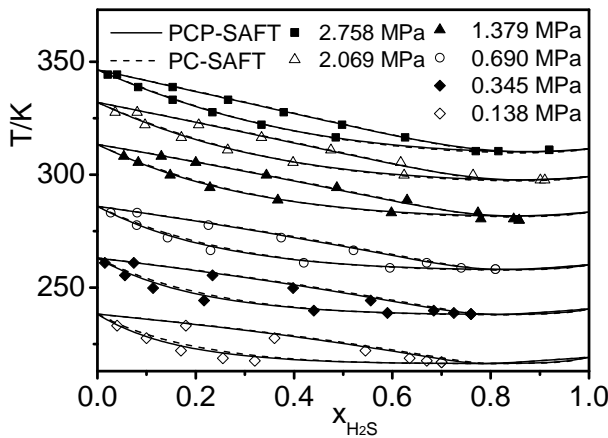
Figure 2.8: *Vapor-liquid equilibrium of H_2S-propane mixtures. Comparison of PCP-SAFT ($k_{ij} = 0.0337$), PC-SAFT ($k_{ij} = 0.0687$) to experimental data (symbols) for various temperatures.*
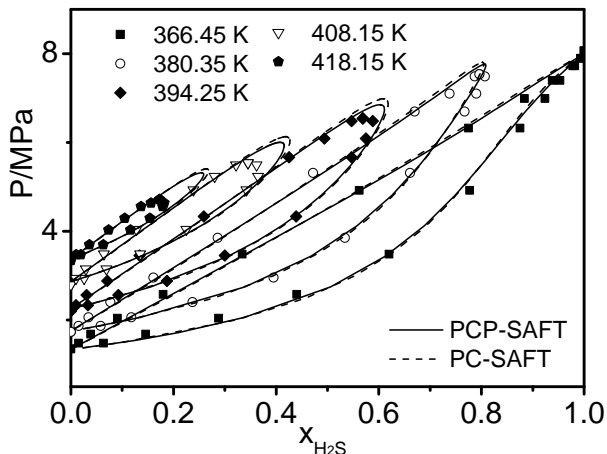
Figure 2.9: *Vapor-liquid equilibrium of H_2S-butane mixtures. Comparison of PCP-SAFT ($k_{ij} = 0.0338$), PC-SAFT ($k_{ij} = 0.0672$) to experimental data (symbols) for various temperatures.*
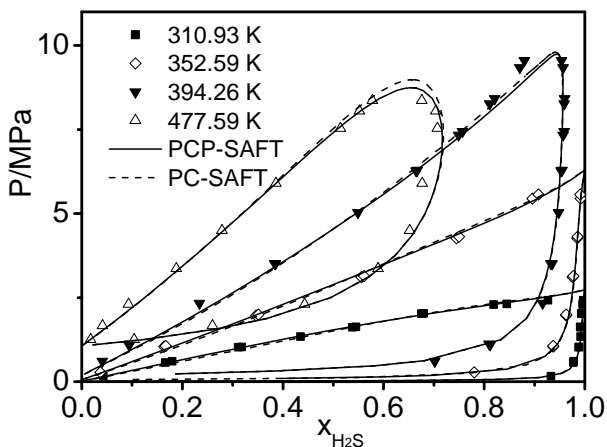
Figure 2.10: *Vapor-liquid equilibrium of H_2S-heptane mixtures. Comparison of PCP-SAFT ($k_{ij} = 0.0428$), PC-SAFT ($k_{ij} = 0.0781$) to experimental data (symbols) for various temperatures.*

Table 2.3: *Correlation Results for Binary Vapor-Liquid Equilibria with PCP-SAFT and PC-SAFT H_2S – aromatics*

H_2S +	PCP-SAFT			PC-SAFT				
	k_{ij}	%AAD		k_{ij}	%AAD		N	Ref
		x	y		x	y		
benzene	-0.012	0.49	0.93	0.025	0.40	0.99	24	[59]
toluene	-0.014	1.15	0.74	0.026	1.61	0.80	27	[60]
n-propylbenzene	0.019	1.29	0.53	0.058	1.40	0.57	25	[68]
average %AAD		0.99	0.73		1.16	0.78	76	

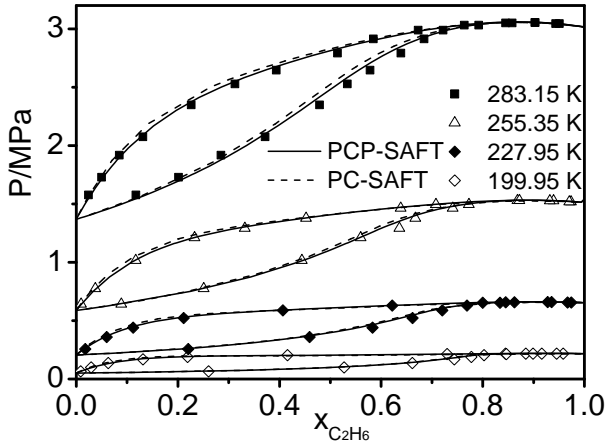**Figure 2.11:** *Vapor-liquid equilibrium of H_2S-toluene mixtures. Comparison of PCP-SAFT ($k_{ij} = -0.0140$), PC-SAFT ($k_{ij} = 0.0256$) to experimental data (symbols) for various temperatures.*

in mixture with carbon dioxide are discussed, focusing on the vapor-liquid phase behavior. The pure component parameters for CO_2 are taken from previous studies[27, 14].

Figure 2.12 compares correlation results of PCP-SAFT to experimental data[69] of the system methane-CO_2. The diagram covers the vapor-liquid region at high temperature and the solid-vapor equilibrium at lower temperature. Both models are in good agreement with the experimental data. PCP-SAFT gives a slightly better description for critical region while PC-SAFT results in a better correlation of the solid-liquid-vapor equilibrium. Donnelly et al.[69] interpolated isopleth-data for the methane-CO_2 mixture from their own experimental data. Figure 2.13 illustrates a very satisfying agreement of isopleth-curves calculated by PCP-SAFT to the interpolated experimental data points. Figure 2.14 presents a $T - x$ diagram of CO_2-methane at 4.641 MPa; the smoothed experimental data[69] are compared to calculated curves. Liquid-vapor, solid-vapor, liquid-solid phase behavior are well described by PCP-SAFT considering the wide temperature range. Figure 2.15 shows the vapor-liquid equilibrium of the CO_2-methane system compared with the investigated models. For clarity in display, not all experimental data that were used for correlation[69, 70, 71] of this system are presented in Figure 2.15. Instead, four representative isotherms are shown. PCP-SAFT leads to a good representation of the vapor phase composition and of the overall phase behavior at higher temperatures. PC-SAFT on the other hand leads to a better description of the lower temperature liquid phase composition. We again speculate that PC-SAFT shows a comparable overall result compared to PCP-SAFT because the octapole moment of methane is not properly accounted for. The cross-interactions to the quadrupolar carbon dioxide are then omitted. This hypothesis is supported by the trend that higher alkanes (with less significant multipole moments) in mixture with CO_2 are significantly better represented by PCP-SAFT compared with the non-polar variant.

Phase equilibria of some CO_2-alkane mixtures, for example, CO_2-butane, CO_2-heptane and CO_2-hexadecane were in an earlier study[27] correlated with the PCP-SAFT equation of state. Table 2.4 extends the previous work on mixtures of carbon dioxide with n-alkanes. Listed are binary interaction parameters k_{ij} and deviation %AAD for both vapor and liquid phases. The marginal difference in k_{ij} values of this work compared with previous work[27] is due to different experimental data which is used for the correlation. Figure 2.16 confirms in one
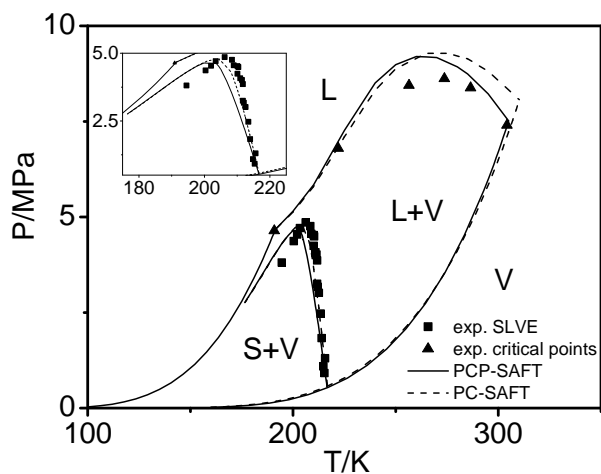
Figure 2.12: $p - T$ diagram of CO_2-methane mixtures. Comparison of PCP-SAFT ($k_{ij} = -0.0325$), PC-SAFT ($k_{ij} = 0.0630$) to experimental data (symbols).
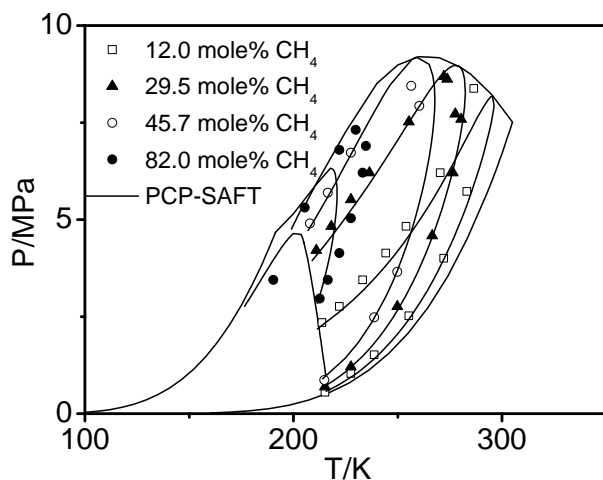
Figure 2.13: $p - T$ diagram of CO_2-methane: isopleths curves. Comparison of PCP-SAFT ($k_{ij} = -0.0325$) to interpolated data (symbols) due to experimental data.
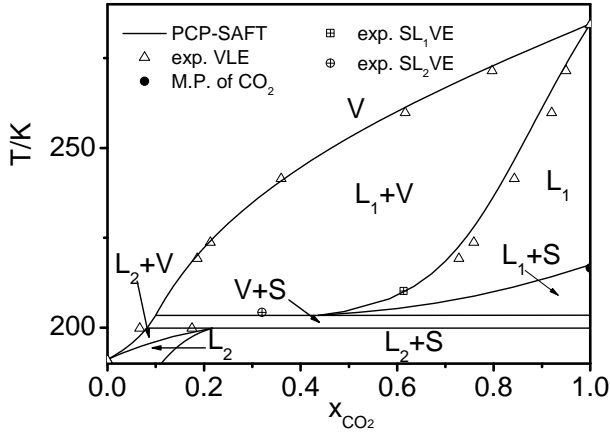
Figure 2.14: *$T - x$ diagram of CO_2-methane mixtures at 4.641 MPa. Comparison of PCP-SAFT ($k_{ij} = -0.0325$) to smoothed experimental data (symbols).*
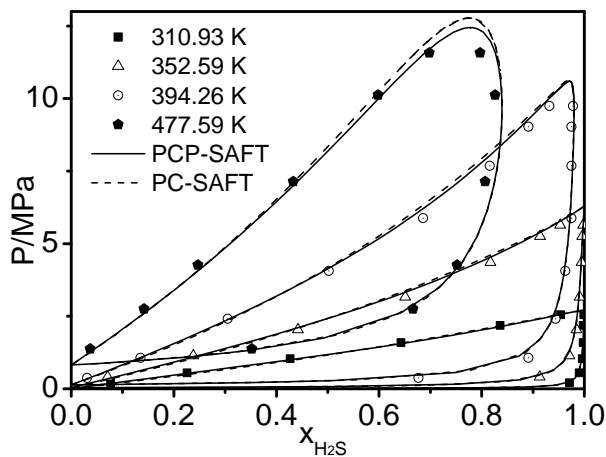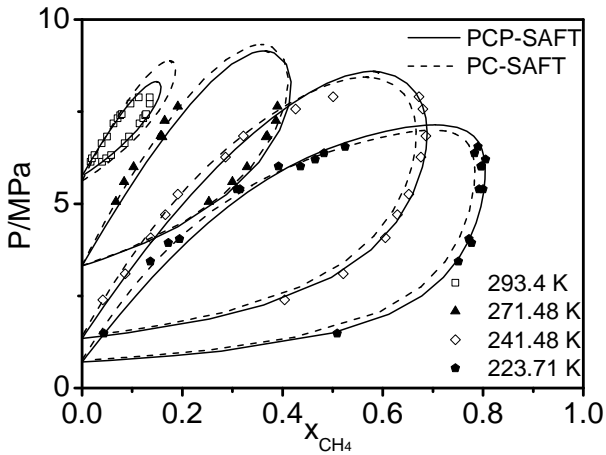

Figure 2.15: *Vapor-liquid equilibrium of CO_2-methane mixtures. Comparison of PCP-SAFT ($k_{ij} = -0.0325$), PC-SAFT ($k_{ij} = 0.0630$) to experimental data (symbols) for various temperatures.*
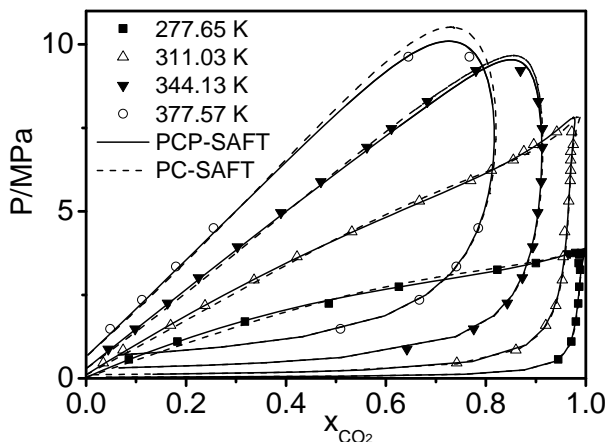
Figure 2.16: *Vapor-liquid equilibrium of CO_2-pentane mixtures. Comparison of PCP-SAFT ($k_{ij} = 0.0413$), PC-SAFT($k_{ij} = 0.120$) to experimental data (symbols) for various temperatures.*

representative example (mixture of CO_2 and n-pentane) that PCP-SAFT adequately describes vapor-liquid equilibria of carbon dioxide with alkanes.

2.4.5   Binary mixtures of CO_2 - aromatics

Mixtures of CO_2-benzene and CO_2-toluene were earlier correlated[27] by PCP-SAFT. Table 2.5 gives more systems of CO_2-aromatics. All aromatic substances are thereby parameterized as non-polar compounds. PCP-SAFT model has significantly lower k_{ij} values and deviations in both phases than the PC-SAFT model. Figure 2.17 shows the polar contribution part in PCP-SAFT plays an important role in accurately describing the phase behavior of the CO_2- ethylbenzene mixture.

2.4.6   Binary mixtures of H_2S - CO_2

Figure 2.18 compares the PCP-SAFT equation of state to experimental data[95] of the system CO_2-H_2S. For PCP-SAFT with $k_{ij} = 0.0614$ (PC-SAFT with $k_{ij} = 0.0679$), the deviation of the liquid and vapor phase mole fraction of carbon dioxide is 0.54 (0.73) and 0.47 (0.68), respectively. Figure 18 gives a graphical

Table 2.4: *Correlation Results for Binary Vapor-Liquid Equilibria with PCP-SAFT and PC-SAFT CO_2 – alkanes*

CO_2 +	PCP-SAFT			PC-SAFT				
	k_{ij}	%AAD		k_{ij}	%AAD		N	Ref
		x	y		x	y		
ethane	0.020	0.44	0.44	0.102	0.73	0.31	51	[72]
propane	0.032	1.06	0.74	0.107	0.93	0.93	79	[54, 72]
n-butane	0.035	0.55	0.49	0.109	1.59	0.55	57	[73, 74, 75]
n-pentane	0.041	0.54	0.25	0.120	1.20	0.36	39	[76]
n-hexane	0.044	1.55	0.75	0.123	2.23	0.78	24	[77]
n-heptane	0.039	0.71	0.62	0.115	1.59	0.70	63	[78]
n-octane	0.055	1.24	0.33	0.132	2.95	0.37	20	[79]
n-nonane	0.044	1.87	0.27	0.122	3.64	0.30	6	[80]
n-decane	0.051	2.03	0.63	0.133	2.91	0.78	40	[68, 78]
n-eicosane	0.060	0.59	-	0.157	0.57	-	45	[81]
isobutane	0.034	0.57	0.58	0.112	0.60	0.82	83	[75, 82, 74]
neopentane	0.044	1.10	0.60	0.123	0.77	0.92	97	[83]
isopentane	0.045	0.55	0.72	0.116	0.69	0.53	25	[74, 71]
cyclopentane	0.036	1.08	0.49	0.114	1.66	0.46	39	[84]
cyclohexane	0.049	1.90	2.57	0.125	1.91	2.63	25	[85]
methyl cyclohexane	0.040	1.19	0.93	0.118	2.15	0.89	23	[86]
propyl cyclohexane	0.074	2.53	0.931	0.154	3.52	1.09	16	[68]
average %AAD		0.97	0.66		1.35	0.77	732	

Table 2.5: *Correlation Results for Binary Vapor-Liquid Equilibria with PCP-SAFT and PC-SAFT CO_2 – aromatics*

CO_2 +	PCP-SAFT			PC-SAFT				
	k_{ij}	%AAD		k_{ij}	%AAD		N	Ref
		x	y		x	y		
benzene	0.007	1.03	0.23	0.087	1.72	0.29	33	[87]
toluene	0.028	1.14	0.71	0.108	2.73	0.75	50	[88]
ethyl-benzene	0.030	1.78	0.15	0.111	3.90	0.18	37	[89]
n-propyl-benzene	0.030	1.91	0.59	0.110	2.94	0.73	26	[80, 90]
1,3,5-trimethyl-benzene[*]	0.022	1.84	0.38	0.102	3.92	0.40	6	[80]
m-xylene	0.021	1.67	0.45	0.102	2.85	0.53	64	[89, 91]
o-xylene	0.022	2.16	0.25	0.103	3.86	0.26	22	[89]
p-xylene	0.022	1.61	0.25	0.103	3.14	0.27	20	[89, 92]
average %AAD		1.57	0.41		2.98	0.47	258	

[*] PC-SAFT parameters: $\epsilon/k = 278.48K$; $\sigma = 3.734$; $m = 3.650$, based on vapour pressure data[93] and liquid density data [94].
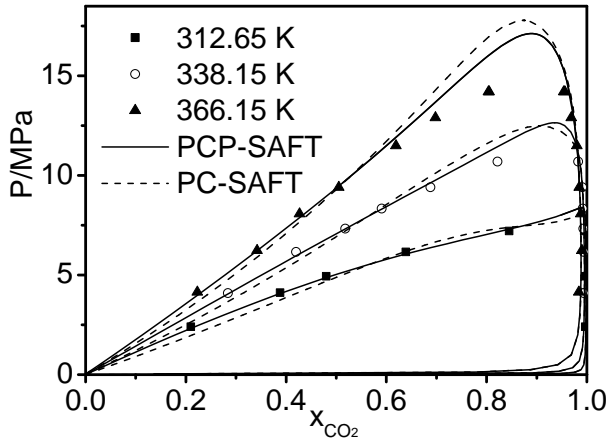
Figure 2.17: *Vapor-liquid equilibrium of CO_2- ethylbenzene mixtures. Comparison of PCP-SAFT ($k_{ij} = 0.0297$), PC-SAFT ($k_{ij} = 0.111$) to experimental data (symbols) for various temperatures.*

illustration of the correlation result and shows that this mixture is very well correlated with the PCP-SAFT equation of state.

2.4.7   Ternary mixtures of H_2S - CO_2 - Methane.

With the above determined binary k_{ij} parameters between CO_2-methane, H_2S-methane, and H_2S-CO_2, the PCP-SAFT model is applied to predict ternary diagrams of H_2S-CO_2-methane system and the calculated results are compared with experimental data[96, 97]. Two examples, both at a pressure of $2.069 MPa$ and temperatures of $T = 238.75K$ and $222.15K$ respectively, are given in Figure 2.19. PCP-SAFT results are in good agreement to experimental data. Figure 2.20 shows the ternary system at three conditions, with two pairings of same pressure and of same temperature. The calculations are in satisfying agreement with the experimental data for a considerable range of pressure and temperature.

2.4.8   Binary mixtures of H_2S - H_2O

Water is often either a constituent of natural gas and oil mixtures or is added for gas and oil treating processes. Water is a strongly associating and polar com-
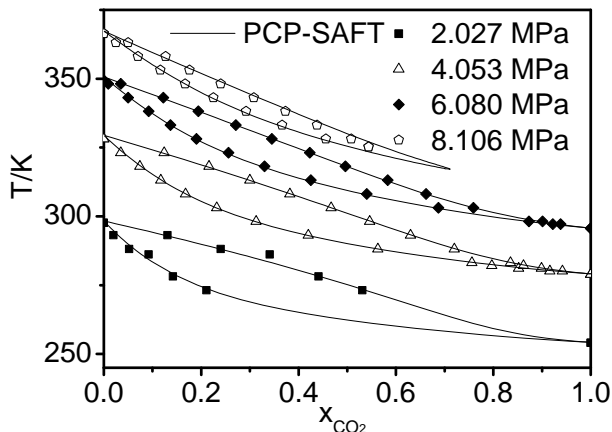
Figure 2.18: *Vapor-liquid equilibrium of CO_2-H_2S mixtures at 4 pressures. Comparison of PCP-SAFT ($k_{ij} = 0.0613$) to experimental data (symbols) for various temperatures.*
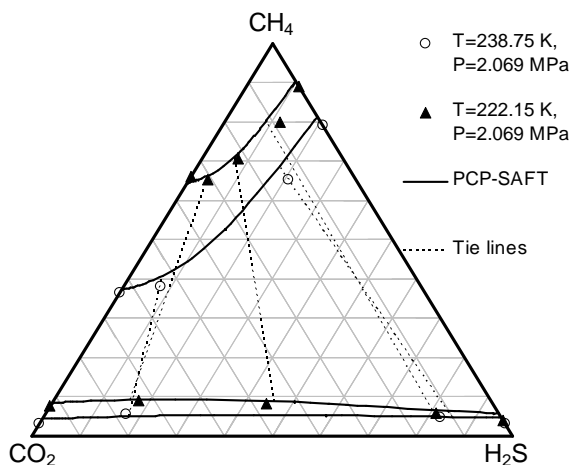
Figure 2.19: *Ternary phase diagram for CO_2-H_2S-CH_4 at 238.15 K and 222.15 K, 2.069 MPa. Comparison of PCP-SAFT to experimental data (symbols).*
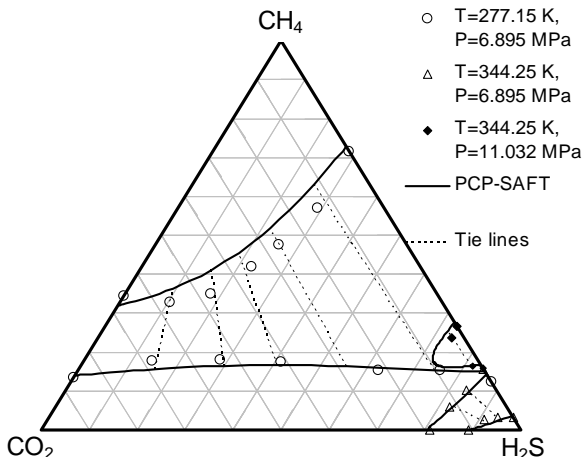
Figure 2.20: *Ternary phase diagram for CO_2-H_2S-CH_4 at 277.15 K, 6.895 MPa; 344.25 K, 6.895 MPa; 344.25 K, 11.032 MPa. Comparison of PCP-SAFT to experimental data (symbols).*

pound. We here omit the multipole moments of water and model it as an only associating substance[98], because the interdependence of associating interactions and dipolar interactions is currently not adequately accounted for. This dependence should ideally be reflected by the dependence of the perturbation theories, where a polar reference fluid with angle-dependent correlation functions should be the reference to the association theory. For water with a high volume-specific dipole moment, this would be particularly important, because the associating interactions are significantly different for a dipolar fluid versus an non-polar isotropic fluid (and vice versa). Since we have not developed a sufficiently interdependent perturbation scheme, water is here treated as associating, but non-polar. In a previous study Kleiner et al.[99] also found weaker results for the phase equilibria of water in mixtures, when the polar moment for water is accounted for. We note, that for H_2S the same argument is in principle true, but the dipole moment (and the associating interactions) there are much smaller compared with water. We will still refer to the applied equation of state as PCP-SAFT, because polar compounds other than water are treated with their polar moments. Two association sites are here assigned to water[98], because (similar to hydrogen sulfide) the results for H_2O and H_2O-binary mixtures are practically identical when 3 or 4

association sites are considered for water. Figure 2.21 and Figure 2.22 compares the PCP-SAFT results ($k_{ij} = 0.0223$) to experimental data[100] of the system hydrogen sulfide – water.
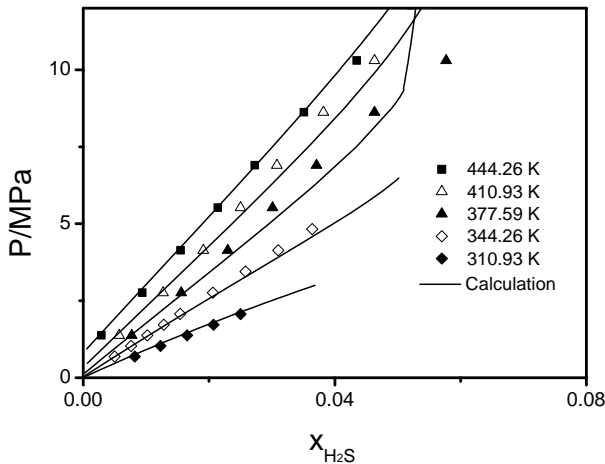
Figure 2.21: *P-x digram for $H_2S + H_2O$ in liquid phase. Comparison of PCP-SAFT ($k_{ij} = 0.0223$) to experimental data (symbols) for various temperatures.*

2.4.9   Binary mixtures of CO_2 - H_2O

Mixtures of water with non-associating (and non-polar or only moderately polar) substances like methane or carbon dioxide are demanding, because water forms hydrate-like structures in a liquid phase around these solutes. The occurrence of these cage structures formed by hydrogen-bonds of water is strongly temperature-dependent. These cages form at low temperatures and disappear at higher temperatures. The hydrogen-bond networks, that are responsible for this effect are not adequately represented in a classical equation of state and we have to expect temperature-dependent binary interaction parameters for such systems. Figure 2.23 and Figure 2.24 compares the correlation results of PCP-SAFT to experimental data of the system CO_2-H_2O. The experimental data considered for adjusting k_{ij} are taken from Ref. [41, 101, 102, 103, 104, 105, 106, 107, 108, 109, 110, 111, 112] with a maximum temperature of $473K$ and a maximum pressure of $70MPa$. For clarity, not all experimental data used to fit binary interaction parameters are
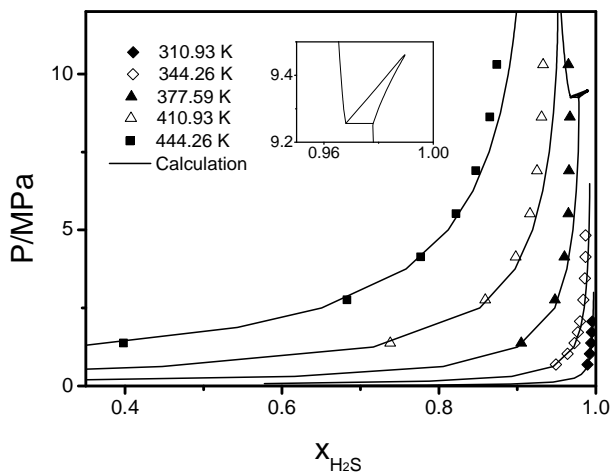
Figure 2.22: *P-x digram for $H_2S + H_2O$ in vapor phase. Comparison of PCP-SAFT ($k_{ij} = 0.0223$) to experimental data (symbols) for various temperatures. Inserted: rescaled view of L_2VE*
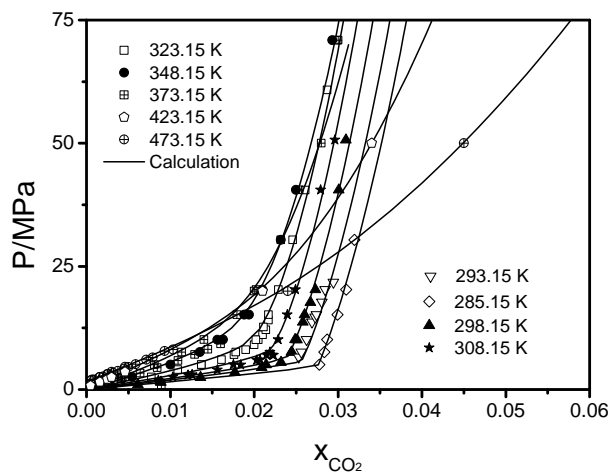
Figure 2.23: *P-x digram for $CO_2 + H_2O$ in liquid phase. Comparison of PCP-SAFT (T-dependent k_{ij}) to experimental data (symbols) for various temperatures.*
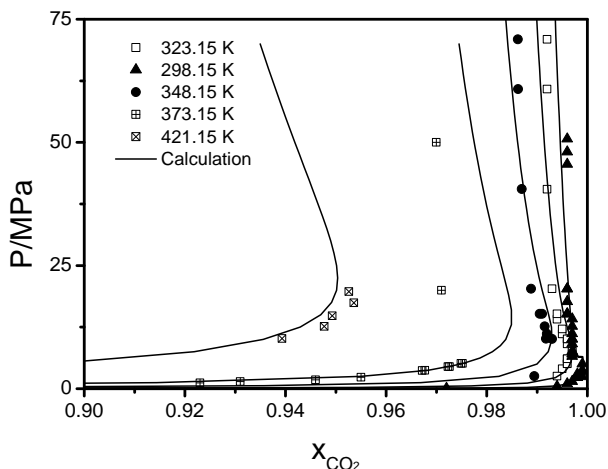
Figure 2.24: *P-x digram for CO_2 + H_2O in vapor phase. Comparison of PCP-SAFT (T-dependent k_{ij}) to experimental data (symbols) for various temperatures.*

shown in Figure 2.23 and Figure 2.24. The correlation results were obtained with second-order polynomial in temperature for the binary interaction parameter, as $k_{ij} = -0.533 + 2.22(T/1000K) - 2.48(T/1000K)^2$ for $T \leq 473K$. The increase of the binary interaction parameter with temperature up to a plateau-value can be explained by the strongly temperature dependent cavity formation[113]. The compositional dependence of the bubble-point pressure is according to Figure 2.23 very well represented by the equation of state.

2.5   Conclusion

The perturbed-chain polar SAFT (PCP-SAFT) equation was applied to mixtures of hydrogen sulfide with hydrocarbons and with water as well as to mixtures of CO_2 with hydrocarbons and with water. The binary mixtures of hydrogen sulfide with methane and carbon dioxide with methane covered a broad range of temperatures and including vapor-liquid, liquid-liquid, solid-liquid, solid-vapor phase equilibria and the appropriate three-phase equilibria. The PCP-SAFT equation of state was found to be in good agreement to the experimental data and well suited to describe all of the mixtures with a temperature-independent binary interaction

parameter. The inclusion of dipole and quadruple term in PCP-SAFT equation of state leads to small improvements for mixtures with hydrogen sulfide and more pronounced systematic improvements for mixtures containing carbon dioxide as compared to the non-polar version (PC-SAFT). The description for mixtures with methane is not improved, perhaps because the octapole moment of methane is not accounted for. The required values of the binary interaction parameter are (especially for CO_2-containing mixtures) considerably lower if the polar moments are accounted for. The ternary mixture H_2S, CO_2 and methane could be modelled with the binary interaction parameters of the binary pairs. H_2S-water and CO_2-water are studied in a large pressure and temperture range. The mixture CO_2-water requires a temperature-dependent binary interaction parameter (like for other mixtures of water with non-associating substances). This observation suggests that the formation of hyrogen-bonding networks of water to form solute-cavities is an important and so-far largely neglected effect in SAFT-type equations of state.

REFERENCES

[1] W. G. Chapman, G. Jackson, and K. E. Gubbins. Phase equilibria of associating fluids. chain molecules with multiple bonding sites. *Mol. Phys.*, 65:1057–1079, 1988.

[2] W. G. Chapman, K. E. Gubbins, G. Jackson, and M. Radosz. SAFT - equation-of-state solution model for associating fluids. *Fluid Phase Equilib.*, 52:31–38, 1989.

[3] M. S. Wertheim. Fluids with highly directional attractive forces. I. statistical thermodynamics. *J. Stat. Phys.*, 35:19–34, 1984.

[4] M. S. Wertheim. Fluids with highly directional attractive forces. II. thermodynamic perturbation theory and integral equations. *J. Stat. Phys.*, 35:35–47, 1984.

[5] M. S. Wertheim. Fluids with highly directional attractive forces. III. multiple attraction sites. *J. Stat. Phys.*, 42:459–476, 1986.

[6] M. S. Wertheim. Fluids with highly directional attractive forces. IV. equilibrium polymerization. *J. Stat. Phys.*, 42:477–492, 1986.

[7] S. H. Huang and M. Radosz. Equation of state for small, large, polydisperse and associating molecules. *Ind. Eng. Chem. Res.*, 29:2284–2294, 1990.

[8] S. H. Huang and M. Radosz. Equation of state for small, large, polydisperse, and associating molecules: Extensions to fluid mixtures. *Ind. Eng. Chem. Res.*, 30:1994–2005, 1991.

[9] A. Gil-Villegas, A. Galindo, P. J. Whitehead, S. J. Mills, G. Jackson, and A. N. Burgess. Statistical associating fluid theory for chain molecules with attractive potentials of variable range. *J. Chem. Phys.*, 106:4168–4186, 1997.

[10] A. Galindo, L. A. Davies, A. Gil-Villegas, and G. Jackson. The thermodynamics of mixtures and the corresponding mixing rules in the SAFT-VR approach for potentials of variable range. *Mol. Phys.*, 93(2):241–252, 1998.

[11] F. J. Blas and L. F. Vega. Prediction of binary and ternary diagrams using the statistical associating fluid theory (SAFT) equation of state. *Ind. Eng. Chem. Res.*, 37:660–674, 1998.

[12] J. C. Pámies and L. F. Vega. Vapor-liquid equilibria and critical behavior of heavy n-alkanes using transferable parameters from the soft-SAFT equation of state. *Ind. Eng. Chem. Res.*, 40:2532–2543, 2001.

[13] J. Gross and G. Sadowski. Application of perturbation theory to a hard-chain reference fluid: An equation of state for squarewell chains. *Fluid Phase Equilib.*, 168:183–199, 2000.

[14] J. Gross and G. Sadowski. Perturbed-chain SAFT: an equation of state based on a perturbation theory for chain molecules. *Ind. Eng. Chem. Res.*, 40:1244–1260, 2001.

[15] S. P. Tan, H. Adidharma, and M. Radosz. Recent advances and applications of statistical associating fluid theory. *Ind. Eng. Chem. Res.*, 47(21):8063–8082, 2008.

[16] H. G. Zhao and C. McCabe. Phase behavior of dipolar fluids from a modified statistical associating fluid theory for potentials of variable range. *J. Chem. Phys.*, 125:104504, 2006.

[17] G. Stell, J. C. Rasaiah, and H. Narang. Thermodynamic perturbation-theory for simple polar fluids. 1. *Mol. Phys.*, 23(2):393–406, 1972.

[18] K. E. Gubbins and C. H. Twu. Thermodynamics of polyatomic fluid mixtures. 1. theory. *Chem. Eng. Sci.*, 33(7):863–878, 1978.

[19] T. Kraska and K. E. Gubbins. Phase equilibria calculations with a modified SAFT equation of state. 1. pure alkanes, alkanols, and water. *Ind. Eng. Chem. Res.*, 35:4727–4737, 1996.

[20] PK Jog and W. G. Chapman. Application of wertheim's thermodynamic perturbation theory to dipolar hard sphere chains. *Mol. Phys.*, 97:307–319, 1999.

[21] P. K. Jog, S. G. Sauer, J. Blaesing, and W. G. Chapman. Application of dipolar chain theory to the phase behavior of polar fluids and mixtures. *Ind. Eng. Chem. Res.*, 40(21):4641–4648, 2001.

[22] J. Gross and G. Sadowski. Perturbed-chain saft: Development of a new equation of state for simple, associating, multipolar and polymeric compounds. *In: Brunner G, ed. Supercritical fluids as solvents and reaction media. Amsterdam, the Netherlands: Elsevier Science*, page 295, 2004.

[23] F. Tumakaka and G. Sadowski. Application of the perturbed-chain SAFT equation of state to polar systems. *Fluid Phase Equilib.*, 217:233–239, 2004.

[24] W. B. Liu, Y. G. Li, and J. F. Lu. A new equation of state for real aqueous ionic fluids based on electrolyte perturbation theory, mean spherical approximation and statistical associating fluid theory. *Fluid Phase Equilib.*, 160:595–606, 1999.

[25] E. K. Karakatsani and I. G. Economou. Perturbed chain-statistical associating fluid theory extended to dipolar and quadrupolar molecular fluids. *J. Phys. Chem. B.*, 110:9252–9261, 2006.

[26] H. G. Zhao, P. Morgado, A. Gil-Villegas, and C. McCabe. Predicting the phase behavior of nitrogen plus n-alkanes for enhanced oil recovery from the SAFT-VR approach: Examining the effect of the quadrupole moment. *J. of Phys. Chem. B*, 110(47):24083–24092, 2006.

[27] J. Gross. An equation-of -state contribution for polar components: quadrupolar molecules. *AIChE*, 51(9):2556–2568, 2005.

[28] J. Gross and J. Vrabec. An equation-of-state contribution for polar componenets: dipolar molecules. *AIChE*, 52(3):1194–1204, 2006.

[29] J. Vrabec and J. Gross. Vapor-liquid equilibria simulation and an equation of state contribution for dipole-quadrupole interactions. *J. Phys. Chem. B*, 112:51–60, 2008.

[30] M. Kleiner and J. Gross. An equation of state contribution for polar components: polarizable dipoles. *AIChE*, 52(5):1951–1961, 2006.

[31] M. S. Wertheim. Theory of polar fluids. 3. *Mol. Phys.*, 34(4):1109–1129, 1977.

[32] M. S. Wertheim. Theory of polar fluids. 5. thermodynamics and thermodynamic perturbation-theory. *Mol. Phys.*, 37(1):83–94, 1979.

[33] L. J. Florusse, C. J. Peters, J. C. Pá mies, L. F. Vega, and H. Meijer. Solubility of hydrogen in heavy n-alkanes: experiments and SAFT modeling. *AIChE J.*, 49(12):3260–3269, 2003.

[34] J. García, L. Lugo, and J. Fernández. Phase equilibria, PVT behavior and critical phenomena in carbon dioxide +n-alkane mixtures using the perturbed-chain statistical associating fluid theory approach. *Ind. Eng. Chem. Res.*, 43:8345–8353, 2004.

[35] F. Llovell and L. F. Vega. Global fluid phase equilibria and critical phenomena of selected mixtures using the crossover Soft-SAFT equation. *J. Phys. Chem. B*, 110(3):1350–1362, 2006.

[36] C. L. Thi, S. Tamouza, J-P. Passarello, P. Tobaly, and J-C. De Hemptinne. Modeling phase equilibrium of H_2 + n-alkane and CO_2 + n-alkane binary mixtures using a group contribution statistical association fluid theory equation of state (GC-SAFT-EOS) with a k_{ij} group contribution method. *Ind. Eng. Chem. Res.*, 45:6803–6810, 2006.

[37] S. Aparicio-Martinez and K. R. Hall. Use of PC-SAFT for global phase diagrams in binary mixtures relevant to natural gases. 3. alkane + non-hydrocarbons. *Ind. Eng. Chem. Res.*, 46:291–296, 2007.

[38] M. C. Dos Ramos, K. D. Goff, H. Zhang, and C. McCabe. Modeling the phase behavior of H_2S+n-alkane binary mixtures using the SAFT-VR+D approach. *J. Phys. Chem. B*, 112:9417–9427, 2008.

[39] D. Nguyen-Huynh, J.-P. Passarello, P. Tobaly, and J.-C. De Hemptinne. Modeling phase equilibria of asymmetric mixtures using a group-contribution SAFT (GC-SAFT) with a k_{ij} correlation method based on london's theory. 1. application to CO_2 + n-alkane, methane + n-alkane, and ethane + n-alkane systems. *Ind. Eng. Chem. Res.*, 47:8847–8858, 2008.

[40] D. Nguyen-Huynh, T. K. S. Tran, S. Tamouza, J.-P. Passarello, P. Tobaly, and J.-C. De Hemptinne. Modeling phase equilibrium of asymmetric mixtures using a group-contribution SAFT (GC-SAFT) with a k_{ij} correlation method based on london's theory. 2. application to binary mixtures containing aromatic hydrocarbons, n-alkanes, CO_2, N_2, and H_2S. *Ind. Eng. Chem. Res.*, 47:8859–8868, 2008.

[41] A. Valtz, A. Chapoy, C. Coquelet, P. Paricaud, and D. Richon. Vapour-liquid equilibria in the carbon dioxide-water system, measurement and modelling from 278.2 to 318.2 K. *Fluid Phase Equilib.*, 226:333–344, 2004.

[42] M. C. dos Ramos, F. J. Blas, and A. Galindo. Phase equilibria, excess properties, and Henry's constants of the water plus carbon dioxide binary mixture. *J. Phys. Chem. C*, 111(43):15924–15934, 2007.

[43] M. C. dos Ramos, F. J. Blas, and A. Galindo. Modelling the phase equilibria and excess properties of the water plus carbon dioxide binary mixture. *Fluid Phase Equilib.*, 261(1-2):359–365, 2007.

[44] X. Y. Ji, S. P. Tan, H. Adidharma, and M. Radosz. SAFT1-RPM approximation extended to phase equilibria and densities of $CO_2 - H_2O$ and $CO_2 - H_2O - NaCl$ systems. *Ind. Eng. Chem. Res.*, 44(22):8419–8427, 2005.

[45] S. P. Tan, H. Adidharma, and M. Radosz. Statistical associating fluid theory coupled with restricted primitive model to represent aqueous strong electrolytes. *Ind. Eng. Chem. Res.*, 44(12):4442–4452, 2005.

[46] M. Seiler, J. Gross, B. Bungert, G. Sadowski, and W. Arlt. Modeling of solid/fluid phase equilibria in multicomponent systems at high pressure. *Chem. Eng. Technol.*, 24:607–612, 2001.

[47] M. Singh, K. Leonard, and K. Lucas. Making equation of state models predictive part 1: quantum chamical computation of molecular properties. *Fluid Phase Equilib.*, 258:16–28, 2007.

[48] A. J. Russell and M. A. Spackman. An ab initio study of vibrational corrections to the electrical properties of the second-row hydrides. *Mol. Phys.*, 90:251–264, 1997.

[49] D. R. Lide, editor. *CRC Handbook of Chemistry and Physics, Table "Dipole Moments"*. CRC Press/Taylor and Francis, Boca Raton, FL, 89 edition, 2009.

[50] P. J. Linstrom and W. G. Mallard, editors. *NIST Chemistry WebBook, NIST Standard Reference Database Number 69*. http://webbook.nist.gov, National Institute of Standards and Technology, Gaithersburg MD, 20899, 2009.

[51] R. L. Scott and P. H. van Konynenburg. Static properties of solutions: Van der waals and related models for hydrocarbon mixtures. *Discuss. Faraday Soc.*, 49:87–97, 1970.

[52] P. H. van Konynenburg and R. L. Scott. Critical lines and phase equilibriums in binary van der waals mixtures. series a: mathematical, physical and engineering sciences. *Philos. Trans. R. Soc. London*, 298(1442):495–540, 1980.

[53] J. P. Kohn and F. Kurata. Heterogeneous phase equilibria of the methane-hydrogen sulfide system. *AIChE*, 4:211–217, 1958.

[54] H. H. Reamer, B. H. Sage, and W. N. Lacey. Phase equilibria in hydrocarbon systems. volumetric and phase behavior of the methane hydrogen sulfide system. *Ind. Eng. Chem.*, 43:976–980, 1951.

[55] H. Kalra, D. B. Robinson, and T. R. Krishnan. The equilibrium phase properties of the ethane-hydrogen sulfide system at subambient temperatures. *J. Chem. Eng. Data*, 22(1):85–88, 1977.

[56] J. Brewer, N. Rodewald, and F. Kurata. Phase equilibria of the propane-hydrogen sulfide system from the cricondeotherm to the solid-liquid-vapor region. *AIChE*, 7(1):13–16, 1961.

[57] A.-D. Leu and B. D. Robinson. Equilibrium phase properties of the n-butane-hydroen sulfide and isobutane-hydrogen sulfide binary systems. *J. Chem. Eng. Data*, 34:315–319, 1989.

[58] H. H. Reamer, B. H. Sage, and W. N. Lacey. Phase equilibria in hydrocarbon systems-volumetric and phase behavior of n-pentane - hydrogen sulfide system. *Ind. Eng. Chem.*, 45:1805–1809, 1953.

[59] S. Laugier and D. Richon. Vapor-liquid equilibria for hydrogen sulfide + hexane, + cyclohexane, + benzene, + pentadecane, and + (hexane + pentadecane). *J. Chem. Eng. Data*, 40:153–159, 1995.

[60] H. J. Ng, H. Kaira, D. B. Robinson, and H. Kubota. Equilibrium phase properties of the toluene-hydrogen sulfide and n-heptane-hdrogen sulfide binary systems. *J. Chem. Eng. Data*, 25(1):51–55, 1980.

[61] B. E. Eakin and W. E. DeVaney. Vapor-liquid equilibria in hydrogen-hydrogen sulfide-C9 hydrocarbon systems. *AIChE. Symp. Ser.*, 70(140):80–90, 1974.

[62] H. H. Reamer, F. T. Selleck, B. H. Sage, and W. N. Lacey. Volumetric and phase behavior of decane-hydrogen sulfide system. *Ind. Eng. Chem.*, 45:1810–1812, 1953.

[63] G.-X. Feng and A. E. Mather. Solubility of hydrogen sulfide in n-eicosane at elevated pressure. *J. Chem. Eng. Data*, 37:412–413, 1992.

[64] A. D. Leu and D. B. Robinson. High-pressure vapor-liquid equilibrium phase properties of the isopentane-hydrogen sulfide and neopentane-hydrogen sulfide binary systems. *J. Chem. Eng. Data*, 37:14–17, 1992.

[65] F. C. Tobler. Correlation of the density of the liquid phase of pure n-alkanes with temperature and vapor pressure. *Ind. Eng. Chem. Res.*, 37:2565–2570, 1998.

[66] S. S. Huang and D. B. Robinson. Equilibrium phase properties of the ethylcyclohexane-hydrogen sulfide and n-propylcyclohexane-hydrogen sulfide binary systems. *J. Chem. Eng. Data*, 30:154–157, 1985.

[67] J. S. Rowlinson and F. L. Swinton, editors. *Liquids and liquid mixtures*. 3rd ed., 1982.

[68] D. Richon, S. Laugler, and H. Renon. High-pressure vapor-liquid equilibrium data for binary mixtures containing N_2, CO_2, H_2S, and an aromatic hydrocarbon or propylcyclohexane in the range 313-473 K. *J. Chem. Eng. Data*, 37(14):264–268, 1992.

[69] H. G. Donnelly and D. L. Katz. Phase equilibria in the carbon dioxide methane system. *Ind. Eng. Chem.*, 46:511–517, 1954.

[70] N. Xu, J. Dong, Y. Wang, and J. Shi. High pressure vapor liquid equilibria at 293 K for systems containing nitrogen, methane and carbon dioxide. *Fluid Phase Equilib.*, 81:175–186, 1992.

[71] B. Bian, Y. Wang, J. Shi, E. Zhao, and B. C. Y. Lu. Simultaneous determination of vapor-liquid equilibrium and molar volumes for coexisting phases up to the critical temperature with a static method. *Fluid Phase Equilib.*, 90:177–187, 1993.

[72] K. Nagahama, H. Konishi, D. Hoshino, and M. Hirata. Binary vapor-liquid equilibria of carbon dioxide-light hydrocarbons at low temperature. *J. Chem. Eng. Japan*, 7(5):323–328, 1974.

[73] H. Kalra, T. R. Krishnan, and D. B. Robinson. Equilibrium phase properties of carbon dioxide - n-butane and nitrogen - hydrogen sulfide systems at sub-ambient temperatures. *J. Chem. Eng. Data*, 21:222–225, 1976.

[74] A.D. Leu and D. B. Robinson. Equilibrium phase properties of the n-butane-carbon dioxide and isobutane-carbon dioxide binary systems. *J. Chem. Eng. Data*, 32:444–447, 1987.

[75] D. B. Robinson and H. Kalra. The phase behavior of selected hydrocarbon - non-hydrocarbon systems: C_2 - H_2S and N_2 - iC_4 systems. *Gas Processors Association, Proceedings of 53rd annual Convention*, 1977.

[76] J. A. Barker and D. Henderson. Perturbation theory and equation of state for fluids. II. A successful theory of liquids. *J. Chem. Phys.*, 47:4714–4721, 1967.

[77] Z. Wagner and I. Wichterle. High-pressure vapour-liquid equilibrium in systems containing carbon dioxide, 1-hexene, and n-hexane. *Fluid Phase Equilib.*, 33:109–123, 1987.

[78] H. Inomata, K. Tuchiya, K. Arai, and S. Saito. Measurement of vapor-liquid equilibria at elevated temperautres and pressures using a flow type apparatus. *J. Chem. Eng. Japan*, 19:386–391, 1986.

[79] W. L. Weng and M. J. Lee. Vapor-liquid equilibrium of the octane/carbon dioxide, octane/ethane, and octane/ethylene systems. *J. Chem. Eng. Data*, 37:213–215, 1992.

[80] D. W. Jennings and R. C. Schucker. Comparison of high-pressure vapor-liquid equilibria of mixtures of CO_2 or propane with nonane and C9 alkyl-benzenes. *J. Chem. Eng. Data*, 41:831–838, 1996.

[81] N. C. Huie, K. D. Luks, and J. P. Kohn. Phase-equilibria behavior of systems carbon dioxide-n-eicosane and carbon dioxide-n-decane-n-eicosane. *J. Chem. Eng. Data*, 18:311–313, 1973.

[82] L. A. Weber. Simple apparatus for vapor-liquid equilibrium measurements with data for the binary systems of carbon dioxide with n-butane and iso-butane. *J. Chem. Eng. Data*, 34:171–175, 1989.

[83] N. N. Shah, M. E. Pozo de Fernandez, J. A. Zollweg, and W. B. Streett. Vapor-liquid equilibrium in the system carbon dioxide + 2,2-dimethylpropane from 262 to 424 K at pressures to 8.4 MPa. *J. Chem. Eng. Data*, 35:278–283, 1990.

[84] C. J. Eckert and S. I. Sandler. Vapor-liquid equilibria for the carbon dioxide-cyclopentane system at 37.7, 45.0, and 60.0C. *J. Chem. Eng. Data*, 31:26–28, 1986.

[85] N. Nagarajan and R. L. Robinson. Equilibrium phase compositions, phase densities, and interfacial tensions for CO_2 + hydrocarbon systems. 3. CO_2 + cyclohexane. 4. CO_2 + benzene. *J. Chem. Eng. Data*, 32:369–371, 1987.

[86] T. Engler, K. Althaus, and F. Moessner, editors. *ITTK Database*. University of Karlsruhe, 1993-2000.

[87] PG Bendale and RM Enick. Use of carbon dixodie to shift benzene/acetonitrile and benzene/cyclohexane azeotropes. *Fluid Phase Equilib.*, 94:227–253, 1994.

[88] S. Fink and H. Hershey. Modeling the vapor-liquid equilibria of 1,1,1-trichloroethane+carbon dioxide and toluene+carbon dioxide at 308, 323, and 353 K. *Ind. Eng. Chem. Res.*, 29:295–306, 1990.

[89] R. S. Mohamed and G. D. Holder. High pressure phase behavior in systems containing CO_2 and heavier compounds with similar vapor pressures. *Fluid Phase Equilib.*, 32:295–317, 1987.

[90] H. Renon, S. Laugier, J. Schwartzentruber, and D. Richon. New determinations of high pressure vapor-liquid equilibria in binary systems containing n-propylbenzene with nitrogen or carbon dioxide consistent with the prausnitz-keeler test. *Fluid Phase Equilib.*, 51:285–298, 1989.

[91] H.-J. Ng, S. S-S Huang, and D. B Robinson. Equilibrium phase properties of selected m-xylene binary systems. m-xylene-methane and m-xylene carbon dioxide. *J. Chem. Eng. Data*, 27((2)):119–122, 1982.

[92] C. Tan, S. Yarn, and J. Hsu. Vapor-liquid equilibria for the systems carbon dioxide-ethylbenzene and carbon dioxide-styrene. *J. Chem. Eng. Data*, 36:23–25, 1991.

[93] *Korea thermophysical properties databank*. Thermodynamics and Properties LAB, Dept. of Chemical Engineering, Korea Univerity, Seoul, Korea, 2009.

[94] F. D. Rossini, K. S. Pitzer, R. L. Arnett, R. M. Braun, and G. C. Pimentel. *Selected Values of Physical and Thermodynamic Properties of Hydrocarbons*. Carnegie Press, Pittsburg, 1953.

[95] J. A. Bierlein and W. B. Kay. Phase-equilibrium properties of system carbon dioxide-hydrogen sulfide. *Ind. Eng. Chem.*, 45:618–624, 1953.

[96] W. E. Hensel and F. E. Massoth. Phase equilibria for the ternary system: CH_4-CO_2-H_2S at low temperatures. *J. Chem. Eng. Data*, 9(3):352–356, 1964.

[97] D. B. Robinson, A. P. Lorenzo, and C. A. Macrygeorgos. The carbon dioxide-hydrogen sulphide-methane system part II. phase behavior at 40 F and 160 F. *Can. J. Chem. Eng.*, 36:212–217, 1959.

[98] J. Gross and G. Sadowski. Application of the peturbed-chain saft equation of state to associating systems. *Ind. Eng. Chem. Res.*, 41:5510–5515, 2002.

[99] M. Kleiner and G. Sadowski. Modeling of polar systems using PCP-SAFT: an approach to account for induced-association interactions. *J. of Phys. Chem. C*, 111(43):15544–15553, 2007.

[100] F. T. Selleck, L. T. Carmichael, and B. H. Sage. Phase behavior in the hydrogen sulfide-water system. *Ind. Eng. Chem.*, 44(9):2219–2226, 1952.

[101] R. Wiebe and V. L. Gaddy. The solubility in water of carbon dioxide at 50, 75 and 100 degrees, at pressures to 700 atmospheres. *J. Am. Chem. Soc.*, 61:315–318, 1939.

[102] M. B. King, A. Mubarak, J. D. Kim, and T. R. Bott. The mutual solubilities of water with supercritical and liquid carbon dioxides. *J. Supercrit. Fluids*, 5(4):296–302, 1992.

[103] C. R. Coan and A. D. King. Solubility of water in compressed carbon dioxide, nitrous oxide, and ethane - evidence for hydration of carbon dioxide and nitrous oxide in gas phase. *J. Am. Chem. Soc.*, 93(8):1857–1862, 1971.

[104] R. Wiebe and V. L. Gaddy. Vapor phase composition of carbon dioxide-water mixtures at various temperatures and at pressures to 700 atmospheres. *J. Am. Chem. Soc.*, 63(2):475–477, 1941.

[105] J. Kiepe, S. Horstmann, K. Fischer, and J. Gmehling. Experimental determination and prediction of gas solubility data for $CO_2 + H_2O$ mixtures containing NaCl or KCl at temperatures between 313 and 393 K and pressures up to 10 MPa. *Ind. .Eng. Chem. Res.*, 41(17):4393–4398, 2002.

[106] R. Dohrn, A. P. Bunz, F. Devlieghere, and D. Thelen. Experimental measurements of phase-equilibria for ternary and quaternary systems of glucose, water, CO_2 and ethanol with a novel apparatus. *Fluid Phase Equilib.*, 83:149–158, 1993.

[107] R. Dsouza, J. R. Patrick, and A. S. Teja. High-pressure phase-equilibria in the carbon-dioxide normal-hexadecane and carbon-dioxide water-systems. *Can. J. Chem. Eng.*, 66(2):319–323, 1988.

[108] A. Bamberger, G. Sieder, and G. Maurer. High-pressure (vapor plus liquid) equilibrium in binary mixtures of (carbon dioxide plus water or acetic acid) at temperatures from 313 to 353 K. *J. Supercrit. Fluid*, 17(2):97–110, 2000.

[109] G. Müller, E. Bender, and G. Maurer. Das dampf-flssigkeitsgleichgewicht des ternren systems ammoniak-kohlendioxide-wasser bei hohen wassergehalten im bereich zwichen 373 und 473 Kelvin. *Ber. der Bunsenges. fur Phys. Chem.*, 92:148–160, 1988.

[110] K. Todheide and E. U. Franck. Das zweiphasengebiet und die kritische kurve im system kohlendioxid-wasser bis zu drucken von 3500 bar. *Z. Phys. Chem. Neue. Fol.*, 37(5):387–401, 1963.

[111] A. Zawisza and B. Malesinska. Solubility of carbon dioxide in liquid water and of water in gaseous carbon dioxide in the range 0.2-5 MPa and at temperatures up to 473 K. *J. Chem Eng. Data.*, 26:388–391, 1981.

[112] T. Sako, T. Sugeta, N. Nakazawa, T. Okubo, M. Sato, T. Taguchi, and T. Hiaki. Phase-equilibrium study of extraction and concentration of furfural produced in reactor using supercritical carbon-dioxide. *J. Chem. Eng. Japan*, 24(4):449–455, 1991.

[113] D. Ben-Amotz. Global thermodynamics of hydrophobic cavitation, dewetting, and hydration. *J. .Chem. Phy.*, 123(18):184504, 2005.

Chapter 3

Renormalization-group corrections to the Perturbed-Chain Statistical Associating Fluid Theory for binary mixtures

Abstract

Classical fluid theories do not describe the long-range fluctuations that occur in the vicinity of a pure component or mixture's critical point. The perturbed-chain statistical associating fluid theory (PC-SAFT) equation of state is extended with a renormalization group theory for mixtures. The theory accounts for the long-range density fluctuations and the results reduce to the results of the classical PC-SAFT equation of state away from the critical point. Two approximation methods, the isomorphic density approximation and individual phase-space cell approximation, are used for the renormalization group corrections of mixtures. The two variants are evaluated by comparison to experimental vapor-liquid data for systems of alkanes, carbon dioxide and hydrogen sulfide. Overall, the considered implementation of the individual phase-space cell approximation is slightly superior to the isomorphic density approximation for the mixtures investigated here. The individual phase-space cell approximation tends to overestimate the renormalization corrections for some cases but generally leads to good agreement with experimental data for binary mixtures.

3.1   Introduction

Long-range density fluctuations play a determining role when approaching the
critical point. The asymptotic singular critical behavior leads to universal (i.e.
substance independent) scaling laws[1, 2, 3]. Classical fluid theories do not des-
cribe the long-range fluctuations and they are unable to correctly represent critical
properties. Perturbation theories are often based on a repulsive reference fluid,
where long-range density fluctuations are absent. The perturbation terms for at-
tractive interactions are formulated as an expansion around the radial distribution
function, $g(r)$, of the repulsive fluid[4] so that only short-range correlations are
accounted for.

Cubic equations of state are in engineering applications regularly parameteri-
zed to enforce the critical temperature and critical pressure, while sacrificing to
some extent the volumetric properties. For models based on the Statistical Asso-
ciating Fluid Theory (SAFT)[5, 6, 7, 8, 9, 10, 11, 12, 13, 14, 15, 16], this has also
been done in order to improve the pressure-temperature-composition behavior in
the vicinity of critical points[17, 18, 19]. Classical models parameterized to en-
force critical properties, like temperature and pressure, however don't reproduce
the universal scaling laws in the vicinity of the critical point while, at the same
time, they compromise some physical properties away from the critical point. In
practice, different sets of parameters need to be handled for conditions away from
the critical region and near to the critical point. In order to obtain an equation of
state for the thermodynamic properties of fluids using only one set of parameters,
it is necessary to incorporate the long range density fluctuations occurring in the
critical region in such a way, that the long wavelength fluctuations disappear for
conditions away from the critical point.

The renormalization group theory[20, 21] applied to critical fluctuations ad-
dresses the difficulty of different length-scales, from molecular scale to density-
fluctuations of diverging length scale, by recursively considering wave-packets of
increasing wavelength. While many theories describing the macroscopic critical
behavior are based on the renormalization group theory (or aspects thereof), we
distinguish two approaches. Crossover equations analyze the critical point and
its surrounding and provide equations that describe the transition to classical
fluid theories. The second approach is to model microscopic properties, such as
intermolecular potentials and pair-correlations of the fluids.

Crossover equations have been developed in order to describe the transition of classical fluid theories to the universal scaling law behavior in the asymptotic limit[22, 23, 24, 25, 26]. The first generation of crossover equations gave an accurate representation of the near-critical region, but the equations did not reduce to ideal gas behavior for low pressures. The practical application was therefore limited to the vicinity of the critical point. The problem was addressed by Pelt et al.[27] and Kiselev[28], leading to crossover equations that can be applied with classical equations of state to the entire fluid state. The approach is useful for engineering purposes, and was successfully applied with several classical equations of state [28, 29, 30, 22, 31, 32, 33, 34]. The method, however, involves many adjustable parameters needed to represent experimental data. A disadvantage in the practical application of the crossover approaches is that the (mixture's) critical temperature and critical density need to be specified. This limits the application to mixtures with very accurately known critical properties. This point was mitigated by estimating the mixture's critical points[35, 36].

White[37] has developed a renormalization group theory based on intermolecular properties. The theory provides simple approximate equations on a mean-field level using the phase-space cell method[21] in order to recursively account for wave-packets of increasing length[38, 39]. Lue and Prausnitz[40, 41] reevaluated the partition function of the system by dividing the intermolecular potential into a repulsive part and an attractive portion. The attractive potential was further divided into a short-ranged part and a successively long-range part, so that the density field could also be decomposed into a short-ranged and a long-ranged fluctuating field. The density functionals appearing in the partition function were simplified with a local density approximation of the Helmholtz energy functional and a saddle point approximation. The resulting equations are essentially the same as those of Salvino and White[38], except they were formulated for mixtures. In addition, the analysis of Lue and Prausnitz added transparency of the assumptions made and gave an interpretation of the involved parameters, such as the average gradient of the wavelet, which was proposed as an adjustable parameter.

Tang[42] also reanalyzed the partition function and extended White's renormalization group theory. Similar to the work of Lue and Prausnitz of the same year, the analysis of Tang shows the fit of fluid theories (perturbation theories and integral equation approaches) within the renormalization group theory. The study is transparent about the assumptions made and lays an emphasis on the

pair correlation functions. White's formalism is extended to fluid theories that
account for the pair correlation function of the involved species, beyond the van
der Waals assumption ($g(r) = 1$). In the subsequent study, Mi et al.[43] reanaly-
zed the renormalization group theory of Tang in Fourier space in order to clearly
differentiate between contributions from local and non-local density fluctuations.
They also applied the approach for vapor-liquid equilibrium for mixtures[44, 45].

Jiang and Prausnitz[46] applied the renormalization group theory to pure chain
fluids. Mi et al. applied White's renormalization group theory with a SAFT
equation of state for pure components[47] and mixtures[48]. Llovell et al. applied
an approach based on Lue and Prausnitz's work to the Soft-SAFT equation of
state to pure components[49] and mixtures[50]. Fu et al.[51] presented results
using the same renormalization procedure with the PC-SAFT equation of state.
Bymaster et al.[52] reconciled previous studies of Llovell et al.[49] and of Fu
et al.[51] showing which additional (so far undocumented) approximations these
studies have used. They studied the renormalization theory with the perturbed-
chain SAFT (PC-SAFT) equation of state.

The renormalization treatment of the PC-SAFT equation of state discussed
in this study is based on White's renormalization approach[38, 37] in the dialect
of Lue and Prausnitz[40], which provides corrections due to long-range density
fluctuations near to the critical region, and reduces to the PC-SAFT equation
of state far from the critical region. This study is an extension of the work of
Bymaster et al.[52] to mixtures. For mixtures we apply on the one hand the
individual phase-space cell approximation (as suggested by Lue and Prausnitz[40,
41]) and on the other hand, the isomorphic density approximation [53, 54]. We
consider binary mixtures of simple compounds, such as alkane-alkane systems,
CO_2-alkane, H_2S-alkane, CO_2-ether and H_2S-alcohol mixtures.

3.2   Renormalization equation of state

3.2.1   Classical equation of state

The PC-SAFT equation of state is based on a coarse-grained molecular model,
where molecules are assumed to be chains of spherical segments exhibiting various
attractive interactions. The complete perturbed-chain statistical associating fluid
theory (PC-SAFT) equation of state is given as the sum of the ideal gas contri-

bution (id), a hard-sphere contribution (hs), a chain term (chain) connecting the spherical segments, a contribution for the dispersive attraction (disp) of chains, and a contribution for associating interactions (assoc), as

$$f^{PC-SAFT} = f^{id} + f^{hs} + f^{chain} + f^{disp} + f^{assoc} \tag{3.1}$$

where $f = F/(N k_B T) \cdot \rho$ is the Helmholtz energy density, with F as the Helmholtz energy, ρ as the molecular number density, N is the number of molecules, T is the temperature, and k_B denotes the Boltzmann constant. For details on the PC-SAFT equation of state we refer to the original literature. The first four terms on the right hand side of Eq.(3.1) were in detail described by Gross and Sadowski[16]. The association term is described by Chapman and colleagues[9, 55, 56]. Helmholtz energy contributions that account for polar interactions of spherical and elongated molecules were recently proposed and applied with the PC-SAFT equation of state[57, 58, 59, 60]. The renormalization procedure studied here, however, can be analyzed without these polar terms.

A non-polar substance i is represented by only three pure component parameters: a segment size parameter σ_i, the number of segments m_i and the segment energy parameter ϵ_i/k. Associating substances require two additional pure component parameters, the association energy ϵ^{AiBi} between association site A and site B, and the effective association volume κ^{AiBi}.

Mixtures are described with regular Berthelot-Lorentz combination rules, where a binary interaction parameter, k_{ij}, is introduced correcting the cross-dispersive energy parameter according to $\epsilon_{ij} = (\epsilon_i \epsilon_j)^{0.5}(1 - k_{ij})$.

3.2.2   Recursive renormalization procedure

The renormalization procedure accounts for density fluctuations of increasing wavelength. The wavelength-coordinate is discretized, i.e. the various wavelengths are binned in intervals (with index n) of representative wave-packets. The renormalization successively accounts for Helmholtz energy contributions δf_n due to density fluctuations of increasing wavelength. The Helmholtz energy density for the nth recursive renormalization step is

$$f_n = f_{n-1} + \delta f_n \tag{3.2}$$

The overall Helmholtz energy density is obtained for $n \to \infty$ and the starting point is the classical equation of state $f_0 = f^{\text{PC-SAFT}}$. The overall Helmholtz energy density is then

$$f = f^{\text{PC-SAFT}} + \sum_{n=1}^{\infty} \delta f_n \tag{3.3}$$

Within the renormalization procedure we consider the attractive interactions in a simplified form, i.e. with a van der Waals term. We follow Lue and Prausnitz's[40] implementation of the Renormalization group theory. The successive corrections to the Helmholtz energy density are given by

$$\delta f_n(\rho) = -K_n \ln \frac{\int_0^{\min(\rho, \rho^{max} - \rho)} \exp\left(-\frac{1}{K_n} G_n^D(\rho, \tau)\right) \, \mathrm{d}\tau}{\int_0^{\min(\rho, \rho^{max} - \rho)} \exp\left(-\frac{1}{K_n} G_n^0(\rho, \tau)\right) \, \mathrm{d}\tau} \tag{3.4}$$

The integrals in τ in this equation are for the amplitude of the density fluctuations. The upper integration bound reflects, that the amplitude is constraint by the condition that the lowest density $(\rho - \tau)$ can not be negative (i.e. $\tau \leq \rho$), and by the condition that the highest density of a fluctuation $(\rho + \tau)$ has to be smaller than a maximum density (i.e. $\tau \leq \rho^{max} - \rho$). The maximum density should be interpreted as the closest segment packing, with $\rho^{max} = \frac{\sqrt{2}}{md^3}$. Further, the coefficient K_n is defined as

$$K_n = \frac{k_B T}{(2^n L)^3} \tag{3.5}$$

where L is an adjustable pure component parameter. It is assumed that density fluctuations of wavelength less than the cutoff length L are accurately captured by the classical equation of state. Eq.(3.4) represents the Helmholtz energy contribution of density fluctuations of wavelengths within the volume $(2^n L)^3$. The factor 2 scales the step-size for the successive renormalization steps. This value was already suggested by White[37]. The value should be large enough to decouple the considered wave-packet from the longer wavelengths. On the other hand it should be small enough to trace the full spectrum of wavelengths with enough renormalization steps.

The abbreviations $G_n^D(\rho, \tau)$ in Eq.(3.4) is the Helmholtz energy contribution of the successively increasing wavelengths (omitting a prefactor) and $G_n^0(\rho, \tau)$ is a normalization of the functional integration, that cuts the short wavelengths

away[42, 40]. These functionals are approximated, as

$$G_n^D(\rho, \tau) = \frac{f_{n-1}(\rho + \tau) + f_{n-1}(\rho - \tau)}{2} - f_{n-1}(\rho) + \alpha(m\tau)^2 \frac{\phi w^2}{2^{2n+1}L^2} \quad (3.6)$$

$$G_n^0(\rho, \tau) = \frac{f_{n-1}(\rho + \tau) + f_{n-1}(\rho - \tau)}{2} - f_{n-1}(\rho) + \alpha(m\tau)^2 \quad (3.7)$$

where $-\alpha(m\rho)^2$ represents an attraction term (for a fluid of molecular density ρ and segment density $m\rho$). We assume a simple van der Waals attraction term so that α reduces to a constant attraction parameter, with

$$\alpha = -\frac{1}{2} \int_\sigma^\infty dr\, 4\pi r^2 \xi u^{attr}(r) = \frac{16\pi\epsilon\sigma^3\xi}{9} \quad (3.8)$$

where the second equality is for a Lennard-Jones potential with the attractive part of the potential $u^{attr} = 4\epsilon((\sigma/r)^{12} - (\sigma/r)^6)$ (here considered for the distance $r > \sigma$). The ξ is a pure component parameter empirically introduced by Bymaster et al.[52].

In Eq.(3.6), ϕ is also a pure component parameter that represents the average dimensionless gradient of the considered wavelet. And w represents the range of the attractive potential, defined as

$$w^2 = -\frac{1}{3!\alpha} \int_\sigma^\infty dr\, 4\pi r^2 r^2 \xi u^{attr}(r) = \frac{9\sigma^2}{7} \quad (3.9)$$

where the last equality is again for a Lennard-Jones potential. The quantity w results from the choice of how the intermolecular potential is divided into a short-ranged and long-ranged part[40]. This choice also determines the values of the parameter ϕ.

We note in passing, that the pure component parameter ξ scales to good approximation inversely with the number of segments per molecules, as $\xi \sim m^{-1}$. It is then possible to abandon the third pure component parameter. This is not pursued here since we feel, that a more in-depth study should be conducted with the attractive term $\alpha(m\rho)^2$ written in terms of the chain molecule's radial distribution function to replace the simple van der Waals expression of Eq.(3.8).

In principle, the recursive procedure should be carried out until n approaches infinity. However, it has been observed by Lue and Prausnitz[40, 41] and many

subsequent studies, that the recursion converges after a few steps ($n = 5$).

3.2.3   Approximation methods for binary mixtures

Two implementations of the renormalization procedure for mixtures are discussed and used for calculations here.

Individual phase-space cell approximation

When mixtures are considered, the fluctuations can be calculated in density of each component independently of the other components density fluctuations[40, 41, 61, 46, 62, 48]. This approach is referred to as 'individual phase-space cell approximation' and has been suggested originally by Wilson[20, 63] for the renormalization procedure. We followed this approach with the successive Helmholtz energy contributions to Eq.(3.3) as

$$
\delta f_n(\rho_1, \rho_2) = -K_n \ln \frac{\int_0^{\min(\rho_2, \rho_2^{max} - \rho_2)} \int_0^{\min(\rho_1, \rho_1^{max} - \rho_1)} \exp\left(-\frac{1}{K_n} G_n^D\right) \, d\tau_1 \, d\tau_2}{\int_0^{\min(\rho_2, \rho_2^{max} - \rho_2)} \int_0^{\min(\rho_1, \rho_1^{max} - \rho_1)} \exp\left(-\frac{1}{K_n} G_n^0\right) \, d\tau_1 \, d\tau_2}
$$

$$(3.10)$$

with $G_n(\rho_1, \tau_1, \rho_2, \tau_2, T)$, according to

$$
G_n^0 = \frac{f_{n-1}(\rho_1 + \tau_1, \rho_2 + \tau_2) + f_{n-1}(\rho_1 - \tau_1, \rho_2 - \tau_2)}{2} - f_{n-1}(\rho_1, \rho_2)
$$
$$
+ \frac{16}{9}\pi\tau^2 \sum_{i=1}^{2}\sum_{j=1}^{2} x_i x_j m_i m_j \sigma_{ij}^3 \frac{\epsilon_{ij}}{kT}\xi_{ij} \quad (3.11)
$$

$$
G_n^D = \frac{f_{n-1}(\rho_1 + \tau_1, \rho_2 + \tau_2) + f_{n-1}(\rho_1 - \tau_1, \rho_2 - \tau_2)}{2} - f_{n-1}(\rho_1, \rho_2)
$$
$$
+ \frac{16}{7}\pi\tau^2 \sum_{i=1}^{2}\sum_{j=1}^{2} x_i x_j m_i m_j \sigma_{ij}^5 \frac{\epsilon_{ij}}{kT}\xi_{ij} \frac{\phi_{ij}}{2^{2n+1} L_{ij}^2} \quad (3.12)
$$

where $x_i = \rho_i/\rho$ denotes the mole fraction of component i and $\tau = \tau_1 + \tau_2$. The mixing rule for the cutoff length L used with Eq.(3.5) in the individual phase-

space cell approximation is defined as

$$L^3 = \sum_{i=1}^{n} x_i \hat{m}_i L_i^3 \qquad (3.13)$$

where the segment ratio $\hat{m}_i = m_i / \overline{m}$ with the average segment number $\overline{m} = \sum_{i=1}^{n} x_i m_i$ was introduced. The combination rules for the three adjustable parameters ϕ_{ij}, L_{ij} and ξ_{ij} are applied as

$$\phi_{ij} = \frac{1}{2} \left(\hat{m}_i \phi_i + \hat{m}_j \phi_j \right) \qquad (3.14)$$

$$L_{ij} = \sqrt{L_i L_j} \qquad (3.15)$$

$$\xi_{ij} = \sqrt{\xi_i \xi_j} \qquad (3.16)$$

Eq.(3.14) is not strictly speaking a combining rule, since the pure component parameters ϕ_i are weighted by the segment ratio. We have observed somewhat better results of this form, compared to the simpler combining rule $\phi_{ij} = \frac{1}{2} \left(\phi_i + \phi_j \right)$. We take an advance on the result chapter in order to illustrate the difference between these two approaches. A representative example for the systems investigated here is given in Figure 3.1, where Eq.(3.14) is seen to improve on the simple geometric combining rule.

Although the parameter ξ has earlier been introduced to the renormalization theory empirically[52], it has a certain interpretation. It corrects for the fact that the integral over the fluids radial distribution function and intermolecular potential, which is assumed as constant in a mean-field approach, in fact depends on the chain-length of a molecule. That is because of segment-segment shielding effects. Twu et al. analyzed nonspherical fluids and their analysis (mildly) suggests a geometric mean for the combining rule for such a parameter[65]. For the cutoff length L in Eq.(3.12), we could have considered an L value from a mixing rule, such as Eq.(3.13). We found a low sensitivity to how L was calculated. The choice of using a combination rule for L_{ij} in Eq.(3.12) rather than a mixing rule for a mean L, is motivated by a simple compositional dependence of Eq.(3.12) that results from this choice.
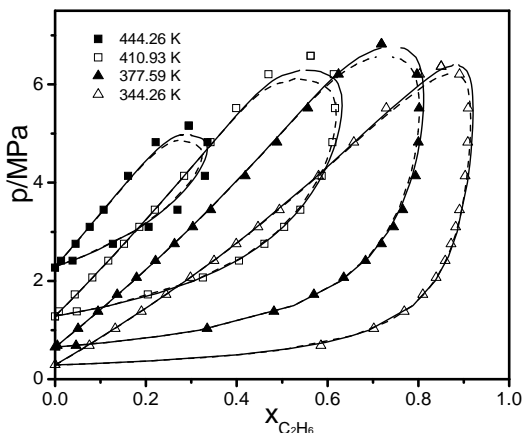
Figure 3.1: *Vapor-liquid equilibrium of ethane – n-pentane at four temperatures. Comparison of PC-SAFT-RG with individual phase-space cell approximation with Eq.(3.14) (solid lines, $k_{ij} = 0.0073$) and with simple combining rule ($\phi_{ij} = \frac{1}{2}(\phi_i + \phi_j)$) (dashed lines, $k_{ij} = 0.0073$) to experimental data[64] (symbols).*

Isomorphic density approximation

The isomorphism assumption proposed by Fisher[53], requires that the thermodynamic potentials in a mixture have the same universal form as the thermodynamic potential of the one-component fluid for the case that an appropriate isomorphic variable is chosen. Here the global density of the system is used as the isomorphic variable. Kiselev and Friend[54] used the mole fractions instead of chemical potentials as independent variables in the isomorphism assumption, and this method was later adopted by Cai and Prausnitz[66], by Sun et al.[67], and by Llovell et al.[50].

According to the isomorphism assumption, the relevant order parameter to describe vapor-liquid equilibria in mixtures is the total density $\rho = \sum_i \rho_i$ of the system, the Helmholtz energy contribution is calculated from Eq.(3.4) as for pure components. For mixtures according to this simplified isomorphic density approximation it is

$$G_n^0(\rho, \tau) = \frac{f_{n-1}(\rho + \tau) + f_{n-1}(\rho - \tau)}{2} - f_{n-1}(\rho) + \overline{\alpha(m\tau)^2} \qquad (3.17)$$

$$G_n^D(\rho, \tau) = \frac{f_{n-1}(\rho + \tau) + f_{n-1}(\rho - \tau)}{2} - f_{n-1}(\rho) + \overline{\alpha(m\tau)^2} \frac{\overline{w}^2 \overline{\phi}}{2^{2n+1} L^2} \quad (3.18)$$

where, for multicomponent mixtures,

$$\overline{\alpha(m\tau)^2} = \frac{16}{9} \pi \tau^2 \sum_{i=1}^n \sum_{j=1}^n x_i x_j m_i m_j \sigma_{ij}^3 \frac{\epsilon}{kT} \xi_{ij} \quad (3.19)$$

and

$$\overline{w}^2 = \frac{9}{7} \sum_{i=1}^n x_i \hat{m}_i \sigma_i^2 \quad (3.20)$$

and

$$\overline{\phi} = \sum_{i=1}^n x_i \hat{m}_i \phi_i \quad (3.21)$$

The quantities L and ξ_{ij} are defined through Eq.(3.13) and Eq.(3.16), respectively.

3.3 Numerical procedure

The renormalization scheme according to White requires the integration of Eq.(3.4) or of Eq.(3.10). A straight-forward implementation is to discretize the density and use a trapezoid rule for the numerical integration. At the end of the renormalization step, the discretized Helmholtz energy as a function of density can be interpolated with cubic splines. This procedure works well for conditions close to the critical point. For phase equilibrium calculations at lower reduced temperature, however, this scheme requires unreasonably fine grids. The reason is that such cases involve low (component) densities for a vapor phase, where the ideal gas contribution to the Helmholtz energy introduces strong non-linear limiting behavior. The density-derivative of the ideal gas contribution introduces a logarithmic density dependence. This makes linear or cubic interpolation schemes inadequate. The result of this problem is visualized as a dashed line in Figure 3.2 for the case of pure n-octane modeled with 400 equi-distant grid points along the vapor pressure line. For low temperatures where the vapor density decreases, the interpolation gets unreasonable.

The ideal-gas contribution was here substracted for every grid-point, before the cubic-spline interpolation was adjusted. Derivatives to density can then be

taken, without an overly pronounced non-linearity. The ideal gas contribution is analytically added to the resulting values. This leads to robust results also at low component densities, as seen from the solid line in Figure 3.2 and a smaller number of grid-points can be used for the calculations. Here, 200 or 400 grid-points were used for pure components and the isomorphic density approximation. For the individual phase-space cell approximation of a binary mixture, the two densities were discretized in a grid of 200×200 points.
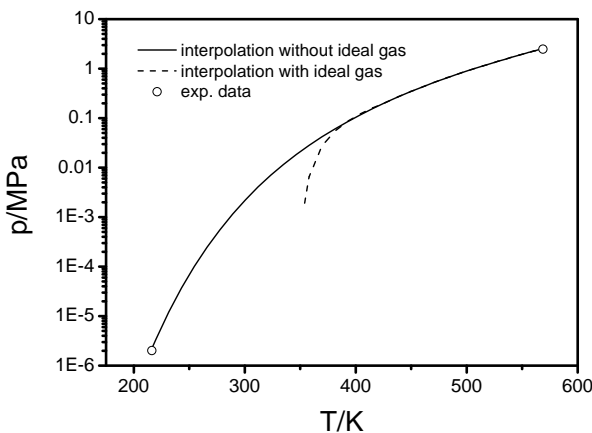
Figure 3.2: *Vapor pressure line of n-octane. Illustration of a numerical artifact as a result of Helmholtz energy interpolations (cubic spline) including the strongly non-linear ideal-gas term (dashed line). An interpolation scheme where the ideal gas contribution is subtracted prior to interpolation (and only added for the desired density) does not suffer from this deficiency (solid line). Calculations with 400 grid-points for both cases. The open circles are the experimental triple point and critical point, respectively.*

For the phase-space cell approximation the evaluation of the 2-dimensional integrals appearing in Eq.(3.11) and Eq.(3.12) was for any mixture isotherm done only once as an initialization of the calculation. The initialization can be done efficiently by realizing that both integrands in Eq.(3.11) and Eq.(3.12) decay to zero with increasing $\{\tau_1, \tau_2\}$, which can be used to truncate the integration. After 5 recursive steps ($n = 5$) the renormalization procedure converged and the resulting Helmholtz energy was correlated using 2-dimensional splines. The thermodynamic derivatives (leading to pressure, chemical potential, etc.) were taken analytically from the spline functions. This procedure leads to an initialization step (where the

numerical integrations are performed) requiring a few seconds on a desktop PC, whereas many equilibrium points of the isotherm were subsequently determined in milliseconds. The isomorphic approximation is computationally less tedious, because it only involves one dimensional integrations. For this case, we have not discretized the density range of both considered components, but as a penalty of the less elaborate implementation the calculations for a complete binary isotherm were in fact slower than those of the previously described algorithm.

3.4 Results and discussion

3.4.1 Pure components

The renormalization group parameters for some n-alkanes considered in this work were taken from Bymaster et al.[52]. All classical equation of state parameters of the PC-SAFT model can be maintained. Additional renormalization group parameters of components considered in this study are listed in Table 3.1 with the classical pure components PC-SAFT parameters taken from previous studies[16, 68]. A comparison of the calculated critical properties and the experimental data is given in Table 3.2. For brevity we refer to the PC-SAFT equation of state applied with the renormalization group theory as PC-SAFT-RG. Results of the regular PC-SAFT model are also tabulated, confirming, that the renormalization group theory gives much better agreement with experimental data.

Figure 3.3 and Figure 3.4 give a graphical comparison of the PC-SAFT-RG model to experimental data for pure component vapor-liquid equilibria. The co-existing densities for methanol, n-decane and dimethyl ether are shown in Figure 3.3, whereas the vapor pressure lines for the same components are presented in Figure 3.4. Calculations of the classical PC-SAFT equation of state are also given. The renormalization group corrections improve the description of the phase equilibrium in the vicinity of the critical points. Both diagrams show that renormalization group correction results remain similar as the results of original PC-SAFT equation of state in the region away from critical point.
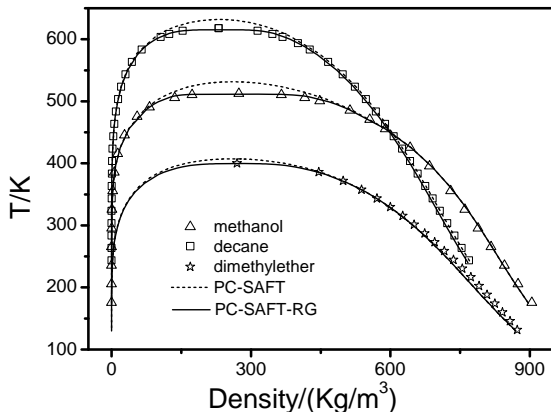
Figure 3.3: *Coexisting vapor and liquid densities of methanol, n-decane and dimethyl ether: Comparison of PC-SAFT-RG results (solid lines) to PC-SAFT results (dashed lines) and experimental data (symbols).*
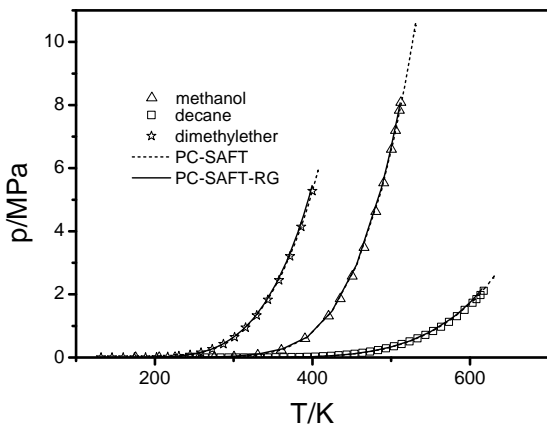
Figure 3.4: *Vapor pressure curves of methanol, n-decane and dimethyl ether. Comparison of PC-SAFT-RG results (solid lines) to PC-SAFT results (dashed lines) and experimental data (symbols).*

Table 3.1: *Pure component parameters*

Component	m	σ / Å	$\epsilon/k_B(K)$	$\epsilon^{AB}/k(K)$	κ^{AB}	ϕ	L/σ	ξ
methane	1.0000	3.7039	150.03	-	-	16.01	1.398	0.6
ethane*	1.6069	3.5206	191.42	-	-	15.38	1.40	0.520
propane*	2.0020	3.6184	208.11	-	-	20.37	1.63	0.397
butane*	2.3316	3.7086	222.88	-	-	23.43	1.75	0.304
pentane*	2.6896	3.7729	231.20	-	-	25.30	1.83	0.261
isopentane	2.5620	3.8296	230.75	-	-	26.13	1.829	0.261
decane	4.6627	3.8384	243.87	-	-	45.0	2.68	0.15
H_2S	1.649	3.0548	229.84	536.6	0.001	15.07	1.332	0.456
CO_2	2.0729	2.7852	169.21	-	-	21.97	1.820	0.433
methanol	1.5255	3.2300	188.90	2899.5	0.0352	17.4	1.57	0.38
dimethylether	2.2623	3.2766	212.93	-	-	19.67	1.629	0.397

* Parameters taken from the work of Bymaster et al.[52].

Table 3.2: *Critical properties for pure component*

n-alkane	T_c/K			P_c/MPa			$\rho_c/kg/m^3$		
	exp	RG	PC-SAFT	exp	RG	PC-SAFT	exp	RG	PC-SAFT
methane	190.6	190.5	191.4	4.60	4.55	4.68	162.2	157.8	148.1
isopentane	460.4	460.0	467.9	3.38	3.42	3.76	235.8	250.0	224.6
decane	617.7	615.3	630.6	2.11	2.17	2.59	230.7	256.5	230.5
H_2S	373.4	373.2	376.3	8.97	9.19	9.38	388.5	370.8	325.4
CO_2	304.2	304.2	310.3	7.38	7.38	8.06	466.1	474.4	441.0
methanol	512.5	511.7	531.5	8.08	8.12	10.66	273.9	276.9	260.0
dimethylether	400.1	399.7	407.3	5.37	5.45	5.94	271.0	286.3	259.8

3.4.2 Binary mixtures

We evaluate the PC-SAFT-RG for various binary mixtures using two approximation methods for the renormalization group theory.

Alkane-alkane systems

Four alkane mixtures with increasing shape-asymmetry are here considered. The vapor-liquid equilibrium of the mixture of ethane-propane is presented in Figure 3.5. The diagram compares results of PC-SAFT and the two variants of the PC-SAFT-RG models to experimental data. The isomorphic density approximation shows improved results near the critical region comparing to PC-SAFT, while the individual phase-space cell approximation overestimates the renormalization group corrections near the critical region for the two highest temperatures.

Results for the mixture propane–n-pentane are given in Figure 3.6. The isomorphic density approximation improves the results compared to the PC-SAFT equation of state. The individual phase-space cell approximation here yields the best agreement with experimental data.

Figure 3.7 shows the $p - x$ diagram for the binary system of ethane-pentane. The binary interaction parameter $k_{ij} = 0.0073$ earlier determined for PC-SAFT is maintained unchanged for the two variants of the renormalization theory. In Figure 3.7, the isomorphic density approximation shown with dashed lines slightly improved the phase behavior in the critical vicinity compared with the PC-SAFT model, while the individual phase-space cell approximation shows a better agreement with experimental data. The individual phase-space cell approximation tends to overestimate the renormalization group corrections near the critical region for the isothermal curves at temperatures of 444.26 K and 410.93 K.

In Figure 3.8, the propane–n-decane mixture is used to analyze the models. The isomorphic density approximation only slightly improves the PC-SAFT equation of state. Results of the individual phase-space cell approximation method show very good agreement with experimental data. We observe, however, that the phase equilibrium calculations do not converge in the very vicinity of the critical point. Although this problem can be due to an insufficient algorithm, we suspect it can also be caused by too aggressive renormalization corrections. We intentionally present diagrams with these last converged phase equilibrium points leaving a gap for these diagrams (where applicable).

Figure 3.5: *Vapor-liquid equilibrium of ethane – n-propane at five temperatures. Comparison of PC-SAFT-RG with individual phase-space cell approximation (solid lines, $k_{ij} = -0.0026$), PC-SAFT-RG with isomorphic density approximation (short dashed lines, $k_{ij} = -0.0046$) and PC-SAFT (dashed lines, $k_{ij} = 0.0036$) to experimental data[69] (symbols).*
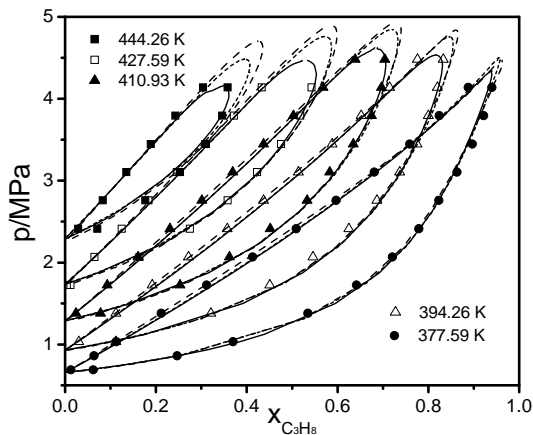
Figure 3.6: *Vapor-liquid equilibrium of n-propane – n-pentane at five temperatures. Comparison of PC-SAFT-RG with individual phase-space cell approximation (solid lines, $k_{ij} = 0.0082$), PC-SAFT-RG with isomorphic density approximation (short dashed lines, $k_{ij} = 0.0082$) and PC-SAFT (dashed lines, $k_{ij} = 0.0182$) to experimental data[70] (symbols).*
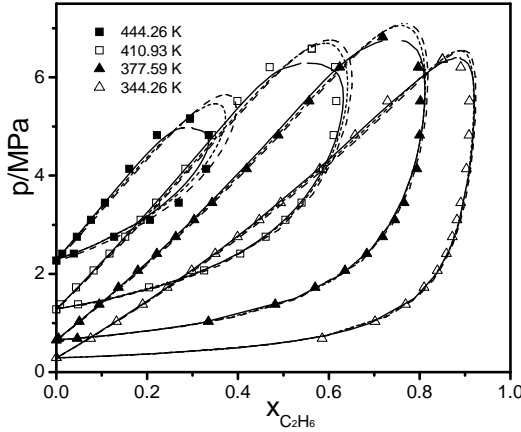
Figure 3.7: *Vapor-liquid equilibrium of ethane – n-pentane at four temperatures. Comparison of PC-SAFT-RG with individual phase-space cell approximation (solid lines, $k_{ij} = 0.0073$), PC-SAFT-RG with isomorphic density approximation (short dashed lines, $k_{ij} = 0.0073$) and PC-SAFT (dashed lines, $k_{ij} = 0.0073$) to experimental data[64] (symbols).*

Figure 3.8: *Vapor-liquid equilibrium of n-propane – n-decane at four temperatures. Comparison of PC-SAFT-RG with individual phase-space cell approximation (solid lines, $k_{ij} = 0.0036$), PC-SAFT-RG with isomorphic density approximation (short dashed lines, $k_{ij} = 0.0066$) and PC-SAFT (dashed lines, $k_{ij} = 0.0066$) to experimental data[71] (symbols).*

Mixtures with CO_2 or H_2S

Mixtures of CO_2-alkane and H_2S-alkane are of particular industrial interest, for example in the removal of acid gases from natural gas. Figure 3.9 illustrates the vapor-liquid equilibrium of CO_2-methane. Only isothermal curves for $T = 288.5$ K and 293.4 K are shown since they lead up to a critical point of the binary mixture and these were overestimated by the PC-SAFT equation of state. Although PC-SAFT-RG calculations using both approximations show improvements for this system over the original PC-SAFT, the results of the individual phase-space cell approximation are better than those of the isomorphic density approximation.

Figure 3.9: *Vapor-liquid equilibrium of CO_2-methane at two temperatures. Comparison of PC-SAFT-RG with individual phase-space cell approximation (solid lines, $k_{ij} = 0.0430$), PC-SAFT-RG with isomorphic density approximation (short dashed lines, $k_{ij} = 0.0450$) and PC-SAFT (dashed lines, $k_{ij} = 0.0630$) to experimental data[72] (symbols).*

The system CO_2 in mixture with butane is shown in Figure 3.10. The individual phase-space cell approximation overestimates the renormalization corrections near the critical point, while the isomorphic density approximation only mildly improves on the original PC-SAFT model.

Dimethylether is considered as a more polar solvent in mixture with carbon dioxide. The mixture was chosen, because it was earlier quite weakly described with PC-SAFT in the vicinity of the critical point. Figure 3.11 shows only two iso-

therms for clarity. Both renormalization theories improve the PC-SAFT equation of state, with the individual phase-space cell approximation as the more accurate model.
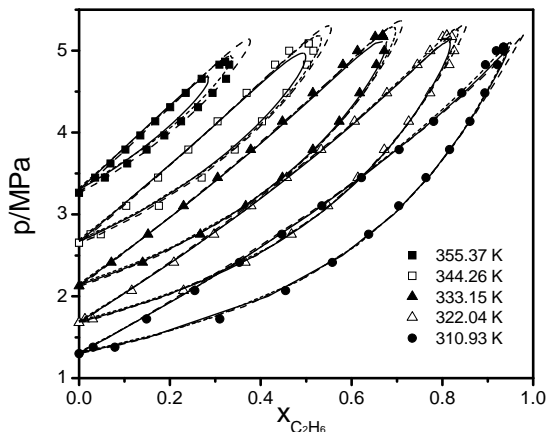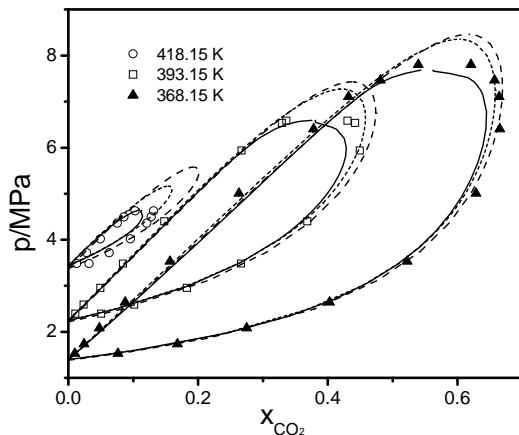

Figure 3.10: *Vapor-liquid equilibrium of CO_2-butane at three temperatures. Comparison of PC-SAFT-RG with individual phase-space cell approximation (solid lines, $k_{ij} = 0.0997$), PC-SAFT-RG with isomorphic density approximation (short dashed lines, $k_{ij} = 0.1090$) and PC-SAFT (dashed lines, $k_{ij} = 0.1090$) to experimental data[73] (symbols).*

A mixture of hydrogen sulfide with butane, is given in Figure 3.12. In this case, both variants of the renormalization theory improve the results of the PC-SAFT model in the critical region. In contrast to the earlier example, the isomorphic density approximation tends to overestimate the corrections to the critical density fluctuations. The individual phase-space cell approximation is in good agreement with the experimental data.

Figure 3.13 shows H_2S in mixture with methanol. Using the same k_{ij} parameter as for the PC-SAFT model, the individual phase-space cell approximation gives much better agreement with experimental data at temperature of 448.15 K compared to the isomorphic density approximation and to the original PC-SAFT model. The more demanding convergence for the individual phase-space cell approximation when approaching the critical point remains in most binary mixtures studied here.
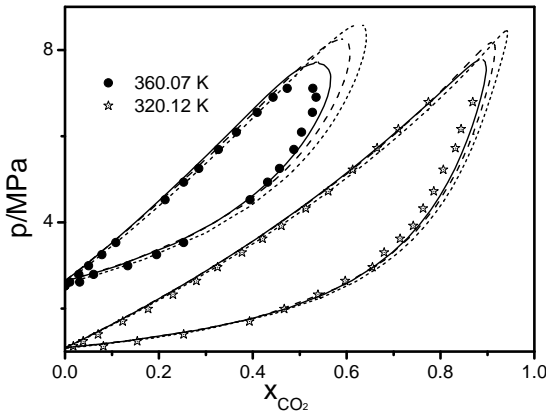
Figure 3.11: *Vapor-liquid equilibrium of CO_2-dimethylether at two temperatures. Comparison of PC-SAFT-RG with individual phase-space cell approximation (solid lines, $k_{ij} = 0.0090$), PC-SAFT-RG with isomorphic density approximation (short dashed lines, $k_{ij} = 0.0090$) and PC-SAFT (dashed lines, $k_{ij} = 0.0090$) to experimental data[74] (symbols).*
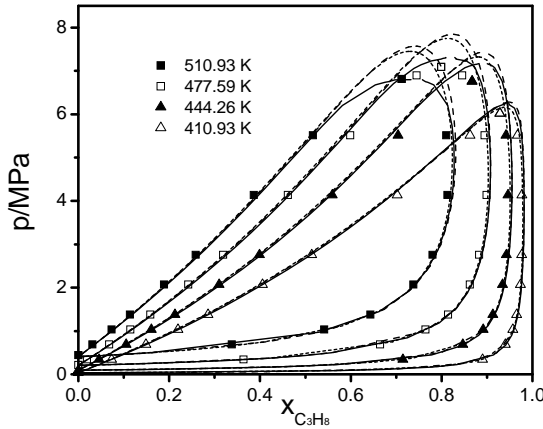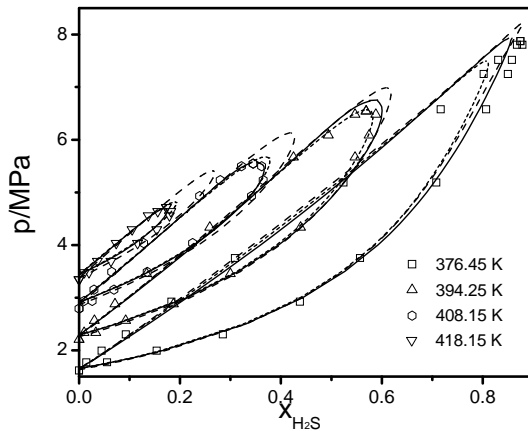

Figure 3.12: *Vapor-liquid equilibrium of H_2S-butane at four temperatures. Comparison of PC-SAFT-RG with individual phase-space cell approximation (solid lines, $k_{ij} = 0.0472$), PC-SAFT-RG with isomorphic density approximation (short dashed lines, $k_{ij} = 0.0572$) and PC-SAFT (dashed lines, $k_{ij} = 0.0672$) to experimental data[75] (symbols).*
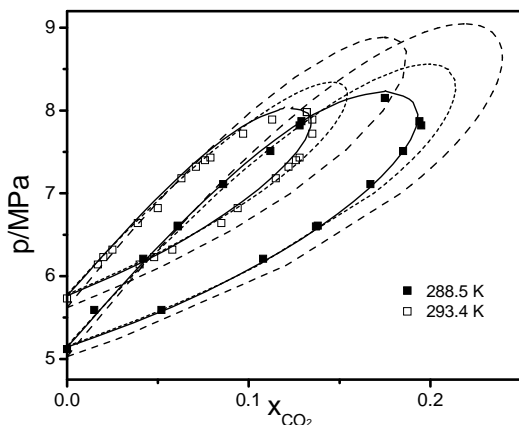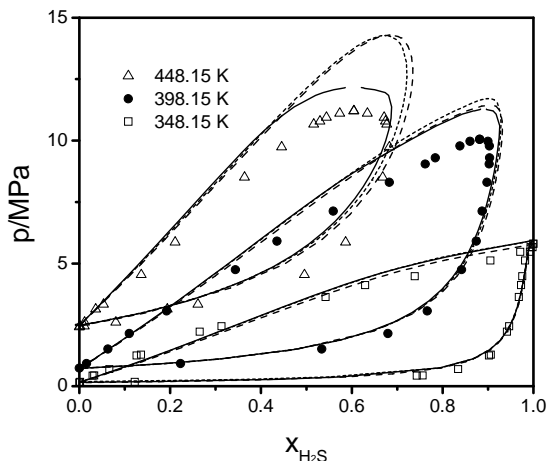
Figure 3.13: *Vapor-liquid equilibrium of H_2S-methanol at three temperatures. Comparison of PC-SAFT-RG with individual phase-space cell approximation (solid lines, $k_{ij} = -0.0589$), PC-SAFT-RG with isomorphic density approximation (short dashed lines, $k_{ij} = -0.0589$) and PC-SAFT (dashed lines, $k_{ij} = -0.0589$) to experimental data[76] (symbols).*

3.5 Conclusion

A renormalization group theory was applied with the PC-SAFT equation of state, in order to account for long-ranged density fluctuations in the vicinity of the critical point. This work can be considered as an extension of the study of Bymaster et al.[52] to mixtures. Two approximations for the renormalization scheme for mixtures were evaluated, i.e. the isomorphic density approximation and the individual phase-space cell approximation. The resulting equations of state were applied to mixtures of alkanes, as well as to mixtures involving hydrogen sulfide and carbon dioxide. Both variants improved the description around the critical point for these mixtures. Despite its tendency to overestimate the renormalization corrections, the individual phase-space cell approximation was found to be slightly superior to the isomorphic density approximation for the systems studied here.

REFERENCES

[1] J. V. Sengers and J. M. H. L. Sengers. Thermodynamic behavior of fluids near the critical point. *Annu. Rev. Phys. Chem.*, 37:189–222, 1986.

[2] M. A. Anisimov, S. B. Kiselev, J. V. Sengers, and S. Tang. Crossover approach to global critical phenomena in fluids. *Physica A*, 188(4):487–525, 1992.

[3] M. A. Anisimov and J. V. Sengers. *Equations of state for fluids and fluid mixtures, Chapter 11. Critical region.* Elsevier, Amsterdam, 1 edition, 2000.

[4] J. P. Hansen and I. R. McDonald. *Theory of Simple Liquids.* Elsevier, Amsterdam, 3 edition, 2006.

[5] M. S. Wertheim. Fluids with highly directional attractive forces. 1. statistical thermodynamics. *J. Stat. Phys.*, 35(1-2):19–34, 1984.

[6] M. S. Wertheim. Fluids with highly directional attractive forces. 2. thermodynamic perturbation-theory and integral-equations. *J. Stat. Phys.*, 35(1-2):35–47, 1984.

[7] M. S. Wertheim. Fluids with highly directional attractive forces. 3. multiple attraction sites. *J. Stat. Phys.*, 42(3-4):459–476, 1986.

[8] M. S. Wertheim. Fluids with highly directional attractive forces. 4. equilibrium polymerization. *J. Stat. Phys.*, 42(3-4):477–492, 1986.

[9] W. G. Chapman, G. Jackson, and K. E. Gubbins. Phase equilibria of associating fluids - chain molecules with multiple bonding sites. *Mol. Phys.*, 65(5):1057–1079, 1988.

[10] W. G. Chapman, K. E. Gubbins, G. Jackson, and M. Radosz. SAFT-equation-of-state solution model for associating fluids. *Fluid Phase Equilib.*, 52:31–38, 1989.

[11] S. H. Huang and M. Radosz. Equation of state for small, large, polydisperse and associating molecules. *Ind. Eng. Chem. Res.*, 29:2284–2294, 1990.

[12] A. GilVillegas, A. Galindo, P. J. Whitehead, S. J. Mills, G. Jackson, and A. N. Burgess. Statistical associating fluid theory for chain molecules with attractive potentials of variable range. *J. Chem. Phys.*, 106(10):4168–4186, 1997.

[13] A Galindo, L. A. Davies, A. Gil-Villegas, and G. Jackson. The thermodynamics of mixtures and the corresponding mixing rules in the SAFT-VR approach for potentials of variable range. *Mol. Phys.*, 93(2):241–252, 1998.

[14] F. J. Blas and L. F. Vega. Prediction of binary and ternary diagrams using the statistical associating fluid theory (SAFT) equation of state. *Ind. Eng. Chem. Res.*, 37(2):660–674, 1998.

[15] J Gross and G Sadowski. Application of perturbation theory to a hard-chain reference fluid: an equation of state for square-well chains. *Fluid Phase Equilib.*, 168(2):183–199, 2000.

[16] J. Gross and G. Sadowski. Perturbed-chain saft: An equation of state based on a perturbed theory for chain molecules. *Ind. Eng. Chem. Res.*, 40(4):1244–1260, 2001.

[17] F. J. Blas and L. F. Vega. Critical behavior and partial miscibility phenomena in binary mixtures of hydrocarbons by the statistical associating fluid theory. *J. Chem. Phys.*, 109(17):7405–7413, 1998.

[18] C. McCabe and G. Jackson. SAFT-VR modelling of the phase equilibrium of long-chain n-alkanes. *Phys. Chem. Chem. Phys.*, 1(9):2057–2064, 1999.

[19] J. C. Pámies and L. F. Vega. Critical properties of homopolymer fluids studied by a Lennard-Jones statistical associating fluid theory. *Mole. Phys.*, 100(15):2519–2529, 2002.

[20] K. G. Wilson. Renormalization group and critical phenomena. 1. renormalization group and the kadanoff scaling picture. *Phys. Rev. B: Condens. Matter*, 4(9):3174–3183, 1971.

[21] K. G. Wilson. Renormalization group and critical phenomena. 2. phase-space cell analysis of critical behavior. *Phys. Rev. B*, 4(9):3184–3205, 1971.

[22] Z. Y. Chen, P. C. Albright, and J. V. Sengers. Crossover from singular critical to regular classical thermodynamic behavior of fluids. *Phys. Rev. A: At. Mol. Opt. Phys.*, 41(6):3161–3177, 1990.

[23] Z. Y. Chen, A. Abbaci, S. Tang, and J. V. Sengers. Global thermodynamic behavior of fluids in the critical region. *Phys. Rev. A: At. Mol. Opt. Phys.*, 42(8):4470–4484, 1990.

[24] G. X. Jin, S. Tang, and J. V. Sengers. Global thermodynamic behavior of fluid mixtures in the critical region. *Phys. Rev. E*, 47(1):388–402, 1993.

[25] S. B. Kiselev. Universal crossover function for the free-energy of single-component and 2-component fluids in the critical region. *High Temp.*, 28(1):42–49, 1990.

[26] S. B. Kiselev and J. V. Sengers. An improved parametric crossover model for the thermodynamic properties of fluids in the critical region. *Int. J. Thermophys.*, 14(1):1–32, 1993.

[27] A. Vanpelt, G. X. Jin, and J. V. Sengers. Critical scaling laws and a classical equation of state. *Int. J. Thermophys.*, 15(4):687–697, 1994.

[28] S. B. Kiselev. Cubic crossover equation of state. *Fluid Phase Equilib.*, 147(1-2):7–23, 1998.

[29] S. B. Kiselev and J. F. Ely. Crossover SAFT equation of state: application for normal alkanes. *Ind. Eng. Chem. Res.*, 38(12):4993–5004, 1999.

[30] S. B. Kiselev, I. G. Kostyukova, and A. A. Povodyrev. Universal crossover behavior of fluids and fluid mixtures in the critical region. *Int. J. Thermodyn.*, 12(5):877–895, 1991.

[31] A. K. Wyczalkowska, J. V. Sengers, and M. A. Anisimov. Critical fluctuations and the equation of state of van der waals. *Physica A*, 334(3-4):482–512, 2004.

[32] H. Adidharma and M. Radosz. Prototype of an engineering equation of state for heterosegmented polymers. *Ind. Eng. Chem. Res.*, 37(11):4453–4462, 1998.

[33] C. McCabe and S. B. Kiselev. Application of crossover theory to the SAFT-VR equation of state: SAFT-VRX for pure fluids. *Ind. Eng. Chem. Res.*, 43(11):2839–2851, 2004.

[34] S. B. Kiselev and J. F. Ely. Generalized crossover description of the thermodynamic and transport properties in pure fluids. II. revision and modifications. *Fluid Phase Equilib.*, 252(1-2):57–65, 2007.

[35] L. X. Sun, H. G. Zhao, S. B. Kiselev, and C. McCabe. Predicting mixture phase equilibria and critical behavior using the SAFT-VRX approach. *J. Phys. Chem. B*, 109(18):9047–9058, 2005.

[36] S. B. Kiselev and J. F. Ely. HRX-SAFT equation of state for fluid mixtures: new analytical formulation. *J. Phys. Chem. C*, 111(43):15969–15975, 2007.

[37] J. A. White. Contribution of fluctuations to thermal properties of fluids with attractive forces of limited range: theory compared with $P\rho T$ and C_v data for argon. *Fluid Phase Equilib.*, 75:53–64, 1992.

[38] L. W. Salvino and J. A. White. Calculation of density fluctuation contributions to thermodynamic properties of simple fluids. *J. Chem. Phys.*, 96(6):4559–4567, 1992.

[39] J. A. White and S. Zhang. Renormalization group theory for fluids. *J. Chem. Phys.*, 99:2012–2019, 1993.

[40] L. Lue and J. M. Prausnitz. Renormalization-group corrections to an approximate free-energy model for simple fluids near to and far from the critical region. *J. Chem. Phys.*, 108(13):5529–5536, 1998.

[41] L. Lue and J. M. Prausnitz. Thermodynamics of fluid mixtures near to and far from the critical region. *AIChE J.*, 44(6):1455–1466, 1998.

[42] Y. Tang. Outside and inside the critical region of the Lennard-Jones fluid. *J. Chem. Phys.*, 109(14):5935–5944, 1998.

[43] J. G. Mi, C. L. Zhong, Y. G. Li, and Y. P. Tang. An improved renormalization group theory for real fluids. *J. Chem. Phys.*, 121(11):5372–5380, 2004.

[44] J. G. Mi, Y. P. Tang, C. L. Zhong, and Y. G. Li. Prediction of global vapor-liquid equilibria for mixtures containing polar and associating components with improved renormalization group theory. *J. Phys. Chem. B*, 109(43):20546–20553, 2005.

[45] J. G. Mi, C. L. Zhong, Y. G. Li, and Y. P. Tang. Prediction of global VLE for mixtures with improved renormalization group theory. *AIChE*, 52(1):342–353, 2006.

[46] J. Jiang and J. M. Prausnitz. Equation of state for thermodynamic properties of chain fluids near-to and far-from the vapor-liquid critical region. *J. Chem. Phys.*, 111:5964–5974, 1999.

[47] J. G. Mi, C. L. Zhong, Y. G. Li, and J. Chen. Renormalization group theory for fluids including critical region. I. pure fluids. *Chem. Phys.*, 305(1-3):37–45, 2004.

[48] J. G. Mi, C. L. Zhong, and Y. G. Li. Renormalization group theory for fluids including critical region. II. binary mixtures. *Chem. Phys.*, 312(1-3):31–38, 2005.

[49] F. Llovell, J. C. Pámies, and L. F. Vega. Thermodynamic properties of lennard-jones chain molecules: renormalization-group corrections to a modified statistical associating fluid theory. *J. Chem. Phys.*, 121(21):10715–10724, 2004.

[50] F. Llovell and L. F. Vega. Global fluid phase equilibria and critical phenomena of selected mixtures using the crossover Soft-SAFT equation. *J. Phys. Chem. B*, 110(3):1350–1362, 2006.

[51] D. Fu, X. Li, S. Yan, and T. Liao. Investigation of critical properties and surface tensions for n-alkanes by perturbed-chain statistical associating fluid theory combined with density-gradient theory and renomrlaization-group theory. *Ind. Eng. Chem. Res.*, 45(24):8199–8206, 2006.

[52] A. Bymaster, C. Emborsky, A. Dominik, and W. G. Chapman. Renormalization-group corrections to a perturbed-chain statistical associating fluid theory for pure fluids near to and far from the critical region. *Ind. Eng. Chem. Res.*, 47(16):6264–6274, 2008.

[53] M. E. Fisher. Renormalization of critical exponents by hidden variables. *Phys. Rev.*, 176(1):257–272, 1968.

[54] S. B. Kiselev and D. G. Friend. Cubic crossover equation of state for mixtures. *Fluid Phase Equilib.*, 162(1-2):51–82, 1999.

[55] G. Jackson, W. G. Chapman, and K. E. Gubbins. Phase equilibria of associating fluids - spherical molecules with multiple bonding sites. *Mol. Phys.*, 65(1):1–31, 1988.

[56] C. G. Joslin, C. G. Gray, and W. G. Chapman. Three-dimensional critical wetting and the statistical mechanics of fluids with short-range forces. *Mol. Phys.*, 62(4):843–860, 1987.

[57] J. Gross. An equation-of-state contribution for polar components: quadrupolar molecules. *AIChE*, 51(9):2556–2568, 2005.

[58] J. Gross and J. Vrabec. An equation-of-state contribution for polar components: Dipolar molecules. *AIChE*, 52(3):1194–1204, 2006.

[59] M. Kleiner and J. Gross. An equation of state contribution for polar components: polarizable dipoles. *AIChE*, 52(5):1951–1961, 2006.

[60] J. Vrabec and J. Gross. Vapor-liquid equilibria simulation and an equation of state contribution for dipole-quadrupole interactions. *J. Phys. Chem. B*, 112(1):51–60, 2008.

[61] J. Jiang and J. M. Prausnitz. Phase equilibria for chain-fluid mixtures near to and far from the critical region. *AIChE*, 46(12):2525–2536, 2000.

[62] J. Jiang and J. M. Prausnitz. Critical temperatures and pressures for hydrocarbon mixtures from an equation of state with renormalization-group theory corrections. *Flude Phase Equilib.*, 169(2):127–147, 2000.

[63] K. G. Wilson and M. E. Fisher. Critical exponents in 3.99 dimensions. *Phys. Rev. Lett.*, 28(4):240–243, 1972.

[64] H. H. Reamer, B. H. Sage, and W. N. Lacey. Phase equilibria in hydrocarbon systems. volumetric and phase behavior of the ethane–n-pentane system. *J. Chem. Eng. Data*, 5(1):44–50, 1960.

[65] C. H. Twu, K. E. Gubbins, and C. G. Gray. Thermodynamics of mixtures of nonspherical molecules. 3. fluid phase equilibria and critical loci. *J. Chem. Phys.*, 64:5186–5197, 1976.

[66] J. Cai and J. M. Prausnitz. Thermodynamics for fluid mixtures near to and far from the vapor-liquid critical point. *Fluid Phase Equilib.*, 219(2):205–217, 2004.

[67] L. Sun, H. Zhao, S. B. Kiselev, and C. McCabe. Application of SAFT-VRX to binary phase behaviour: alkanes. *Fluid Phase Equilib.*, 228-229:275–282, 2005.

[68] X. Tang and J. Gross. Modeling the phase equilibria of hydrogen sulfide and carbon dioxide in mixture with hydrocarbons and water using the PCP-SAFT equation of state. *Fluid Phase Equilib.*, 147(1-2):7–23, 2010.

[69] D. E. Matschke and G. Thodos. Vapor-liquid equilibria for the ethane–propane system. *J. Chem. Eng. Data*, 7(2):232–234, 1962.

[70] B. H. Sage and W. N. Lacey. Phase equilibria in hydrocarbon systems - propane–n-pentane system. *Ind. Eng. Chem.*, 32:992–996, 1940.

[71] H. H. Reamer and B. H. Sage. Phase equilibria in hydrocarbon systems - volumetric and phase behavior of propane–n-decane system. *J. Chem. Eng. Data*, 11(1):17–24, 1966.

[72] H. G. Donnelly and D. L. Katz. Phase equilibria in the carbon dioxide–methane system. *Ind. Eng. Chem.*, 46:511–517, 1954.

[73] A.D. Leu and D. B. Robinson. Equilibrium phase properties of the n-butane–carbon dioxide and isobutane–carbon dioxide binary systems. *J. Chem. Eng. Data*, 32:444–447, 1987.

[74] C. Y. Tsang and W. B. Streett. Vapor-liquid equilibrium in the system carbon dioxide–dimethyl ether. *J. Chem. Eng. Data*, 26(2):155–159, 1981.

[75] A.-D. Leu and B. D. Robinson. Equilibrium phase properties of the n-butane–hydroen sulfide and isobutane–hydrogen sulfide binary systems. *J. Chem. Eng. Data*, 34:315–319, 1989.

[76] A. D. Leu, J. J. Carroll, and D. B. Robinson. The equilibrium phase properties of the methanol–hydrogen sulfide binary system. *Fluid Phase Equilib.*, 72:163–172, 1992.

Density functional theory for calculating surface tensions with a simple renormalization formalism for the critical point

Abstract

The calculation of interfacial properties, such as the surface tension, from the density functional theory suffers from the overestimation of the critical temperature of all classical Helmholtz energy functionals. A Helmholtz energy functional is here proposed, where the long-range density fluctuations leading to the universal critical scaling behavior are accounted for using a renormalization group theory. The appeal of the approach is its simple implementation, where the renormalization is treated in a local density approximation (LDA). The model is almost exact at the critical point. Away from the critical point, the model reduces to the perturbed chain statistical associated fluid theory (PC-SAFT) equation of state. The conventional PC-SAFT pure component parameters are supplemented with a single substance-specific renormalization parameter, which is adjusted to reproduce the bulk phase critical temperature. The surface tension is obtained with excellent agreement to experimental data for some non-polar and moderately polar substances (alkanes, ethers, acetates, aromatic substances) up to the critical point.

4.1   Introduction

The liquid-vapor surface tension influences and controls many processes in chemical or reservoir engineering applications. Membrane absorption contactors that are considered for the separation of acid gas from natural gas, for example, rely on non-wetted pores in order to ensure sufficiently high diffusion through the membrane layer. The control and modification of interfacial properties require predictive models that are based on molecular theories.

The most versatile and successful approach to describe interfaces from fluid theories is the classical density functional theory (DFT)[1, 2, 3]. The treatment of the inhomogeneous liquid-gas interface by van der Waals in 1894 is probably the first density functional study[4]. Despite this early development, the DFT was only further developed after the quantum DFT approach for the electron gas was developed. Hohenberg and Kohn[5] formalized the variational principle deriving a form that is the basis to all current implementations. In recent years accurate Helmholtz energy functionals have been proposed with the DFT and many applications were developed. We refer to recent reviews[6, 7, 8] for an overview.

There has been significant effort in developing equations of state that can be used to describe the thermodynamics and bulk phase equilibria of fluids and fluid mixtures. A successful family of equations of state is the statistical associating fluid theory (SAFT) which has been developed by Chapman et al.[9, 10] based on Wertheim's thermodynamic perturbation theory of first order (TPT1)[11, 12, 13, 14]. Several variants were suggested [15, 16, 17, 18, 19, 20, 21, 22], with widespread applications[23, 24]. For interfaces, a number of studies[25, 26, 27, 28, 29, 30] used the SAFT equation of state and the perturbed-chain SAFT (PC-SAFT) model with the Van der Waals' density-gradient theory to correlate the surface tension of pure components and binary mixtures. This appoach gives good agreement for the observed properties, however, with an additional adjustable parameter per component. The TPT1 of Wertheim is formulated in density functional form and it has successfully been applied to inhomogeneous associating fluids[31, 32, 33, 34, 35, 36, 37, 38, 39, 40, 41, 42, 43, 44]. Zhou improves the accuracy of functionals for the dispersive attraction[45, 46]. Helmholtz energy functionals for the chain formation[47, 48, 49, 50, 51, 52, 53] have been developed and accurate expressions have been proposed by Tripathi and Chapman[39, 40].

Gross[54] has applied the density functional theory with the PCP-SAFT equation of state using the approach of Gloor et al.[42] for vapor-liquid interfaces and obtained very accurate results without any additional parameter or reparameterization. Several studies consider the structural properties of hetero-segmented substances, such as block-copolymers [55, 56, 57, 41, 58, 59, 60]. The Helmholtz energy functionals of hetero-segmented fluids have the same form as for mixtures of different substances. However, studies applying the DFT to surface tensions of mixtures are somewhat scarce. Llovell et al. extended the SAFT-VR DFT treatment to deal with mixtures of chainlike molecules and their study provides a comprehensive review of applications of DFT to mixtures[61].

Most Helmholtz energy functionals that have been proposed, however, overestimate the critical point. For bulk phases, on the other hand, the renormalization-group theory[62, 63] has successfully been applied with classical equations of state in order to account for the long-range density fluctuations that appear in the vicinity of a critical point. White[64] has developed a renormalization group theory based on intermolecular properties. Lue and Prausnitz[65, 66] re-analyzed the partition function of the system adding some clear interpretation of the involved parameters. The renormalization group theory in the dialect considerd here, was applied to pure components by Jiang and Prausnitz[67], Mi et al.[68], Llovell et al.[69], Fu et al.[70] and to mixtures[71, 72]. The renormalization group theory was applied with the perturbed-chain SAFT (PC-SAFT) equation of state by Bymaster et al.[73] and by us[74] for pure components and mixtures, respectively.

It is very desirable to account for critical fluctuations also in the Helmholtz energy functionals applied to the calculation of interfacial properties. The surface tension, for example, vanishes at the critical point and errors in the calculated critical temperature lead to systematic offsets in the description of the surface tension. Kiselev and Ely [75] developed the generalized version of the corresponding states model combined with the density functional theory and crossover theory for the vapor-liquid interface and surface tension. McCabe and Kiselev[76] combined DFT with the variable-range SAFT equation of state applying a crossover scheme. Fu and Wu [35] proposed an equation of state based on the Yukawa intermolecular potential and they applied the model to bulk properties and interfaces using DFT. A renormalization group theory was considered to correct for critical fluctuations of bulk fluids but it was not applied in the DFT framework. Fu [77] applied an equation of state by using the density-gradient expansion, in which

the so-called influence parameter was obtained from the direct correlation func-
tion. However, solving the DFT and renormalization group theory was found to
be computationally difficult, so that for interfaces a constant influence parameter
was assumed reducing the DFT to the density-gradient theory.

In this work, a Helmholtz energy functional is proposed that accouts for critical
fluctuations through a renormalization theory. The renormalization is applied
with a local density approximation (LDA), leading to a simple model, which is
almost exact at the critical point. The renormalization theory is supplemented
with a stability constraint, since the LDA requires the evaluation of the Helmholtz
energy for densities, which for bulk fluids are in the instable region. The approach
is demonstrated for alkanes, aromatics, acetates, ethers far and near the critical
point.

4.2   Bulk phase equation of state

4.2.1   Classical PC-SAFT equation of state

The PC-SAFT equation of state is based on a coarse-grained molecular model,
where molecules are assumed to be chains of spherical segments exhibiting various
attractive interactions. The complete perturbed-chain statistical associating fluid
theory (PC-SAFT) equation of state is given as the sum of the ideal gas contri-
bution (id), a hard-sphere contribution (hs), a chain term (chain) connecting the
spherical segments, a contribution for the dispersive attraction (disp), a term for
associating interactions (assoc). The whole PC-SAFT equation of state written
in terms of Helmholtz energy is

$$F = F^{\mathrm{id}} + F^{\mathrm{hs}} + F^{\mathrm{chain}} + F^{\mathrm{disp}} + F^{\mathrm{assoc}} \tag{4.1}$$

For details on the PC-SAFT model we refer to the literature: The first four
terms on the right hand side of Eq. (4.1) were in detail described by Gross and
Sadowski[22]. The association term is a simplified version of Wertheim's TPT1
proposed by Chapman et al.[9, 78, 79] and together with the PC-SAFT equation
of state applied in several studies[80, 81, 82]. A substance i is represented by
only three pure component parameters: a segment size parameter σ_i, the number
of segments m_i, and the segment energy parameter ϵ_i/k. Associating substances
require two additional pure component parameters, the association energy $\epsilon^{A_i B_i}/k$

between association site A and site B, and the effective association volume $\kappa^{A_i B_i}$.

4.2.2 Renormalization group theory for PC-SAFT

The renormalization treatment with the PC-SAFT equation of state discussed in this study is in its outset based on the work of Bymaster et al.[73] providing corrections due to longrange density fluctuations near critical region. This approach has in a previous study been extended to mixtures[74]. While the approach required three adjustable parameters for the renormalization theory, we will here reduce the number to only a single parameter.

In the renormalization group theory the wavelength-coordinate is discretized so that wavelengths are binned in intervals (with index n) of representative wavepackets. The renormalization successively adds Helmholtz energy density contributions δf_n due to density fluctuations of increasing wavelength and the Helmholtz energy density for the nth recursive renormalization step is $f_n = f_{n-1} + \delta f_n$. Far from the critical point long-range fluctuations don't contribute to the Helmholtz energy and the equation of state then reduces to the PC-SAFT model. The Helmholtz energy density is calculated as

$$f = f^{\text{PC-SAFT}} + \sum_{n=1}^{\infty} \delta f_n \tag{4.2}$$

The recursive procedure should be carried out with n counting to infinity. In practice, the series converges after just a few iterations ($n = 5$)[83]. The term that corrects for long-wavelength fluctuations is for pure components

$$\delta f_n(\rho) = -K_n \ln \frac{\int_0^{\min(\rho, \rho^{max} - \rho)} \exp\left(-\frac{1}{K_n} G_n^D(\rho, \tau)\right) \, d\tau}{\int_0^{\min(\rho, \rho^{max} - \rho)} \exp\left(-\frac{1}{K_n} G_n^0(\rho, \tau)\right) \, d\tau} \tag{4.3}$$

The integrals in τ in this equation are for the amplitude of the density fluctuations. The upper integration bound limits the minimally and maximally allowed density to within the range from zero to $\rho^{max} = \frac{\sqrt{2}}{md^3}$. The coefficient K_n is defined as

$$K_n = \frac{k_B T}{(2^n L)^3} \tag{4.4}$$

where L is an adjustable pure component parameter. It is assumed that density

fluctuations of wavelengths below the cutoff length L are accurately captured by the classical equation of state. Eq. (4.3) represents the Helmholtz energy contribution of density fluctuations of wavelengths within the volume $(2^n L)^3$. The factor 2 scales the step-size for the successive renormalization steps[64].

The abbreviations $G_n^D(\rho, \tau)$ in Eq.(4.3) is the Helmholtz energy contribution of the successively increasing wavelengths (omitting a prefactor) and $G_n^0(\rho, \tau)$ is a normalization of the functional integration, that cuts the short wavelengths away[84, 65]. These functionals are approximated, as

$$G_n^D(\rho, \tau) = \frac{f_{n-1}(\rho+\tau) + f_{n-1}(\rho-\tau)}{2} - f_{n-1}(\rho) + \alpha(m\tau)^2 \frac{\phi w^2}{2^{2n+1}L^2} \qquad (4.5)$$

$$G_n^0(\rho, \tau) = \frac{f_{n-1}(\rho+\tau) + f_{n-1}(\rho-\tau)}{2} - f_{n-1}(\rho) + \alpha(m\tau)^2 \qquad (4.6)$$

where $-\alpha(m\rho)^2$ represents an attraction term (for a fluid of molecular density ρ and segment density $m\rho$). Further, ϕ is the average gradient of the wavelet function and is a pure component parameter. For fluids with Lennard-Jones segments, the two parameters α and w^2 are

$$\alpha = -\frac{1}{2} \int_\sigma^\infty \mathrm{d}r \, 4\pi r^2 \xi u^{attr}(r) = \frac{16\pi\epsilon\sigma^3\xi}{9} \qquad (4.7)$$

$$w^2 = -\frac{1}{3!\alpha} \int_\sigma^\infty \mathrm{d}r \, 4\pi r^2 r^2 \xi u^{attr}(r) = \frac{9\sigma^2}{7} \qquad (4.8)$$

Here, ξ is a pure component parameter ξ that was empirically introduced by Bymaster et al.[73]. The parameter scales to good approximation inverse with the number of segments per molecules. We omit this pure component parameter using the definition for α and w^2 as

$$\alpha = \frac{16\pi\epsilon\sigma^3}{9m} \qquad (4.9)$$

$$w^2 = \frac{9\sigma^2 m}{7} \qquad (4.10)$$

The segment number m in Eq. (4.10) is included to compensate the m in Eq. (4.9) so that Eq. (4.5) effectively remains unchanged. Another pure com-

ponent parameter, namely the cut-off length is set to $L = 2\sigma$ for all substances. This leaves the average gradient of the wavelet function ϕ in Eq. (4.5) as the only adjustable pure component parameter of the renormalization theory. For brevity, we refer to the resulting renormalized PC-SAFT equation of state as PC-SAFT-RG.

4.3   Classical density functional theory

In DFT the Helmholtz energy $F[\rho(\mathbf{r})]$ of an inhomogeneous fluid can be expressed as a functional of the density $\rho(\mathbf{r})$, where $\mathbf{r}$ can generally be a vector that characterizes the configuration (position, orientation, conformation, etc.) of molecules. In our modelling framework, the configuration of a fluid is not resolved and the vector $\mathbf{r}$ is only a positional vector and the appropriate density is the average segment density of a molecule. The grand potential $\Omega(T, \mu, [\rho(\mathbf{r})])$ is thereby expressed as the Helmholtz energy functional and the chemical potential which acts (as a Lagrangian multiplier) as a constraint on the number of particles. In the absence of an external field, it is

$$\Omega = F[\rho(\mathbf{r})] - \mu \int \mathrm{d}\mathbf{r} \, \rho(\mathbf{r}) \tag{4.11}$$

For a system in equilibrium, the grand potential functional is minimal

$$\left(\frac{\delta\Omega}{\delta\rho(\mathbf{r})} \right)_{\rho(\mathbf{r})=\rho_{eq}(\mathbf{r})} = 0 \tag{4.12}$$

With this condition, the density functional theory allows the calculation of equilibrium density-profiles $\rho_{eq}(\mathbf{r})$ in inhomogeneous systems. For a compact notation we omit the index 'eq' for the equilibrium density profile. These profiles are obtained by

$$0 = \frac{\delta F[\rho]}{\delta\rho(\mathbf{r})} - \mu \tag{4.13}$$

A Helmholtz energy functional based on the PC-SAFT equation of state was recently proposed[54]. It has the same structure as the Helmholtz energy for bulk

phases, Eq. (4.1), with

$$\frac{\delta F[\rho]/kT}{\delta \rho(\mathbf{r})} = \frac{\delta F^{\text{ig}}[\rho]/kT}{\delta \rho(\mathbf{r})} + \frac{\delta F^{\text{hs}}[\rho]/kT}{\delta \rho(\mathbf{r})} + \frac{\delta F^{\text{chain}}[\rho]/kT}{\delta \rho(\mathbf{r})}$$
$$+ \frac{\delta F^{\text{disp}}[\rho]/kT}{\delta \rho(\mathbf{r})} + \frac{\delta F^{\text{assoc}}[\rho]/kT}{\delta \rho(\mathbf{r})} \qquad (4.14)$$

The functional based on the PC-SAFT equation of state was shown to predict surface tensions quantitatively except for the immediate vicinity of the critical point. We refer to ref.[54] for details on the functional.

4.3.1   Combining PC-SAFT-RG and DFT

The hard-sphere functional of Eq. (4.14) according to the modified Fundamental Measure Theory[85, 86, 87, 88] is fully compatible with the PC-SAFT equation of state. The same holds for the expression accounting for the chain connectivities proposed by Tripathi and Chapman[39, 40]. The dispersion term of the PC-SAFT equations of state, however, is not formulated in density functional form. Gloor et al.[42, 43, 44] have proposed a scheme to adapt a bulk-phase equations of state to a DFT formalism. A DFT treatment for such a dispersive term is established based on perturbation theory written in functional form, while the (small) difference between this perturbation term and the dispersion term of the bulk-phase equations of state can be described with a local density approximation. It has been shown in our previous study that a first order non-local perturbation theory is sufficiently accurate and the addition of a non-local second order term does not change the results appreciably[54]. Following this approach we here formulate a simple functional for the dispersion term that contains a renormalization treatment for the critical point. It is given as a first order perturbation term (1PT) which is treated non-local and the excess of the renormalized PC-SAFT model to the 1PT-term, which is approximated locally (i.e. with a local density approximation), according to

$$\frac{\delta F^{\text{disp}}[\rho]}{\delta \rho} = \frac{\delta F^{\text{1PT}}[\rho]}{\delta \rho} + (\mu^{\text{disp,PC-SAFT-RG}} - \mu^{\text{1PT}}) \qquad (4.15)$$

Here, the superscript 'disp,PC-SAFT-RG' indicates the dispersive term of the PC-SAFT equation of state along with renormalization corrections from the sum

over δf_n of Eq. (4.2). The first order perturbation term $F^{1\mathrm{PT}}[\rho(\mathbf{r})]$ is obtained from a perturbation theory[54] which, for pairwise additive potentials, is exact

$$F^{PT}[\rho(\mathbf{r});T]/kT = \frac{1}{2}\int_0^1 d\varphi \sum_\alpha \sum_\beta \int\int d\mathbf{r}d\mathbf{r}' \, g_{\varphi,\alpha\beta}\left(\mathbf{r},\mathbf{r}';T\right)\rho_\alpha(\mathbf{r})\rho_\beta(\mathbf{r}')\frac{\phi_{\alpha\beta}^{PT}(\mathbf{r},\mathbf{r}')}{kT}$$

(4.16)

here the indices α and β run over all segments of polysegmented molecule 1 and 2, respectively. The parameter φ is a coupling parameter, that accomplishes a continuous transition from the reference fluid to the target fluid. The potential for each segment-segment interaction has the form $\phi(r) = \phi_0(r) + \varphi\phi^{PT}(r)$. The index $\alpha\beta$ is omitted in the potential, because all segments of a chain interact with the same potential. Eq. 4.16 is difficult to solve, because the pair correlation function $g_{\varphi,\alpha\beta}(\mathbf{r},\mathbf{r}';T)$ is not available for fluids with any value of φ between zero and one. Since, for dispersive interactions, the reference fluids pair correlation function is similar to that of the target fluid, we expand around the reference fluids pair correlation function. Hard-chains are here considered as the reference fluid. We simplify the treatment by not resolving the difference in the local density of various segments in the chain[38], so that $\rho_\alpha(\mathbf{r}) = \rho(\mathbf{r})$. For inhomogeneous conditions, the (hard-chain) pair correlation function is not well known and we have to make approximations: First, as proposed by Sokolowski and Fischer [89] we assume the segment pair correlation function of the homogeneous fluid at an average of the densities in $\mathbf{r}$ and $\mathbf{r}'$, with $\hat{\rho} = \frac{1}{2}(\rho(\mathbf{r}) + \rho(\mathbf{r}'))$. And secondly, we consider an average over the segment pair correlation function. The average segment-segment radial distribution is

$$g^{hc}\left(\hat{r},\hat{\rho}\right) = \frac{1}{m^2}\sum_\alpha\sum_\beta g_{\alpha\beta}^{hc}\left(\hat{r},\hat{\rho}\right)$$

(4.17)

where the index (hc) refers to segments of the hard-chain fluid and $\hat{r} = |\mathbf{r} - \mathbf{r}'|$ is a segment-segment distance for segments on two different chain-molecules. The first order perturbation term (index '1PT') then gets

$$F^{1\mathrm{PT}}[\rho]/kT = \frac{1}{2}\int\int d\mathbf{r}d\mathbf{r}' \, m^2 \, \rho(\mathbf{r}) \, \rho(\mathbf{r}') \, g^{hc}\left(\hat{r},\hat{\rho}\right) \frac{u^{PT}(\hat{r})}{kT}$$

(4.18)

This equation constitutes a non-mean field dispersion term, where a radial distribution function for chain fluids according to the Percus-Yevick closure, is

used[54].

The density fluctuations are long-ranged and the renormalization group theory applied here accounts for these density waves in a mean field local density approximation. The approach of Eq. (4.15), although simple, should give a reasonable account of the critical density fluctuations.

4.3.2   Surface tension

The surface tension of the system is the difference of the grand potential of the interface and of the bulk phase, according to

$$\gamma_{\mathrm{DFT}} = \frac{1}{A} \left(\Omega - \Omega_{bulk} \right) \tag{4.19}$$

where A denotes the surface area. The subscript 'DFT' has been introduced to the surface tension in Eq. (4.19) in order to indicate that this is the surface tension of a planar interface in the absence of long-range capillary waves. The reason is that we have approximated the grand potential omitting the influence of capillary waves. To include the capillary wave contribution, a simple approximation for the macroscopic surface tension is given as

$$\gamma = \gamma_{\mathrm{DFT}} \left(1 + \frac{3}{8\pi} \frac{T}{T_c} \frac{1}{(2.55)^2} \frac{1}{\kappa} \right)^{-1} \tag{4.20}$$

This model is based on the mode coupling theory[90] and is derived from a first order expansion of the universal critical scaling behavior. The relation can be extrapolated outside the critical region. In Eq. (4.20) the κ is the amplitude ratio. For the Ising model, the value is $\kappa = 0.24$[91]. In our previous study the amplitude ratio was used as a model constant that depends only on segment number m. It was adjusted to reproduce the surface tension of the alkane series[54], leading to $\kappa = 0.0045 + 0.0674m$. For detailed information, we refer to previous literature[54]. For not too large molecules the resulting value of κ is close to the value of the Ising model, while in this parameterization, the capillary wave contribution vanishes for substances with a large segment number m. Generally, capillary waves and the bulk phase density fluctuations that diverge at the critical point are physically related but a unified molecular theory bridging the DFT approach to the capillary wave theory has not yet been accomplished[92, 93, 94]. The critical renormalization does not fully account for the capillary wave contribution

which acts through the curvature of the interface.

4.4   Numerical implementation

The renormalization group theory is here applied with a local density approxima-tion within the DFT framework. This requires the evaluation of the Helmholtz energy for the complete density region between the two coexisting densities. This becomes a problem for the Helmholtz energy contributions to wave-packets of in-creasing wavelength, G_n^D. These, in some cases, give values smaller than zero in the instable region. That is an artifact of the approach, where a Van der Waals dispersion term is assumed to be driving the fluctuations, whereas other attac-tive contributions are accounted for in the bulk-phase equation of state. We have introduced the constraint, that $G_n^0 = 0$ and $G_n^D = 0$ when the original renorma-lization scheme gives values of G_n^0 or G_n^D lower than zero. The results with and without this constraint are illustrated in Figure.4.1. The results show an unreaso-nable deviation to the experimental data that is soley due to the renormalization procedure when the stability constraint is omitted. Quantitative agreement with the experimental data is obtained when the stability constraint is accounted for. No parameters were thereby adjusted to the interfacial data.

The renormalization scheme requires the integration of Eq. (4.3). We discreti-zed the density using 200 steps in the density interval from zero to ρ^{max} and used a trapez-rule for the numerical integration. At the end of the renormalization step, the discretized Helmholtz energy as a function of density was interpolated with cubic splines. Before interpolating the Helmholtz energy, however, we subtracted the ideal gas contribution for every grid point, because it introduces a logarith-mic density dependence for low densities. This makes linear or cubic interpolation schemes inadequate. The ideal gas contribution was analytically added only after completion of the renormalization procedure. This leads to robust results also at low component densities.

For the numerical procedure for solving the density functional theory, Eq. (4.13), we refer to a previous study[54].
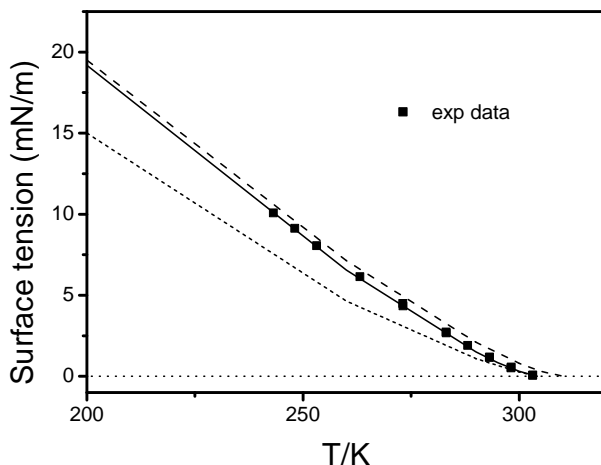
Figure 4.1: *Comparison of the proposed DFT with stability constraint (solid line) and without the stability constraint (short dashed line) to experimental data[95, 96] for the surface tension of CO_2 (closed symbols). Results of the non-renormalized PC-SAFT-DFT is given for comparison (dashed line)*

4.5   Results and discussion

The renormalized PC-SAFT equation of state (abbreviated as PC-SAFT-RG) reduces to the classical PC-SAFT equation of state at conditions sufficiently far from the critical point. The pure component parameters of the classical PC-SAFT equation of state can therefore be used without modification[22]. As opposed to Bymaster et al.[73] and our previous work[74] where three additional renormalization parameters were needed, the renormalization procedure proposed here requires the average wavelet gradient ϕ as the only additional pure component parameter. It is determined from bulk phase calculations. All pure component parameters are summarized in Table 4.1. The critical point calculated from the PC-SAFT-RG and the PC-SAFT model is in Table 4.2 compared with experimental data. The renormalization procedure clearly improves the agreement with experimental data for critical temperature and critical pressure. The renormalization parameter ϕ is determined by enforcing the experimental critical temperature. The parameter ϕ is thereby well-behaved with segment number, as illustrated in Figure 4.2.
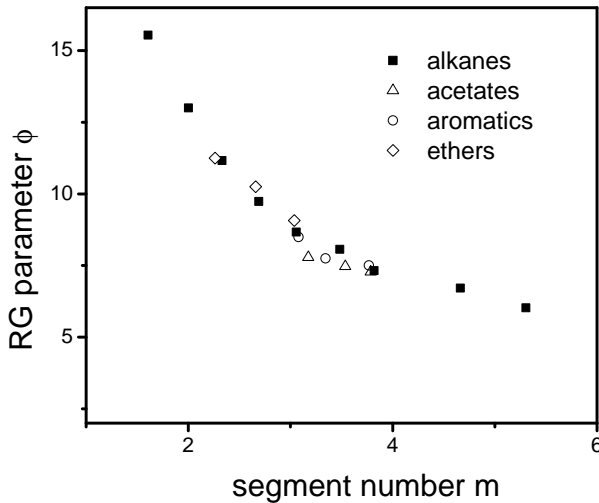
Figure 4.2: *The renormalization group theory parameter ϕ is well-behaved with segment number m, for alkanes, acetates, aromatics and ethers*

Results of PC-SAFT-RG and PC-SAFT models for the surface tension of some n-alkanes (butane, octane, and dodecane) are in Figure 4.3 compared with experimental data (closed symbols). Throughout this work open symbols represent extrapolated results of experimental data using empirical correlations taken from reference[97]. Far from the critical region, both models show quantitative agreement with the experimental data. Close to the critical region the classical PC-SAFT equation of state overestimates the critical temperature and thus also the surface tension. The renormalized equation of state is also in this region in quantitative agreement to the experimental values. For hexane the model is also applied neglecting the capillary wave contribution, in order to illustrate the contribution of Eq. (4.20). Figure 4.3 shows that capillary waves give a small but non-negligible contribution to the results in our parameterization.

Table 4.1: *Molecular Parameters and RG Parameter ϕ*

Component	m	σ (Å)	$\epsilon/k_B(K)$	ϕ
CO_2	2.0727	2.7852	169.21	11.38
ethane	1.6069	3.5206	191.42	15.54
propane	2.2220	3.6184	208.11	13.00
butane	2.3316	3.7086	222.88	11.16
pentane	2.6896	3.7729	231.20	9.74
hexane	3.0576	3.7983	236.77	8.67
heptane	3.4831	3.8049	238.40	8.07
octane	3.8176	3.8373	242.78	7.32
decane	4.6632	3.8373	242.78	6.71
dodecane	5.3060	3.8959	249.21	6.02
methylacetate	3.1756	3.1872	234.107	7.79
ethylacetate	3.5371	3.3079	230.801	7.47
propylacetate	3.7863	3.4227	235.758	7.285
ethylbenzene	3.0801	3.7974	287.348	8.49
n-propylbenzene	3.3435	3.8438	288.128	7.75
n-butylbenzene	3.7668	3.8727	283.072	7.50
dimethylether	2.2623	3.2766	212.934	11.25
methylethylether	2.6587	3.3729	216.010	10.25
diethylether	3.0369	3.4857	217.641	9.07

Table 4.2: *Critical Constants Compared with Experimental Data*

Component	$T_c(K)$			$P_c(MPa)$			$\rho_c(kg/m^3)$		
	exp	RG	PC-SAFT	exp	RG	PC-SAFT	exp	RG	PC-SAFT
CO_2	304.2	304.2	310.3	7.38	7.45	8.06	468	473	441
ethane	305.3	305.3	308.9	4.87	4.96	5.16	203	203	192
propane	369.8	369.8	375.1	4.25	4.34	4.61	217	222	209
butane	425.1	425.1	432.5	3.80	3.90	4.22	228	231	219
pentane	469.7	469.7	479.3	3.37	3.46	3.83	232	238	223
hexane	507.6	507.6	519.3	3.03	3.14	3.54	232	246	229
heptane	540.2	540.2	552.1	2.74	2.87	3.25	234	251	230
octane	568.7	568.7	583.1	2.49	2.60	3.02	232	256	231
decane	617.7	617.7	630.6	2.11	2.27	2.59	231	257	231
dodecane	658.0	658.0	673.3	1.83	1.95	2.27	226	261	228
methylacetate	506.6	506.6	521.8	4.75	4.93	5.78	325	353	320
ethylacetate	523.3	523.3	537.8	3.88	4.05	4.74	308	332	303
propylacetate	549.7	549.6	564.2	3.36	3.55	4.14	296	278	294
ethylbenzene	617.2	617.2	632.3	3.61	3.77	4.28	284	302	280
n-propylbenzene	638.4	638.4	656.2	3.2	3.36	3.9	273	310	280
n-butylbenzene	660.5	660.5	676.3	2.89	3.01	3.46	270	296	269
dimethylether	400.1	400.1	407.3	5.37	5.49	5.94	271	279	260
methylethylether	437.8	437.8	445.5	4.40	4.62	5.04	272	280	264
diethylether	466.7	466.7	476.0	3.64	3.81	4.23	266	276	256

Figure 4.3: *Comparison of the DFT with the PC-SAFT equation of state including renormalization corrections (solid line) and without renormalization theoy (dashed line) to experimental data (closed symbols) for the surface tension of three alkanes: n-butane[96, 95, 98, 99, 100], n-hexane[100], and n-dodecane[96]. For hexane, results omitting the capillary wave contribution are also shown (dashed dotted line)*

Figure 4.4 compares the two models with experimental data (closed symbols) of ethylbenzene, n-propylbenzene, and n-butylbenzene as representatives of aromatic substances. The insert in the figure gives a rescaled view around the critical temperature. Near the critical region, the renormalization group contributions lead to excellent results of the PC-SAFT-RG model.

The surface tension of two further chemical families are studied here, i.e. acetates in Figure 4.5 and ethers in Figure 4.6. These confirm the observation, that the renormalization treatment can be considered in a local density approximation to the DFT. Quantitative results are obtained for all substances of moderate polarity. In our previous study we have already shown, that small compounds with high dipolar moment require a resolution of the orientational distribution function. Dimethylether, in Figure 4.6 is an example of a substance where the orientational distribution function has to be resolved for a better agreement with experimental data.
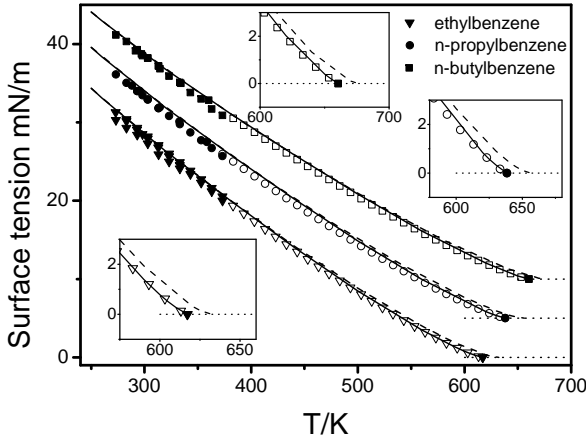
Figure 4.4: *Comparison of the DFT with the PC-SAFT equation of state including renormalization corrections (solid line) and without renormalization theoy (dashed line) to experimental data (closed symbols) for the surface tension of three aromatics: ethylbenzene[101, 96, 102], n-propylbenzene[101, 103, 104], and n-butylbenzene[101, 103, 104]*
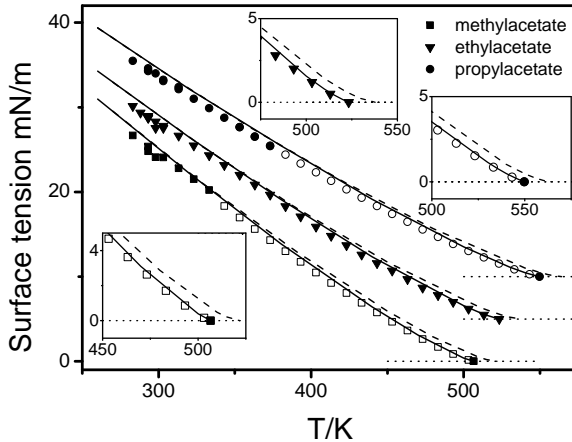
Figure 4.5: *Comparison of the DFT with the PC-SAFT equation of state including renormalization corrections (solid line) and without renormalization theoy (dashed line) to experimental data (closed symbols) for the surface tension of three acetates: methylacetate[105, 96], ethylacetate[106, 107, 108, 105, 96, 100], and n-propylacetate[107, 105, 96]*
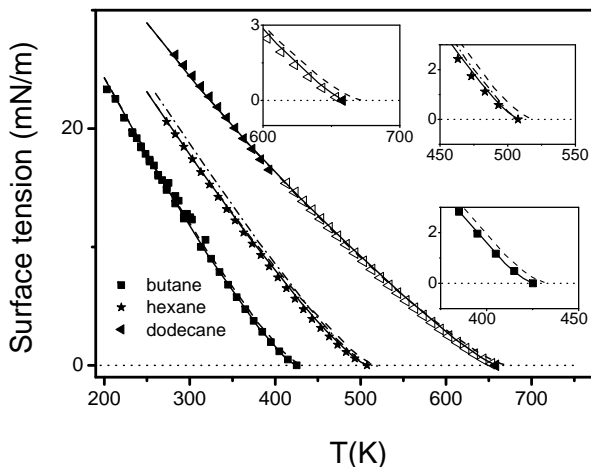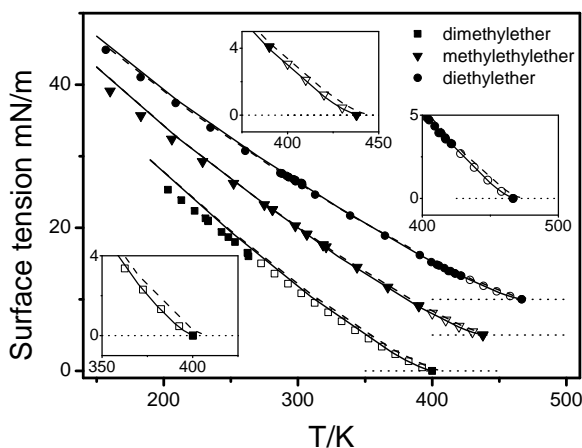
Figure 4.6: *Comparison of the DFT with the PC-SAFT equation of state including renormalization corrections (solid line) and without renormalization theoy (dashed line) to experimental data (closed symbols) for the surface tension of three acetates: methyl-ethyl-ether[109, 108, 110], dimethyl-ether[95, 96, 107], and diethylether[96, 108, 110, 107, 103, 111]*

4.6   Conclusion

A simple Helmholtz energy functional based on the PC-SAFT equation of state is proposed, where a renormalization group theory leads to excellent results of the critical point. Away from the critical point, the results of the PC-SAFT equation are recovered. The pure component parameters of the model are those of the classical PC-SAFT equation, supplemented with a single pure component parameter for the renormalization scheme. The calculated surface tension for real substances is found in excellent quantitative agreement with the experimental data up to the critical point. No parameters were adjusted to interfacial properties.

REFERENCES

[1] R. Evans. *Fundamentals of Inhomogeneous Fluids*, chapter 3. CRC Press, New York, 1 edition, 1992.

[2] H.T. Davis. *Statistical Mechanics of Phases and Interfaces, and Thin Films.* Wiley-VCH, Weinheim, 1996.

[3] J. S. Rowlinson and B. Widom. *Molecular Theory of Capillarity*. Oxford University Press, Oxford, 1989.

[4] J. D. van der Waals. The thermodynamic theory of capillarity under the hypothesis of a continuous variation of density, translated and reprinted in J. Statical Physics 20, 200 (1979). *Zeitschrift für Physikalische Chemie Stöchiom. Verwandtschaftsl.*, 13:657, 1894.

[5] P. Hohenberg and W. Kohn. Inhomogeneous electron gas. *Phys. Rev. B*, 136(3B):B864–B871, 1964.

[6] H. Löwen. Density functional theory of inhomogeneous classical fluids: recent developments and new perspectives. *J. Physics: Condensed Matter*, 14(46):11897–11905, 2002.

[7] J. Z. Wu. Density functional theory for chemical engineering: from capillarity to soft materials. *AIChE*, 52(3):1169–1193, 2006.

[8] J. Z. Wu and Z. Li. Density-functional theory for complex fluids. *Annu. Rev. Phys. Chem.*, 58(1):85–112, 2007.

[9] W. G. Chapman, G. Jackson, and K. E. Gubbins. Phase equilibria of associating fluids. chain molecules with multiple bonding sites. *Mol. Phys.*, 65:1057–1079, 1988.

[10] W. G. Chapman, K. E. Gubbins, G. Jackson, and M. Radosz. SAFT-equation-of-state solution model for associating fluids. *Fluid Phase Equilib.*, 52:31–38, 1989.

[11] M. S. Wertheim. Fluids with highly directional attractive forces. I. Statistical thermodynamics. *J. Stat. Phys.*, 35:19–34, 1984.

[12] M. S. Wertheim. Fluids with highly directional attractive forces. II. Thermodynamic perturbation theory and integral equations. *J. Stat. Phys.*, 35:35–47, 1984.

[13] M. S. Wertheim. Fluids with highly directional attractive forces. III. Multiple attraction sites. *J. Stat. Phys.*, 42:459–476, 1986.

[14] M. S. Wertheim. Fluids with highly directional attractive forces. IV. Equilibrium polymerization. *J. Stat. Phys.*, 42:477–492, 1986.

[15] S. H. Huang and M. Radosz. Equation of state for small, large, polydisperse and associating molecules. *Ind. Eng. Chem. Res.*, 29:2284–2294, 1990.

[16] S. H. Huang and M. Radosz. Equation of state for small, large, polydisperse, and associating molecules: extensions to fluid mixtures. *Ind. Eng. Chem. Res.*, 30:1994–2005, 1991.

[17] A. Gil-Villegas, A. Galindo, P. J. Whitehead, S. J. Mills, G. Jackson, and A. N. Burgess. Statistical associating fluid theory for chain molecules with attractive potentials of variable range. *J. Chem. Phys.*, 106:4168–4186, 1997.

[18] A. Galindo, L. A. Davies, A. Gil-Villegas, and G. Jackson. The thermo-dynamics of mixtures and the corresponding mixing rules in the SAFT-VR approach for potentials of variable range. *Mol. Phys.*, 93(2):241–252, 1998.

[19] F. J. Blas and L. F. Vega. Prediction of binary and ternary diagrams using the statistical associating fluid theory (SAFT) equation of state. *Ind. Eng. Chem. Res.*, 37:660–674, 1998.

[20] J. C. Pámies and L. F. Vega. Vapor-liquid equilibria and critical behavior of heavy n-alkanes using transferable parameters from the Soft-SAFT equation of state. *Ind. Eng. Chem. Res.*, 40:2532–2543, 2001.

[21] J. Gross and G. Sadowski. Application of perturbation theory to a hard-chain reference fluid: An equation of state for squarewell chains. *Fluid Phase Equilib.*, 168:183–199, 2000.

[22] J. Gross and G. Sadowski. Perturbed-chain SAFT: an equation of state based on a perturbation theory for chain molecules. *Ind. Eng. Chem. Res.*, 40:1244–1260, 2001.

[23] S. P. Tan, H. Adidharma, and M. Radosz. Recent advances and applications of statistical associating fluid theory. *Ind. Eng. Chem. Res.*, 47(21):8063–8082, 2008.

[24] X. Tang and J. Gross. Modeling the phase equilibria of hydrogen sulfide and carbon dioxide in mixture with hydrocarbons and water using the PCP-SAFT equation of state. *Fluid Phase Equilib.*, 293:11–21, 2010.

[25] H. Kahl and S. Enders. Calculation of surface properties of pure fluids using density gradient theory and SAFT-EOS. *Fluid Phase Equilib.*, 172(1):27–42, 2000.

[26] H. Kahl and S. Enders. Interfacial properties of binary mixtures. *Phys. Chem. Chem. Phys.*, 4(6):931–936, 2002.

[27] D. Duque, J. C. Pámies, and L. F. Vega. Interfacial properties of lennard-jones chains by direct simulation and density gradient theory. *J. Chem. Phys.*, 121:11395–11401, 2004.

[28] D. Fu. Investigation of surface tensions for pure associating fluids by perturbed-chain statistical associating fluid theory combined with density-gradient theory. *Ind. Eng. Chem. Res.*, 46:7378–7383, 2007.

[29] D. Fu and Y. Z. Wei. Investigation of vapor-liquid surface tension for carbon dioxide and hydrocarbon mixtures by perturbed-chain statistical associating fluid theory combined with density-gradient theory. *Ind. Eng. Chem. Res.*, 47(13):4490–4495, 2008.

[30] E. A. Muller and A. Mejia. Interfacial properties of selected binary mixtures containing n-alkanes. *Fluid Phase Equilib.*, 282(2):68–81, 2009.

[31] C.J. Segura, W.G. Chapman, and K.P. Shukla. Associating fluids with four bonding sites against a hard wall: density functional theory. *Mol. Phys.*, 90(5):759–771, 1997.

[32] C.J. Segura, E.V. Vakarin, W.G. Chapman, and M.F. Holovko. A comparison of density functional and integral equation theories vs Monte Carlo simulations for hard sphere associating fluids near a hard wall. *Mol. Phys.*, 108(12):4837–4848, 1998.

[33] O. Pizio, A. Patrykiejew, and S. Sokolowski. Evaluation of liquid-vapor density profiles for associating fluids in pores from density-functional theory. *J. Chem. Phys.*, 113(23):10761–10767, 2000.

[34] Y. X. Yu and J. Z. Wu. A fundamental-measure theory for inhomogeneous associating fluids. *J. Chem. Phys.*, 116(16):7094–7103, 2002.

[35] D. Fu and J. Z. Wu. Vapor-liquid equilibria and interfacial tensions of associating fluids within a density functional theory. *Ind. Eng. Chem. Res.*, 44(5):1120–1128, 2005.

[36] P. Bryk, S. Sokolowski, and O. Pizio. Density functional theory for inhomogeneous associating chain fluids. *J. Chem. Phys.*, 125(2):024909, 2006.

[37] H. Kahl and J. Winkelmann. Modified PT-LJ-SAFF density functional theory - I. Prediction of surface properties and phase equilibria of non-associating fluids. *Fluid Phase Equilib.*, 270(1-2):50–61, 2008.

[38] A. Dominik, S. Tripathi, and W. G. Chapman. Bulk and interfacial properties of polymers from interfacial SAFT density functional theory. *Ind. Eng. Chem. Res.*, 45(20):6785–6792, 2006.

[39] S. Tripathi and W. G. Chapman. Microstructure of inhomogeneous polyatomic mixtures from a density functional formalism for atomic mixtures. *J. Chem. Phys.*, 122(9):094506, 2005.

[40] S. Tripathi and W.G. Chapman. Microstructure and thermodynamics of inhomogeneous polymer blends and solutions. *Phys. Rev. Lett.*, 94(8):087801, 2005.

[41] S. Jain, A. Dominik, and W. G. Chapman. Modified interfacial statistical associating fluid theory: A perturbation density functional theory for inhomogeneous complex fluids. *J. Chem. Phys.*, 127(24):244904, 2007.

[42] G. J. Gloor, F. J. Blas, E. M. del Rio, E. de Miguel, and G. Jackson. A SAFT-DFT approach for the vapour-liquid interface of associating fluids. *Fluid Phase Equilib.*, 194:521–530, 2002.

[43] G. J. Gloor, G Jackson, F. J. Blas, EM del Rio, and E de Miguel. An accurate density functional theory for the vapor-liquid interface of associating chain molecules based on the statistical associating fluid theory for potentials of variable range. *J. Chem. Phys.*, 121(24):12740–12759, DEC 22 2004.

[44] Guy J. Gloor, George Jackson, F. J. Blas, E. Martin del Rio, and E. de Miguel. Prediction of the vapor-liquid interfacial tension of nonassociating and associating fluids with the SAFT-VR density functional theory. *J. Phys. Chem. C*, 111(43):15513–15522, NOV 1 2007.

[45] S. Q. Zhou. How to extend hard sphere density functional approximation to nonuniform nonhard sphere fluids: Applicable to both subcritical and supercritical temperature regions. *J. Chem. Phys.*, 124:144501, 2006.

[46] S. Q. Zhou. Reformulation of liquid perturbation theory for low temperatures. *Phys. Rev. E*, 79:011126, 2009.

[47] M. S. Wertheim. Thermodynamic perturbation-theory of polymerization. *J. Chem. Phys.*, 87(12):7323–7331, 1987.

[48] E. Kierlik and M. L. Rosinberg. A perturbation density-functional theory for polyatomic fluids. 1. Rigid molecules. *J. Chem. Phys.*, 97(12):9222–9239, 1992.

[49] E. Kierlik and M. L. Rosinberg. A perturbation density-functional theory for polyatomic fluids. 2. Flexible molecules. *J. Chem. Phys.*, 99(5):3950–3965, 1993.

[50] E. Kierlik and M. L. Rosinberg. Perturbation density-functional theory for polyatomic fluids. 3. Application to hard chain molecules in slitlike pores. *J. Chem. Phys.*, 100(2):1716–1730, 1994.

[51] M. Muller and L. G. MacDowell. Interface and surface properties of short polymers in solution: Monte Carlo simulations and self-consistent field theory. *Macromolecules*, 33(10):3902–3923, 2000.

[52] Y. X. Yu and J. Z. Wu. Density functional theory for inhomogeneous mixtures of polymeric fluids. *J. Chem. Phys.*, 117(5):2368–2376, 2002.

[53] A. Malijevsky, P. Bryk, and S. Sokolowski. Density functional approach for inhomogeneous star polymer fluids. *Phys. Rev. E*, 72(3):032801, 2005.

[54] J. Gross. A density functional theory for vapor-liquid interfaces using the PCP-SAFT equation of state. *J. Chem. Phys.*, 131:204705, 2009.

[55] D. Cao and J. Wu. Microstructure of block copolymers near selective surfaces: theoretical predictions and configurational-bias Monte Carlo simulation. *Macromolecules*, 38(3):971–978, 2005.

[56] J. Jin and J. Wu. A theoretical study for nanoparticle partitioning in the lamellae of diblock copolymers. *J. Chem. Phys.*, 128(7):074901, 2008.

[57] Z. Ye, H. Chen, H. Liu, Y. Hu, and J. Jiang. Density functional theory for copolymers confined in a nanoslit. *J. Chem. Phys.*, 126(13):134903, 2007.

[58] A. Bymaster, S. Jain, and W. G. Chapman. Microstructure and depletion forces in polymer-colloid mixtures from an interfacial statistical associating fluid theory. *J. Chem. Phys.*, 128(16):164910, 2008.

[59] S Jain and W. G. Chapman. Effect of confinement on the ordering of symmetric diblock copolymers: application of interfacial statistical associating fluid theory. *Mol. Phys.*, 107(1):1–17, 2009.

[60] S. Jain, V. V. Ginzburg, P. Jog, J. Weinhold, R. Srivastava, and W. G. Chapman. Modeling polymer-induced interactions between two grafted surfaces: comparison between interfacial statistical associating fluid theory and self-consistent field theory. *J. Chem. Phys.*, 131(4):044908, 2009.

[61] F. Llovell, A. Galindo, F. J. Blas, and G. Jackson. Classical density functional theory for the prediction of the surface tension and interfacial properties of fluids mixtures of chain molecules based on the statistical associating fluid theory for potentials of variable range. *J. Chem. Phys.*, 133:024704, 2010.

[62] K. G. Wilson. Renormalization group and critical phenomena. 1. Renormalization group and the Kadanoff scaling picture. *Phys. Rev. B: Condens. Matter*, 4(9):3174–3183, 1971.

[63] K. G. Wilson. Renormalization group and critical phenomena. 2. Phase-space cell analysis of critical behavior. *Phys. Rev. B*, 4(9):3184–3205, 1971.

[64] J. A. White. Contribution of fluctuations to thermal properties of fluids with attractive forces of limited range: theory compared with PρT and C_v data for argon. *Fluid Phase Equilib.*, 75:53–64, 1992.

[65] L. Lue and J. M. Prausnitz. Renormalization-group corrections to an approximate free-energy model for simple fluids near to and far from the critical region. *J. Chem. Phys.*, 108(13):5529–5536, 1998.

[66] L. Lue and J. M. Prausnitz. Thermodynamics of fluid mixtures near to and far from the critical region. *AIChE J.*, 44(6):1455–1466, 1998.

[67] J. Jiang and J. M. Prausnitz. Equation of state for thermodynamic properties of chain fluids near-to and far-from the vapor-liquid critical region. *J. Chem. Phys.*, 111:5964–5974, 1999.

[68] J. G. Mi, C. L. Zhong, Y. G. Li, and J. Chen. Renormalization group theory for fluids including critical region. I. Pure fluids. *Chem. Phys.*, 305(1-3):37–45, 2004.

[69] F. Llovell, J. C. Pámies, and L. F. Vega. Thermodynamic properties of Lennard-Jones chain molecules: renormalization-group corrections to a modified statistical associating fluid theory. *J. Chem. Phys.*, 121(21):10715–10724, 2004.

[70] D. Fu, X. Li, S. Yan, and T. Liao. Investigation of critical properties and surface tensions for n-alkanes by perturbed-chain statistical associating fluid theory combined with density-gradient theory and renomrlaization-group theory. *Ind. Eng. Chem. Res.*, 45(24):8199–8206, 2006.

[71] J. G. Mi, C. L. Zhong, and Y. G. Li. Renormalization group theory for fluids including critical region. II. Binary mixtures. *Chem. Phys.*, 312(1-3):31–38, 2005.

[72] F. Llovell and L. F. Vega. Global fluid phase equilibria and critical phenomena of selected mixtures using the crossover Soft-SAFT equation. *J. Phys. Chem. B*, 110(3):1350–1362, 2006.

[73] A. Bymaster, C. Emborsky, A. Dominik, and W. G. Chapman. Renormalization-group corrections to a perturbed-chain statistical associating fluid theory for pure fluids near to and far from the critical region. *Ind. Eng. Chem. Res.*, 47(16):6264–6274, 2008.

[74] X. Tang and J. Gross. Renormalization-group corrections to the perturbed-chain statistical associating fluid theory for binary mixtures. *Ind. Chem. Eng. Res.*, 49:9436–9444, 2010.

[75] S. B. Kiselev and J. F. Ely. Generalized corresponding states model for bulk and interfacial properties in pure fluids and fluid mixtures. *J. Chem. Phys.*, 119(16):8645–8662, 2003.

[76] C. McCabe and S. B. Kiselev. Application of crossover theory to the SAFT-VR equation of state: SAFT-VRX for pure fluids. *Ind. Eng. Chem. Res.*, 43(11):2839–2851, 2004.

[77] D. Fu. Investigation of surface tensions for pure fluids outside and inside the critical region. *Chinese Journal of Chemistry*, 24(10):1315–1320, 2006.

[78] G. Jackson, W. G. Chapman, and K. E. Gubbins. Phase equilibria of asso-
ciating fluids - spherical molecules with multiple bonding sites. *Mol. Phys.*,
65:1–31, 1988.

[79] C. G. Joslin, C. G. Gray, and W. G. Chapman. Theory and simulation of
associating liquid mixtures. II. *Mol. Phys.*, 62:843–860, 1987.

[80] J. Gross and G. Sadowski. Application of the peturbed-chain SAFT equa-
tion of state to associating systems. *Ind. Eng. Chem. Res.*, 41:5510–5515,
2002.

[81] N. V. Solms, M. L. Michelsen, and G. M. Kontogeorgis. Computational and
physical performance of a modified PC-SAFT equation of state for highly
asymmetric and associating mixtures. *Ind. Eng. Chem. Res.*, 42(5):1098–
1105, 2003.

[82] N. V. Solms, M. L. Michelsen, and G. M. Kontogeorgis. Applying association
theories to polar fluids. *Ind. Eng. Chem. Res.*, 43:1803–1806, 2004.

[83] L. Lue and J. M. Prausnitz. Thermodynamics of fluid mixtures near to and
far from the critical region. *AIChE*, 44(6):1455–1466, 1998.

[84] Y. Tang. Outside and inside the critical region of the Lennard-Jones fluid.
J. Chem. Phys., 109(14):5935–5944, 1998.

[85] Y. Rosenfeld.   Free-energy model for the inhomogeneous hard-sphere
fluid mixture and density-funtional theory of freezing.   *Phys. Rev. Lett.*,
63(9):980–983, 1989.

[86] R. Roth, R. Evans, A. Lang, and G. Kahl. Fundamental measure theory for
hard-sphere mixtures revisited: the white bear version. *J. Phys. Condens.
Matter*, 14(46):12063–12078, 2002.

[87] Y.X. Yu and J.Z. Wu. Structures of hard-sphere fluids from a modified
fundamental - measure theory. *J. Chem. Phys.*, 117:10156–10164, 2002.

[88] S. Phan, E. Kierlik, M. L. Rosinberg, B. Bildstein, and G. Kahl. Equivalence
of two free-energy models for the inhomogeneous hard-sphere fluid. *Phys.
Rev. E*, 48(1):618–620, 1993.

[89] S. Sokolowski and J. Fischer. The role of attractive intermolecular forces
in the density functional theory of inhomogeneous fluids. *J. Chem. Phys.*,
96(7):5441–5447, 1992.

[90] J. Meunier. Liquid interfaces - role of the fluctuations and analysis of ellip-
sometry and reflectivity measurements. *J. Phys.*, 48(10):1819–1831, 1987.

[91] K. Binder. Monte Carlo calculation of the surface tension for two- and three-dimensional lattice-gas models. *Phys. Rev. A*, 25(3):1699–1709, Mar 1982.

[92] D. Bedeaux. *Advances in Chemical Physics: Nonequilibrium Thermodynamics and Statistical Physics of Surfaces*, volume 64. John Wiley and Sons, Inc., 1986.

[93] K. R. Mecke and S. Dietrich. Effective hamiltonian for liquid-vapor interfaces. *Phys. Rev. E*, 59(6):6766–6784, Jun 1999.

[94] P. Tarazona, R. Checa, and E. Chacón. Critical analysis of the density functional theory prediction of eenhanced capillary waves. *Phys. Rev. Lett.*, 99(19):196101, 2007.

[95] W. Braker and A. L. Mossman. *The Matheson Unabridged Gas Data Book*, volume 4. Matheson Gas Products, East Rutherford, New Jersey, 1974.

[96] J. J. Jasper. The surface tension of pure liquid compounds. *J. Phys. Chem. Ref. Data*, 1(4):841–1009, 1972.

[97] Bruce E. Poling, John M. Prausnitz, and John P. O'connell. *The Properties of Gases and Liquids*, chapter 12. McGraw-Hill, New York, 5 edition, 2001.

[98] J. C. Calado, I. A. McLure, and V. A. Soanes. Surface tension for octa-fluorocyclobutane, n-butane and their mixtures from 233 K to 254 K, and vapour pressure, excess Gibbs function and excess vlume for the mixtures at 233 K. *Fluid Phase Equilib.*, 2:199–213, 1978.

[99] D. L. Katz and W. Saltman. Surface tension of hydrocarbons. *J. Ind. Eng. Chem.*, 31:91–94, 1939.

[100] N. B. Vargaftik, Y. K. Vinogradov, and V. S. Yargin. *Handbook of Physical Properties of Liquids and Gases, Pure Substances and Mixtures*. begell house, New York, Wallingford, 3 edition, 1996.

[101] *Selected Values of Properties of Hydrocarbons and Related Compounds, American Petroleum Institute Research Project 44, loose-leaf sheet, extant.* Thermodynamic Research Center, Texas A & M University, College Station, Texas, 56 edition, 1980.

[102] A. Watanabe and S. Sugiyama. Temperature coefficient of surface tension for organic liquids of homologous series. *Nippon Kagaku Kaishi*, pages 2047–2051, 1973.

[103] A. I. Vogel. Physical properties and chemical constitution: Part X. n-alkyl benzenes. *J. Chem. Soc.*, pages 607–610, 1948.

[104] R. E. Donaldson and O. R. Quayle. A study of organic parachors. X. Para-
chors of American petroleum institute - national bureau of standards hydro-
carbons: Benzene and homologs of benzene. *J. Am. Chem. Soc.*, 72:35–36,
1950.

[105] S. A. Mumford and J. W. C. Phillips. The physical properties of some
aliphatic compounds. *J. Chem. Soc.*, pages 75–84, 1950.

[106] R. E. Kirk. *Encyclopedia of Chemical Technology*, volume 22. Wiley Inter-
science, New York, 2 edition, 1966.

[107] J. A. Riddick and W. B. Bunger. *Organic Solvents: Physical Properties and
Methods of Purificatio*. Wiley Interscience, New York, 3 edition, 1970.

[108] J. Timmermans. *Physico-Chemical Constants of Pure Organic Substances*,
volume 2. Elsevier, Amsterdam, London, 1965.

[109] E. W. Washburn. *International Critical Tables of Numerical Data, Physics,
Chemistry, and Technology*, volume 7. McGraw-Hill, New York, 1926-1933.

[110] S. Sugden. The variation of surface tension with temperature and some
related functions. *J. Chem. Soc.*, 125:32–41, 1924.

[111] T. O. Jeffries, M. Derrick, and B. Musgrave. Surface tension of ether and
pentane. *J. Chem. Phys.*, 23:1730, 1955.

Modeling the phase equilibria of carbon dioxide and hydrogen sulfide in aqueous electrolyte systems at elevated pressure

Abstract

The solubility of carbon dioxide (CO_2) and hydrogen sulfide (H_2S) in basic aqueous electrolyte solutions is determined by a combined phase and reaction equilibrium. A cubic equation of state is applied to model the vapor-liquid equilibria of these reacting systems. The Peng-Robinson equation of state with Wong-Sandler mixing rules is combined with an extended UNIQUAC model for electrolytes where ion-specific interactions are determined from a Debye-Hückel term. The thermodynamic model is parameterized for aqueous systems containing carbon dioxide and hydrogen sulfide along with water and potassium carbonate solutions at high pressure. The UNIQUAC binary interaction parameters are estimated by minimizing deviations in the liquid phase composition of the model with respect to the experimental data. The data is taken from literature and is supplemented by own experimental work conducted as part of this study.

5.1   Introduction

Hydrocarbon gas streams may contain high levels of CO_2 and/or H_2S as contaminants. These contaminants have to be removed to meet product quality and to prevent greenhouse gas emissions. A prominent technology for the separation of the contaminants is absorption/desorption using aqueous electrolyte solutions[1, 2, 3, 4, 5, 6, 7]. For the design and optimization of these processes, a sound model of the occurring phase equilibria is mandatory.

For mixtures with electrolytes, useful methods for practical phase equilibrium calculations have been studied [8, 9, 10]. Models for the correlation of salt effect in aqueous solutions[11, 12, 13, 14, 15, 16] have been reviewed by Sander et al.[17].The model applied by Thomsen et al.[18] combines a Debye-Hückel term with the UNIQUAC equation. This model was used for the liquid phase in combination with the Soave-Redlich-Kwong equation for the vapor phase[19]. Aqueous electrolyte solutions containing CO_2 and/or NH_3 were well described with this approach[19]. But when using two different models for the liquid phase and the vapor phase, the properties of the two phases will not become identical, so that the vapor-liquid critical region behavior is incorrectly described.

Wong and Sandler[20] developed a scheme where an excess Gibbs energy model is used within a mixing rule of a cubic equation of state. This circumvents the inconsistencies of different models for the vapor and the liquid phase, while maintaining the flexibility of the excess Gibbs energy models. In 1995, the original Wong-Sandler mixing rule was reformulated by Orbey and Sandler[21] in a way that eliminates one of its parameters and makes a smooth transition from activity coefficient-like behavior to the classical van der Waals mixing rule.

In this work, we apply an electrolyte variant of the UNIQUAC model (extended UNIQUAC) with the Peng-Robison equation of state. We solve for the simultaneous phase equilibrium and reaction equilibrium and apply the model to the solubility of CO_2 in aqueous solutions of potassium carbonate. Wide ranges of concentration are thereby covered in a temperature region of 273 K to 383 K and pressures up to 90 bar for this system.

5.2   Equation of state

The first practical cubic equation of state was proposed by J. D. van der Waals
in 1873[22] and written as

$$P = \frac{RT}{V - b} - \frac{a}{V^2} \tag{5.1}$$

with the constant b is the excluded volume, i. e. that part of the molar volume
which is not available to a molecule due to the presence of others. The parameter
a is a measure of the attractive forces between the molecules. When a and b are
taken as zero the ideal gas equation is recovered.

The van der Waals equation can only be used in a small, temperature-range,
because with constant parameters, it quickly deviates from the behaviour of real
fluids. Redlich-Kwong (1949)[23, 24] introduced temperature dependence and
slightly different volume dependence

$$P = \frac{RT}{V - b} - \frac{a(T)}{V(V + b)} \tag{5.2}$$

with the expressions for $a(T)$, and b

$$a(T) = 0.42748 \frac{R^2 T_c^{\;2}}{P_c} \alpha(T) \tag{5.3}$$

$$b = 0.08664 \frac{RT_c}{P_c} \tag{5.4}$$

with the dimensionless function $\alpha(T) = (\frac{T}{T_c})^{-\frac{1}{2}}$ depending on the temperature
and the critical temperature.

A breakthrough came from Soave's modification (1972)[25] for the α parame-
ter,

$$\sqrt{\alpha(T)} = 1 + \kappa(1 - \sqrt{\frac{T}{T_c}}) \tag{5.5}$$

and $\kappa = 0.480 + 1.574\omega - 0.176\omega^2$, where ω is the acentric factor. This
breakthrough resulted in more accurate pressure predictions.

A slightly different approach was introduced[26] by Peng and Robinson (1976),
who used a different volume dependence to give improved liquid volumes and chan-

ged the temperature dependence of α to give accurate vapour pressure predictions

$$P = \frac{RT}{V - b} - \frac{a(T)}{V(V + b) + b(V - b)} \tag{5.6}$$

with parameter $a(T)$ and b writen as

$$a(T) = 0.45724 \frac{R^2 T_c^{\ 2}}{P_c} \alpha(T) \tag{5.7}$$

and

$$b = 0.07780 \frac{RT_c}{P_c} \tag{5.8}$$

where $\alpha(T)$ is defined as same as in Eq.(5.5),
   while

$$\kappa = 0.37464 + 1.54226\omega - 0.26992\omega^2 \tag{5.9}$$

Although other α functions have been proposed, the Peng-Robinson and Soave-Redlich-Kwong equations are widely used in industry, especially for refinery and reservoir simulation. The real power of the equation of state description lies in that starting with relatively little information (Tc, Pc, and ω of the pure components), the phase equilibrium, phase densities, and other thermodynamic properties can be obtained.

However, these equations do have some important shortcomings. For example, liquid densities are not well predicted, the generalized parameters are not accurate for nonhydrocarbons, and these equations do not lead to accurate predictions for long-chain molecules.

Since Peng-Robinson equation of state is only useful for hydrocarbons and inorganic gases (O_2, N_2, CO_2, etc)[27]. To get accurate vapour-liquid equilibrium including polar fluids (water, organic acids, alcohols, etc) a modified Peng-Robinson equation is introduced by Stryjek and Vera (1986) which is referred to by PRSV equation of state[24] This modification introduces another constant that is specific for each pure compound and is given in Ref. [24]. In their approach Eq.(5.9) is replaced by the relation

$$\kappa = \kappa_0 + \kappa_1 (1 + \sqrt{\frac{T}{T_c}})(0.7 - \frac{T}{T_c}) \tag{5.10}$$

with $\kappa_0 = 0.378893 + 1.4897153\omega - 0.17131848\omega^2 + 0.0196554\omega^3$

Table 5.1: *Parameters of pure CO_2, H_2S, H_2O and electrolytes*

Component	T_c/K[a]	P_c/bar[a]	ω[a]	κ_1[a]	ΔG_f[b] /(kJ/mol) (Aq.)	ΔH_f[b] /(kJ/mol) (Aq.)	r[c]	q[c]	a[c]	b[c]	c[c]
CO_2	304.2	73.83	0.224	0.04285	-385.98	-413.8	1.30[g]	1.12[g]	243.057[f]	0[f]	0[f]
H_2S	373.09[d]	89.43[d]	0.1[d]	0.0316[d]	–	–	2.333[e]	2.326[e]	–	–	–
H_2O	647.1	220.55	0.345	-0.0663	-237.13	-285.83	0.92[a]	1.4[a]	58.37	0.03896	523.88
HCO_3^-	–	–	–	–	-586.77	-691.99	11.073	13.529	-51.5	0	0
H^+	–	–	–	–	0	0	0.13779	10-15	0	0	0
CO_3^{2-}	–	–	–	–	-527.81	-677.14	11.222	10.53	-268.0	0	0
OH^-	–	–	–	–	-157.24	-229.99	9.3973	8.8171	1418.2	-3.4446	-51473
K^+	–	–	–	–	-283.27	-252.38	2.2304	2.4306	415.09	-0.8142	-16316

[a] Ref.[28]
[b] Ref.[29]
[c] Ref.[30]
[d] Ref.[31]
[e] Ref.[32]
[f] Ref.[19]
[g] Ref.[33]

This modification of the Peng-Robinson equation of state (PRSV) is applied in Chapter 5 to describe the vapour-liquid equilibrium of CO_2 and water (highly polar).

The Peng-Robinson equation of state according to Stryjek and Vera (PRSV)[24] is applied in this work to describe the vapor-liquid equilibrium of CO_2/H_2S in water and in aqueous electrolyte solutions. The equations of state requires four pure component parameters, i.e. the critical temperature and pressure (Tc, Pc), the acentric factor ω, and pure component parameter κ_1 for each component.

The thermodynamic model used within the G^E-mixing rule is the extended UNIQUAC model described by Nicolaisen[34]; it extends the original UNIQUAC model[33] by a Debye-Hückel term to account for the specific contributions from the charged species. The extended UNIQUAC model consists of three terms

$$G^{Ex} = G^{Ex}_{Combinational} + G^{Ex}_{Residual} + G^{Ex}_{Debye-Huckel} \tag{5.11}$$

The UNIQUAC model requires two pure component parameters, i.e the volume r_i and the surface q_i parameter and the model provides the energy parameters u^0_{ki} and u^T_{ki} as adjustable parameters for every pair of components, with

$$u_{ki} = u^0_{ki} + u^T_{ki}(T/K - 298.15) \tag{5.12}$$

The pure component parameters are taken from literature and are summarized in Table 5.1.

5.3   Phase and reaction equilibrium

For the binary pairs CO_2/water and H_2S/water, the dissociation of CO_2 and H_2S in the liquid phase is very low and it can at our conditions be neglected[35]. However, for CO_2/potassium carbonate aqueous solutions system, the dissociation of carbon dioxide in the liquid phase increases the solubility of CO_2. When carbon dioxide is added to an aqueous solution of potassium carbonate in small amounts, the CO_2 gas is almost completely chemically dissolved. However, at higher concentrations when most potassium carbonate has reacted, carbon dioxide becomes more and more physically dissolved leading to an increase of the total pressure. We consider ionic species to be present only in the liquid phase and limit chemical equilibrium calculations to the liquid phase. The equilibrium can

then be formulated as

Phase equilibrium

$$CO_{2(g)} \longleftrightarrow CO_{2(l)} \tag{5.13}$$

$$H_2O(g) \longleftrightarrow H_2O(l) \tag{5.14}$$

Reaction equilibrium

$$CO_{2(l)} + H_2O_{(l)} \longleftrightarrow HCO_3^- + H^+ \tag{5.15}$$

$$HCO_3^- \longleftrightarrow CO_3^{2-} + H^+ \tag{5.16}$$

$$H_2O_{(l)} \longleftrightarrow H^+ + OH^- \tag{5.17}$$
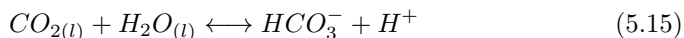
The influence of the dissociation of the electrolytes on the solubility of CO_2 in potassium carbonate is accounted for by the Debye-Hückel term in the extended UNIQUAC model and by the chemical reaction equilibria. The balance equation for the amount of substance (the number of moles) of a species i in the liquid solution is

$$n_i = n_i^0 + \sum_j n_{i,j} \xi_j \tag{5.18}$$

where ξ_j is the extent of reaction j and n_i^0 denotes the initial amount of component i. The reaction equilibrium constants were determined in the standard way[28]. Correlations of heat capacity values with temperature are needed for the calculation of the reaction equilibrium constant; these correlations for C_p^0 (in $J/mol^{-1}K^{-1}$) are taken from literature [18] with parameters a, b and c summarized in Table 5.1. The values for $\Delta^f G^0$ and $\Delta^f H^0$ for components in the aqueous phase are also given in Table 5.1.

5.4   Parameter optimization

A modified Levenberg-Marquardt algorithm was used to adjust binary interaction energy parameters (u_{ki}^0, u_{ki}^T) of the model to experimental data. The objective function is written as the relative absolute deviations in mole fractions. All derivatives for the gradient-based algorithm are taken by numerical differentiation.

5.5   Experiments

CO_2 was obtained from Hoek Loos (Schiedam, the Netherlands), with a supplier given purity of 99.995 mol-%. Potassium carbonate was obtained from J.T. Baker (Deventer, the Netherlands), purchased with a purity of 99.0 mass-% minimum. The water content was determined to be 1.2 mass-% since the container was exposed to air. The uncertainty in the temperature measurements is better than 0.03 K for the measurements, and the pressure uncertainty was 0.003 MPa at pressures below 50 bar and 0.01 MPa at higher pressure, with a Cailletet apparatus[36]. The experiments were performed according to the synthetic method using high-pressure view cells. Details about these setups, instrumentation, uncertainties, and experimental procedure are given by Steen and Loos [37].

5.6   Results and discussion

5.6.1   Binary system of CO_2 - water and H_2S - water

The estimation of UNIQUAC binary interaction energy parameters, u_{ki}^0 and u_{ki}^T are carried out by minimizing the deviation in the relative liquid phase composition $|x_i^{calc} - x_i^{exp}|/x_i^{exp}$ of the model with respect to the experimental data. No additional binary interaction parameters k_{ij} are used along with the Wong-Sandler mixing rule. The resulting deviations to the experimental data for CO_2/water and H_2S/water are summarized in Table 5.2 and Table 5.3, respectively. The deviations are reported according to

$$(\%AARD)(x) = \frac{100}{N} \sum_{i=1}^{N} \frac{|x_i^{exp} - x_i^{cal}|}{x_i^{exp}} \tag{5.19}$$

The determined UNIQUAC binary interaction energy parameters u_{ki}^0 and u_{ki}^T

for CO_2/water are given in Table 5.4 and Table 5.5 , respectively; for H_2S/water
we obtain $u_{ki}^0 = 1272.4$ and $u_{ki}^T = 1.402$. The estimated UNIQUAC binary inter-
action energy parameters are suitable to describe the solubility of CO_2 in water
in the temperature range of 288.15-373.15 K and pressures up to 200 bar with an
overall accuracy of 3.51%. For H_2S in water, the temperature range is 311-444
K and pressure is up to 121 bar with an overall accuracy of 11.65%. A compari-
son between the model correlation results and the experimental data is given in
Figure 5.1 and Figure 5.2. A fair agreement is obtained, with deviations getting
more pronounced with increasing pressure.

Table 5.2: *Solubility of CO_2 in water: Literature references and deviations of calcula-
tion results to the experimental data*

T/K	P/bar	N data points	% AARD(x)	Reference
288.15	60.8-202.7	8	3.88%	[38]
293.15	65.9-202.7	8	0.80%	[38]
298.15	76.0-202.7	6	2.11%	[38]
313.15	50-200	6	5.65%	[30]
323.15	1.54-25.05	6	4.89 %	[39]
	50-200	6		[30]
348.15	3.37-35.91	3	3.36%	[39]
	50-200	5		[30]
353.15	20-100	8	1.57%	[40]
373.15	3.25-23.07	7	4.47%	[41]
	3.56-45.60	3		[39]
	50-200	5		[30]
Total		71	3.51%	

Table 5.3: *Solubility of H_2S in water: Literature references and deviations of calcula-
tion results to experimental data*

T/K	P/bar	N data points	% AARD(x)	Reference
310.93	0-21	5	12.04%	[42]
344.26	0-50	9	13.57%	[42]
377.59	0-105	7	13.76%	[42]
410.93	0-121	8	11.67%	[42]
444.26	0-121	8	7.37%	[42]
Total		37	11.65%	[42]

Table 5.4: $u_{ki}^0 = u_{ik}^0$ *parameters for* CO_2 *in* K_2CO_3 *aqueous solution*

U^0	CO_2	H_2O	HCO_3^-	H^+	CO_3^{2-}	OH^-	K^+
CO_2	0						
H_2O	387.5	0					
HCO_3^-	1527.9	154.4	0				
H^+	1010	1010	1010	0			
CO_3^{2-}	189.1	1134.1	55.0	1010	0		
OH^-	1010	1010	1010	1010	1010	0	
K^+	907.1	601.6	177.1	1010	194.8	220.6	0

Table 5.5: $u_{ki}^T = u_{ik}^T$ *parameters for* CO_2 *in* K_2CO_3 *aqueous solution*

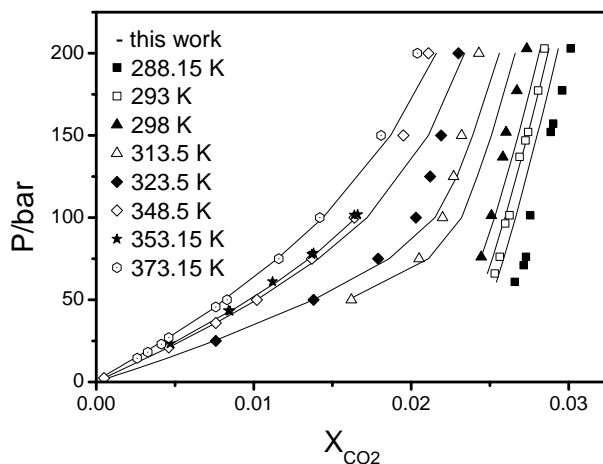| U^T	CO_2	H_2O	HCO_{3-}	H^+	CO_3^{2-}	OH^-	K^+
CO_2	0						
H_2O	2.088	0					
HCO^{3-}	0.900	1.106	0				
H^+	0	0	0	0			
CO_3^{2-}	1.09	0.800	1.010	0	0		
OH^-	0	0	0	0	0	0	
K^+	0	0	0	0	0	0	0

Figure 5.1: *Solubility of* CO_2 *in water system. Comparison of correlation results (lines) to experimental data (symbols) for various temperatures.*
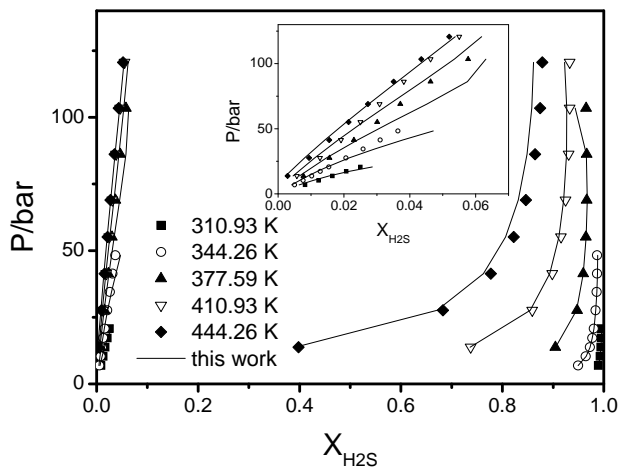
Figure 5.2: *Vapor-liquid equilibrium of H_2S - water system. Comparison of correlation results (lines) to experimental data (symbols) for various temperatures. Insert: rescaled view of the liquid phase mole fractions.*

5.6.2 System containing CO_2 - aqueous solution of potassium carbonate

Park et al. [43] report the solubility of CO_2 in aqueous solutions of potassium carbonate in the low pressure range. The experimental data by Kamps et al. [44], are for temperatures of 313.15 K and 353.15 K and two different amounts of potassium carbonate, 5.6 and 19.14 mass%, respectively. No precipitation of potassium carbonate occurs for these experimental data points. The average absolute relative deviation is given in Table 5.6 with reference to the data points. A comparison of the calculated solubility of CO_2 in aqueous solutions of potassium carbonate with the experimental data is shown in Figure 5.3. The estimated UNIQUAC binary interaction energy parameters given in Table 5.4 and Table 5.5 are valid for the temperature range of 298.15 to 353.15 K and pressures up to 90 bar. Some of the u_{ki}^0 parameters have been assigned the value 10^{10}, and for the corresponding u_{ki}^T parameter the values are zero. These values are assigned because H^+ and OH^- are not present in any significant amount in the solution. The u_{ki}^T for K^+ has also been assigned the value of zero, because at the moment the experimental data used to estimate the parameters is not sufficient. For the estimation of 15 parameters, only 41 experimental data points are used. It is clear

that reducing this ratio is desirable for future work.
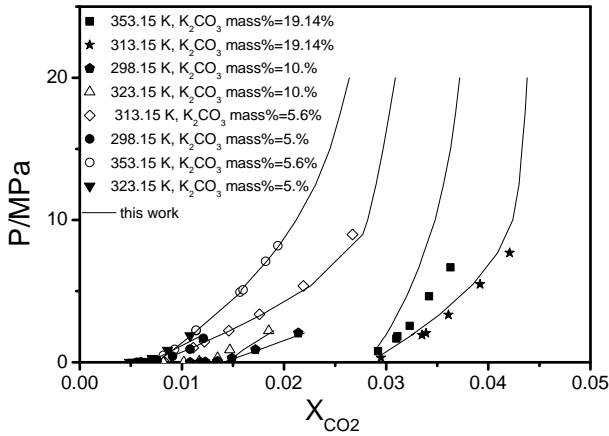
Figure 5.3: *Solubility of CO_2 in aqueous solutions of potassium carbonate at $T = 313.15$ K and 353.15 K for different amounts of potassium carbonate. Comparison of correlation results (lines) to experimental data (symbols) for various temperatures.*
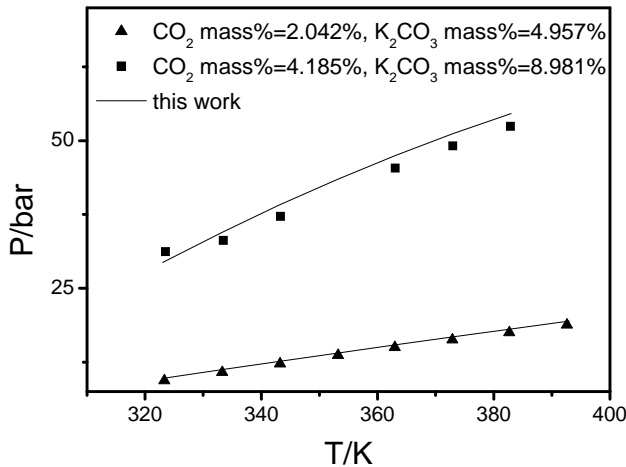
Figure 5.4: *Bubble-point lines for two compositions of aqueous potassium carbonate solution in mixture with carbon dioxide. Comparison of own preliminary data (symbols) with calculation results of the proposed model (lines).*

Table 5.6: *Solubility of CO_2 in K_2CO_3 aqueous solution: Literature references and deviations of calculation results to experimental data.*

T/K	P/bar	K_2CO_3 mass%	N data points	% AARD(x)	Reference
298.2	0.7-16.81	5.	5	5.38%	[43]
298.2	0.8-20.58	10.	4	3.33%	[43]
313.15	4.3-89.8	5.6	7	1.84%	[44]
313.15	3.29-77.	19.14	6	2.45%	[44]
323.2	2.79-18.78	5.	3	7.15%	[43]
323.2	3.195-22.3	10.	3	7.40%	[43]
353.15	4.9-82.	5.6	7	0.78%	[44]
353.15	7.7-67.	19.14	6	4.92%	[44]
Total			41	4.16%	

Experiments were done by the authors to generate more data for CO_2-potassium carbonate solution system. The comparison of the preliminary experimental data and calculated data is given in Figure 5.4. The mass concentrations of K_2CO_3 in aqueous solution are 4.957% and 8.981%, respectively. CO_2 is subsequently added to the mixture; the overall CO_2 mass concentration in system is 2.042% and 4.185%. The temperature range is 323.15 K to 393.15 K. The pressure range is up to 55 bar. The data was not yet considered in adjusting the binary interaction parameters, but the model shows a good agreement to the experimental data.

5.7 Conclusion

The Peng-Robinson equation of state with Wong-Sandler mixing rules together with an extended UNIQUAC Gibbs excess energy model were applied to the reactive phase equilibria of aqueous electrolyte solutions. The binary interaction energy parameters for mixtures of hydrogen sulfide with water and carbon dioxide with water as well as for mixtures of carbon dioxide in potassium carbonate solutions were determined by adjusting them to experimental data. The model showed to be suitable for describing these systems in the considered range of conditions.

It is desirable to use a molecular-based equation of state for the mild basic electrolyte aqueous system. Systems of CO_2-H_2O and H_2S-H_2O are already studied using PC-SAFT equation of state in Chapter 2. The PC-SAFT equation of state gives slightly better results using one temperature-independent k_{ij} parameter for

the system H_2S-H_2O, compared with the results of the Peng-Robinson model using a temperature dependent k_{ij}. For the system of CO_2-H_2O, a temperature dependent k_{ij} is used in PC-SAFT equation of state, but this is due to the cage structures formation of water. The PC-SAFT equation of state gives precise results in a wide range of temperature and pressure for the system CO_2-H_2O. Using a molecular-based equation of state like PC-SAFT, someone can reduce the number of interaction parameters for the mixture of complex mild basic electrolyte solutions and CO_2, comparing with the cubic equation of state.

REFERENCES

[1] H. E. Bensen, J. H. Field, and W. P. Haynes. Improved process for CO_2 absorption uses hot carbonate solutions. *Chem. Eng. Prog.*, 52(10):433–438, 1956.

[2] H. E. Benson, J. H. Field, and R. M. Jimeson. CO_2 absorption employing hot potassium carbonate solution. *Chem. Eng. Prog.*, 50(7):352–364, 1954.

[3] A. H. G. Cents, D. W. F. Brilman, and G. F. Versteeg. CO_2 absorption in carbonate/bicarbonate solutions: The danckwerts-criterion revisited. *Chem. Eng. Sci.*, 60:5830, 2005.

[4] M. S. Litvinenko. Equilibrium in the system hydrogen sulfide and carbon dioxide and solutions of sodium or potassium carbonate. *J. Appl. Chem. USSR*, 25:516, 1952.

[5] P. Petit. Carbonate of potash for purifing gas. *Journal of Gas Lighting and Water Supply*, Sept. 21:645, 1915.

[6] J. S. Tosh, J. H. Field, H. E. Benson, and R. B. Anderson. Equilibrium pressures of hydrogen sulfide and carbon dioxide over solutions of potassium carbonate. *Bur. Mines Rep. Invest. 5622*, 1960.

[7] J. S. Tosh, J. H. Field, H. E. Benson, and W. P. Haynes. Equilibrium study of the system potassium carbonate, potassium bicarbonate, carbon dioxide, and water. *Bur. Mines Rep. Invest. 5484*, 1959.

[8] H. Cabezas and J. P. O'Connell. Thermodynamic properties of aqueous strong electrolytes from fluctuation theory. *AIChE National Meeting, Atlanta, GA*, 1984.

[9] S. A. Ed. Newman. Thermodynamics of aqueous systems with industrial applications. *ACS Symp. Ser.*, page 133, 1980.

[10] C. Christensen, B. Sander, A. Fredenslund, and P. Rasmussen. Towards the extension of UNIFAC to mixtures with electrolytes. *Fluid Phase Equilib.*, 13(Oct):297–309, 1983.

[11] E. Bekerman and D. Tassios. Correlation of vapor-liquid equilibrium systems containing two solvents and one salt. *Adv. Chem. Ser.*, 155:3, 1976.

[12] J. E. Boone, R. W. Rousseau, and E. M. Schoenbom. The correlation of vapor-liquid equilibrium data for salt containing systems. *Adv. Chem. Ser.*, 155:36, 1976.

[13] E. Hala. *Third International Conference on Phase Equilibria and Fluid Properties for Chemcial Process Design, Callaway Gardens, GA*, 1983.

[14] A. I. Johnson and W. F. Futer. Salt effect in vapor-liquid equilibrium. part II. *Can J. Chem. Eng.*, (38):78, 1960.

[15] R. W. Rousseau and J. E. Boone. Vapor-liquid equilibrium for salt containing systems: correlation of binary solvent data and prediction of behavior in multicomponent solvents. *AIChE*, 24:718, 1978.

[16] D. Schmitt and A. Vogelpohl. Prediction of the salt effect on the vapour-liquid equilibrium of binary mixtures. *Fluid Phase Equilib.*, 9:162, 1982.

[17] B. Sander, A. Fredenslund, and P. Rasmussen. Calculation of vapor-liquid equilibria in mixed solvent/salt systems using an extended UNIQUAC equation. *Chem. Enfng Sci.*, 41:1171–1183, 1986.

[18] K. Thomsen, P. Rasmussen, and R. Gani. Correlation and prediction of thermal properties and phase behavior for a class of aqueous electrolyte systems. *Chem. Eng. Sci.*, 51(14):3675–3683, 1996.

[19] K. Thomsen and P. Rasmussen. Modeling of vapour-liquid-solid equilibrium in gas-aqueous electrolyte systems. *Chem. Eng. Sci.*, 54:1787–1802, 1999.

[20] S. I. Sandler and D. S. H. Wong. A theoretically correct new mixing rule for cubic equations of state. *AIChE*, 38:671–680, 1992.

[21] H. Orbey and S. I. Sandler. Reformulation of Wong-Sandler mixing rule for cubic equations of state. *AIChE*, 41:683–690, 1995.

[22] J. M. Smith, H. C. Van Ness, and M. M. Abbott, editors. *Introduction to Chemical Engineering Thermodynamics*. McGraw-Hill Education, 7 edition, 2005.

[23] H. Orbey and S. I. Sandler. *Modeling vapor-liquid equilibria: cubic equation of state and their mixing rules.* Cambridge University Press, 1 edition, 1998.

[24] R. Stryjek and J. H. Vera. PRSV: An improved peng-robinson equation of state for pure compounds and mixtures. *Can. J. Chem. Eng.*, 64:323–333, 1986.

[25] G. Soave. Equilibrium constants from a modified redlich-kwong equation of state. *Chem. Eng. Sci.*, 27:1197–1203, 1972.

[26] D. Y. Peng and D. B. Robinson. A new two-constant equation of state. *Ind. Eng. Chem. Fundam.*, 15:59–64, 1976.

[27] S. I. Sandler. *Chemical and Engineering Thermodynamics*. John Wiley and Sons,Inc, 3 edition, 1999.

[28] R. C. Reid, J. M. Prausnitz, and B. E. Poling. *The Properties of Liquids and Gases*. 1987.

[29] P. Atkins and J. de Paula, editors. *Atkins' Physical Chemistry*. Oxford University Press Inc., Oxford, 8 edition, 2006.

[30] R. Wiebe and V.L. Gaddy. The solubility of carbon dioxide in water at various temperatures from 12 to 40 and at pressures to 500 atmospheres. critical phenomena. *J. Am. Chem. Soc.*, 62(4):815–817, 1940.

[31] P. Proust and J. H. Vera. PRSV: The Stryjek-Vera modification of the Peng-Robinson equation of state. parameters for other pure compounds of industrial interest. *Can. J. Chem. Eng.*, 67, 1989.

[32] J. Li, I. Vanderbeken, S. Ye, H. Carrier, and P. Xans. Prediction of the solubility and gas-liquid equilibria for gas-water and light hydrocarbon-water systems at high tempertures and pressures with a group contribution equation of state. *Fluid Phase Equilib.*, 131:107–118, 1997.

[33] D. S. Abrams and J. M. Prausnitz. Statistical thermodynamics of liquid mixtures: a new expression for the excess gibbs energy of partly or completely miscible systems. *AIChE*, 21:116–128, 1975.

[34] H. Nicolaisen, P. Rasmussen, and J. M. Sorensen. Correlation and prediction of mineral solubilities in the reciprocal slat system $(Na^+, K^+)(Cl^-, SO_4^{2-})$-$H_2O$ at $0 - 100$ C. *Chem. Eng. Sci.*, 48:3149–3158, 1993.

[35] D. D. Perrin. *Dissociation constants of inorganic acids and bases in aqueous solution*. Butterworths, London, 1969.

[36] Th. W. De Loos, H. J. Van der Kooi, and P. L. Ott. Vapour + liquid equilibria in the system ethane+ 2-methylpropane. *J. Chem. Eng. Data*, 31:166, 1986.

[37] J. van de Steen, Th. W. De Loos, and J. de Swaan Arons. The volumetric analysis and predictio of liquid-liquid-vapor equilibria in certain carbon dioxide + n-alkane systems. *Fluid Phase Equilib.*, 51:353–367, 1989.

[38] M. B. King, A. Mubarak, J.D. Kim, and T.R. Bott. The mutual solubilities of water with supercritical and liquid carbon dioxides. *J. Supercrit. Fluids*, 5(4):296–302, 1992.

[39] A. Zawisza and B. Malesinska. Solubility of carbon dioxide in liquid water and of water in gaseous carbon dioxide in the range 0.2 - 5 MPa and at temperatures up to 473 K. *J. Chem Eng. Data.*, 26:388–391, 1981.

[40] J. A. Nighswander, N.Kalogerakis, and A. K. Mehrotra. Solubilities of carbon dioxide in water and 1 wt % *nacl* solution at pressure up to 10 MPa and temperatures from $80 - 200$ C. *J. Chem Eng. Data.*, 34:355–360, 1989.

[41] G. Müller, E. Bender, and G. Maurer. Das dampf - flssigkeitsgleichgewicht des ternren systems ammoniak-kohlendioxide-wasser bei hohen wassergehalten im bereich zwichen 373 und 473 Kelvin. *Ber. der Bunsenges. fur Phys. Chem.*, 92:148–160, 1988.

[42] F. T. Selleck, L. T. Carmichael, and B. H. Sage. Phase behavior in the hydrogen sulfide-water system. *Ind. Eng. Chem.*, 44(9):2219, 1952.

[43] S. B. Park, C. S. Shim, H. Lee, and K. H. Lee. Solubilities of carbon dioxide in the aqueous potassium carbonate and potassium carbonate-poly(ethylene glycol) solutions. *Fluid Phase Equilib.*, 134:141–149, 1997.

[44] A. P.-S. Kamps, E. Meyer, B. Rumpf, and G. Maurer. Solubility of CO_2 in aqueous solutions of KCl and in aqueous solutions of K_2CO_3. *J. Chem. Eng. Data*, 52(3):817 –832, 2007.

Chapter 6

Conclusions and Perspectives

Mixtures of acid gases, like hydrogen sulfide (H_2S) and carbon dioxide (CO_2), with hydrocarbons and with water or with basic aqueous solutions are *technically and socially important*, because H_2S is hazardous and CO_2 is a climate active component. It is desirable to leave these acid gases within a reservoir in the production process of, say, natural gas. At the same time, it is *academically challenging* to develop a sound thermodynamic model for the physical properties of these mixtures, because on the one hand the appropriate phase equilibria involve vapor-liquid-liquid and solid phases, that are all relevant in processing these mixtures. Secondly, the components exhibit specific, anisotropic molecular interactions, such as polar, associating (H-bonding) and ionic interactions. Third, the phase equilibrium is superpositioned by reactions in the liquid phase. Last, the conditions of interest often involve conditions close to the critical point of the mixtures, where long-range density fluctuations dominate the physical behavior.

This thesis proposes a sound thermodynamic model for the physical properties of mixtures involving acid gas components, hydrocarbons, water and reactive (electrolyte) aqueous solutions. The perturbed-chain polar statistical associating fluid theory (PCP-SAFT) equation of state, which is a molecular-based equation of state, was parameterized to represent experimental data for these mixtures (Chapter 2). The equation of state was applied to correlate phase equilibria for mixtures of hydrogen sulfide (H_2S) and carbon dioxide (CO_2) with alkanes, with aromatics, and with water over wide temperature and pressure ranges. The considered phase equilibria cover vapor-liquid, liquid-liquid, solid-liquid, solid-vapor phase equilibria and the appropriate three-phase equilibria (and four-phase end-points).

For cubic equations of state that do not specifically account for associating interactions, most binary mixtures require temperature-dependent binary interaction parameters, k_{ij}. The PCP-SAFT equation of state was found to be in good agreement to the experimental data using a temperature-independent binary interaction parameter. An exception is the system of CO_2-water, where water is known to form specific hydrate-like structures around solutes, such as carbon dioxide. Accounting for the hyrogen-bonding network of water around solutes is a so-far unsolved problem, that could, for example, be addressed with theories developed for hydrates. The Helmholtz energy hydrate-structures can expected to be similar, compared with the water-cages around solutes.

The inclusion of the dipole and quadruple term in PCP-SAFT equation of

state leads to some improvement for mixtures with hydrogen sulfide and more pronounced systematic improvements for mixtures containing carbon dioxide as compared to the non-polar version of the equation of state (PC-SAFT). The description for mixtures with methane is not improved, possibly because the octapole moment of methane is not accounted for. The required values of the binary interaction parameter are (especially for CO_2-containing mixtures) considerably lower if the polar moments are accounted for. The ternary mixture H_2S, CO_2 and methane could be modeled with the binary interaction parameters of the binary pairs. That confirms that the PCP-SAFT equation of state can be used for multicomponent mixtures using binary interaction parameters determined from the binary pairs.

Classical fluid theories do not describe the long-range density-fluctuations that occur in the vicinity of a pure component or mixture's critical point. A renormalization group theory was applied with the PC-SAFT equation of state, in order to account for long-ranged density fluctuations in the vicinity of the critical point, to improve the phase behaviors in the critical regions (Chapter 3). This chapter extended the renormalization group corrections approach for pure fluids to mixtures, which make the renormalization group corrections suitable for complex systems. The theory accounts for the long-range density fluctuations and the results reduce to those of the classical PC-SAFT equation of state away from the critical point.

Two approximations for the renormalization scheme for mixtures were evaluated, the isomorphic density approximation and the individual phase-space cell approximation. The resulting equations of state were applied to mixtures of alkanes, as well as to mixtures involving hydrogen sulfide and carbon dioxide. Both variants improved the description around the critical point for these mixtures. Despite its tendency to overestimate the renormalization corrections, the individual phase-space cell approximation was found to be slightly superior to the isomorphic density approximation for the systems studied here.

The surface tension is important for predicting the (undesired) pore-wetting in membrane contactors. Membrane contactors receive a certain degree of attention in this study, because we suggested an absorption process within the ISAPP program, which could also be realized underground, in the bore well. A membrane contactor is suggested as a promising separation device for an absorption/desorption process that could be establised underground (see Appendix A).

To calculate the surface tension in the critical region, a Helmholtz energy functional is proposed, where the long-range density fluctuations leading to the universal critical scaling behavior are for the first time accounted for using a renormalization group theory (Chapter 4). The density functional theory (DFT) approach is elegant, because of its simple implementation. The model is almost exact at the critical point. Away from the critical point, the model reduces to the perturbed chain statistical associated fluid theory (PC-SAFT) equation of state. The number of pure component renormalization parameters is reduced from three to a single parameter. The conventional PC-SAFT pure component parameters are then supplemented with this single substance-specific renormalization parameter, that is adjusted to reproduce the bulk phase critical temperature. The surface tension is obtained with excellent agreement to experimental data for non-polar and moderately polar substances (alkanes, ethers, acetates, aromatic substances) up to the critical point. An extension of the approach to mixtures remains to be done. The procedure for doing so, however, is quite straight-forward. Further, water has been omitted in our calculations, because the non-isotropic orientational distribution of water has not been resolved in our DFT-formalism.

To study the system of CO_2 with aqueous electrolyte solutions, the Peng-Robinson equation of state with Wong-Sandler mixing rules together with an extended UNIQUAC Gibbs excess energy model was applied to the reactive phase equilibria of aqueous electrolyte solutions (Chapter 5). The ion-specific interactions are determined from a Debye-Huckel term. The thermodynamic model is parameterized for aqueous systems containing carbon dioxide and hydrogen sulfide along with water and potassium carbonate solutions at high pressure. The UNIQUAC binary interaction parameters are estimated by minimizing deviations in the liquid phase composition of the model with respect to the experimental data. The data is taken from literature and is supplemented by own experimental data conducted as part of this study. The model showed to be suitable for describing these systems in the considered range of conditions.

An adequate model based on the PC-SAFT equation of state for electrolytes which is needed for an improved modelling of the electrolyte solutions with reacting acid gas components remains to be developed. The cubic equation of state presented in Chapter 5 has as a distinct disadvantage, that the number of adjustable mixture parameters is high. The model is therefore applicable only for mixtures with a few constituents, where, at the same time, a broad basis of ex-

perimental data exists. For mixtures with less data, a more robust and more predictive model needs to be developed. This could certainly be a SAFT model. The most common electrolyte terms (Debye-Hckel, Mean Spherical Approximation, Hypernetted Chain Approximation, Henderson's Perturbation Theory) should, however, be systematically evaluated and further developed in order to ensure a sound physical basis. A computational framework was developed in this study (Chapter 5), where the reaction equilibrium and the phase equilibrium can be solved simutaneously. This may enable the developmet of an exteded SAFT model.

The model development in this thesis can facilitate the design of more energy efficient and environmentally begnin processes. The energetic requirement of a separation process is in practice determined with process simulation and optimization tools, where the phase equilibria and caloric properties are the only input (apart from solving the appropriate component and energy balances). The physical property models developed here can be used in these process simulators. More detailed models for individual process units, for example a membrane contactor, in addition require heat- and mass-transport models. Such transport equations also require (the same) thermodynamic models in order to express, for example the driving force for diffusion.

The methods developed in this thesis, like the renormalization procedure for mixtures or the Helmholtz energy functional for calculating interfacial properties are generic and can be used for any system.

Appendix A

Acid gas separation processes

A.1 ISAPP program

The Integrated System Approach Petroleum Production (ISAPP) programme aims to increase hydrocarbon recovery through the application of innovative reservoir development and management technologies. TNO, TU Delft and Shell envisage that future hydrocarbon production systems will be more intelligent, enabling:

- faster and higher recoveries from oil and gas fields to be realised

- cost reductions through automated and unmanned operations

- greater flexibility to manage unexpected events that jeopardise production

- greenhouse gas emission to be reduced through downhole processing and storage

A.2 Subsurface separation of acid gases from oil and gas

Oil and gas reservoirs which contain high purity of oil and natural gas, are becoming scarcer nowadays. Fields containing not only oil and natural gas but also large amount of acid gases, such as carbon dioxide and hydrogen sulfide, are targeted for production. Since sour gases give rise to extra costs and potential

149

enviromental and safety hazards, it is necessary to dispose them from the oil and gas products. One idea is to purify natural gas and oil in their production process underground in the wells which connect reservoirs and earth surfaces. Acid gases captured subsurface can be left within the reservoir or re-injected into sublayers without producing them to the earth surface, see Figure A.1.
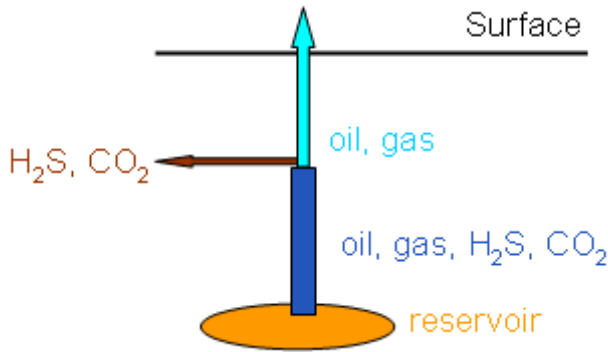

Figure A.1: *Natural gas and oil are purified in their production process underground, and acid gases captured subsurface can be left within the reservoir or can be re-injected into geological sublayers*

Processes underground need to deal with particular temperature and high pressure ranges. Pressure at any point underground can be calculated roughly as the sum of atmosphere pressure and the hydrostatic pressure of water at the considered depth. Subsurface temperature can be estimated roughly as the sum of the surface temperature and the increments of temperature with the depth $(2-3^oC$ per 100 meters). The depth of the location considered for the separation process is in the range of $1 \ km$ to $3 \ km$ from the earth surface. Figure A.2 shows the pressure and temperature range considered. The fluid dynamic conditions underground often strongly vary, e.g. with slugs of liquid (water-rich) phase.

There are different kinds of technologies for acid gases capture from gas streams, absorption using solvents, adsorption on solids, selective membrane separation, cryogenic/condensation separations. Due to the difficulties of handling solid
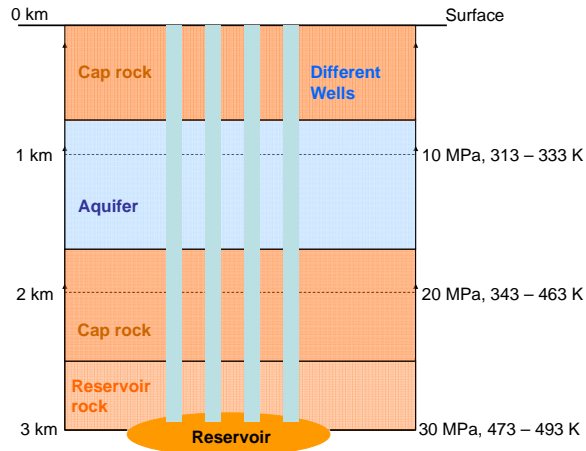
Figure A.2: *Pressure and temperature range for subsurface separation process*

phases in the narrow wells underground, techniques containing solid phases, like adsorption and cryogenic separation, are not considered for subsurface separations. Temperature at subsurface is very difficult to control, thus condensation separation is not considered here for subsurface process. Most selective membranes(See section A.5) available are vulnerable to high pressure/temperature, or to the presence of water/impurities in gas/oil. So selective membrane separation process is not considered here. We consider to use absorption/desorption technology for subsurface separation, which is a simple technique and has no issue under elevated pressure and temperature. The analogous principle in extraction can be considered for acid gases separated from oil.

A.3   Acid gas solubilities in various solvents

In absorption/desorption processes, different sorts of solvents are used, such as water, neutral salt aqueous solutions, organic (physical) solvents, mildly basic aqueous electrolyte solutions and strong chemical solvents. *Strong chemical solvents* are commonly used for the absorption of H_2S/CO_2 at low pressure conditions since at high pressures, the regeneration process can be an issue. *Physical*

solvents are usually considered for elevated pressure conditions. Substances like methanol, ethanol and acetone have a fairly high vapor pressure so that solvent-loss is a technical challenge. Glycols would continuously be diluted with the water in the course of the process for an application in the bore-well means. *Aqueous solutions* are suitable for the operating conditions subsurface. Carbonate aqueous solutions, for example, aqueous K_2CO_3 and Na_2CO_3 solutions can lead to balanced absorption as well as desorption behaviors under the conditions at hand. Table A.1 gives a summary for the experimental study of CO_2 and H_2S solubilities in different solvents.

Figure A.3 gives CO_2 solubilities in aqueous K_2CO_3 solutions [1], in aqueous $NaNO_3$ solutions[2] and in H_2O at 353 K. CO_2 solubilities in strong electrolytes aqueous solutions such as aqueous $NaNO_3$ solutions is shown to be lower than in the pure water, due to salting-out effect. The solubility of CO_2 in aqueous K_2CO_3 solution[1, 3, 4, 5] were explored. While choosing aqueous K_2CO_3/Na_2CO_3 solution as absorbents, the precipitation problems of $KHCO_3/NaHCO_3$ need to be prevented. Due to the reactions in CO_2-aqueous K_2CO_3 solution systems, the solubility of CO_2 in aqueous K_2CO_3 solution is higher than in H_2O and in aqueous $NaNO_3$ solutions, as shown in Figure A.3.

A.4 Separation of acid gases by absorption using a membrane contactor

Aqueous K_2CO_3-solution is used as the solvent for the absorption process since it is not an issue with the solvent loss and it is environmentally benign. Membrane contactor is following attributes of mature absorption process based only on vapor-liquid equilibrium (i.e., non-selective robust in terms of fluid dynamics behavior). It is easy to install no moving parts and the operation conditions are very predictable based on models.

Lumped-parameter models are used to describe the resistance and absorption process. The volumetric overall mass transfer coefficient through a hollow fiber membrane contactor was found to be greater than that for the conventional packed towers[21, 22, 23]. These investigations employed a simplified approach to analyse the mass transfer process using individual film and overall mass transfer coefficients to account for the shell, membrane and tube side resistance. A more

Table A.1: *Summary of acid gas solubilities in different solvents*

| Solvent	T(K)	P(MPa)	Gas	Ref.
H_2O	273 - 533	$\leq$200	CO_2	[6]
H_2O	313 - 393	$\leq$9.3	CO_2	[7]
H_2O	353 - 471	$\leq$10.2	CO_2	[8]
H_2O	323	$\leq$ 6	CO_2	[9]
H_2O	296 - 594	$\leq$13.9	H_2S	[10]
H_2O	324 - 375	$\leq$58	CH_4	[11]
$NaCl + H_2O$	273 - 533	$\leq$200	CO_2	[6]
$NaCl + H_2O$	313 - 353	$\leq$10.5	CO_2	[7]
$NaCl + H_2O$	313 - 413	$\leq$9	CO_2	[9]
$NaCl + H_2O$	155 - 320	$\leq$13.8	H_2S	[10]
$NaCl + H_2O$	313 - 393	$\leq$10	H_2S	[12]
$KCl + H_2O$	313 - 433	$\leq$9.4	CO_2	[1]
$Na_2SO_4 + H_2O$	288 - 368	$\leq$14	CO_2	[13]
$Na_2SO_4 + H_2O$	313 - 433	$\leq$10	CO_2	[14]
$Na_2SO_4 + H_2O$	313 - 393	$\leq$10	H_2S	[12]
$(NH_4)_2SO_4 + H_2O$	313 - 393	$\leq$10	NH_3, CO_2	[15]
$(NH_4)_2SO_4 + H_2O$	313 - 393	$\leq$10	H_2S	[12]
$NH_4Cl + H_2O$	313 - 393	$\leq$10	H_2S	[12]
$NaNO_3 + H_2O$	313 - 433	$\leq$10	CO_2	[2]
$NaNO_3 + H_2O$	313 - 433	$\leq$10	H_2S	[16]
$NaHCO_3 + H_2O$	324 - 403	$\leq$58	CO_2, CH_4	[11]
$K_2CO_3 + H_2O$	298	0.78-1.29	CO_2	[4]
$K_2CO_3 + H_2O$	313 - 393	$\leq$9.2	CO_2	[1]
Diethylene glycol	298 - 398	$\leq$21.1	CO_2, H_2S	[17]
CH_3OH	298	$\leq$5.08	H_2S	[18]
TEGMME	313 - 373	$\leq$8.8	CO_2	[19]
Methanol	291 - 323	$\leq$8.0	CO_2	[20]
Ethanol	291 - 313	$\leq$7.9	CO_2	[20]
Acetone	291 - 313	$\leq$7.4	CO_2	[20]
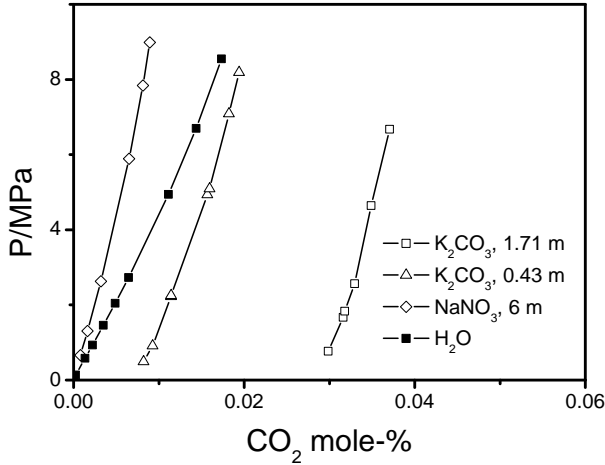
Figure A.3: *Experimental data of CO_2 solubilities in aqueous K_2CO_3[1](concentration of 1.71 mol/kg and 0.43 mol/kg) solution, aqueous $NaNO_3$[2](concentration of 6 mol/kg) solutions and H_2O[7] at 353 K.*

detailed analysis of the transport processes and a survey of literature, listed in Table A.2, shows that non-wetted pores, are an essential prerequisite for the efficiency of membrane contactors. The non-wetted mode for membrane pores is preferred so that the limiting breakthorough pressure needs to be investigated. This limiting pressure depends on the surface tension of the fluid.

A.4.1   Geometry and configuration of the membrane contactor

In our model of a membrane contactor for absorption, an aqueous K_2CO_3-solution is used as a solvent to absorb CO_2. A gas mixture of 90 mol-% methane and 10 mol-% carbon dioxide is investigated as the inlet gas mixture. The absorption process is investigated over a wide temperature and pressure range ($298.15K \leq T \leq 323.15K$ and $0.1MPa \leq P \leq 10MPa$). A mathematical model based on Fick's law is developed to understand the mass transfer process taking place in a hollow fiber membrane contactor, which is a reacting system.

Table A.2: *A survey of literature on detailed analysis of membrane absorption processes*

T/C	P/bar	Gas mixture	Solvent	Diffusion	wetting-mode	Ref.
25	1	CO_2/CH_4	$NaOH^a$	Axial	partial/ complete	[24]
25	1	CO_2/CH_4	Water	Axial/radial	non-wetted	[25]
25	1	CO_2/N_2	Wate, DEA^b	Radial	non-wetted	[26]
25	0 - 2.07	CO_2	Water	Radial	wetted/ non-wetted	[27]
		SO_2				
		CO_2/N_2				
		SO_2/Air				
25	1.7 - 3.08	CO_2	$K_2CO_3^c$	Radial	non-wetted	[28]
30	1	CO_2	Water, MEA^d, $NaOH^a$	Radial	non-wetted	[29]
20-60	1	CO_2/N_2	Water, MEA^d, AMP^e, $MDEA^f$	Radial	non-wetted	[30]

[a] $NaOH$ - Aqueous sodium hydroxide solution;
[b] DEA - Aqueous di-ethanolamine solution;
[c] K_2CO_3 - Aqueous potassium carbonate solution;
[d] MDEA - Methyldiethanoamine aqueous solution;
[e] AMP - 2-amino-2-methyl-1-propanol aqueous solution;
[f] MEA - Mono ethanolamine aqueous solution.

The configuration of a hollow fiber membrane contactor is shown in Figure A.4. Figure A.4 (a) gives a top view of the membrane contactor containing a number of membrane tubes, while Figure A.4 (b) represents a single membrane tube, consisting of three sections: the tube side, the membrane side and the shell side. Figure A.4 (c) and (d) show the cross-section of a membrane tube (top view and side view), where the liquid absorbent is considered to flow in the lumen of the hollow fiber membrane tubes, while the gas mixture(methane and CO_2) flows countercurrently in the shell side, as assumed by many authors[24, 27, 28]. A possible reason for this preference could be the fact that the flow of liquid in the shell side has not been clearly understood yet[31]. The results for some reports on the experimental and analytical studies on the shell-side mass transfer[32, 33, 34] vary significantly, possibly arising from the irregularity of the fiber spacing, the polydispersity of fiber dimeters and the influence from the module wall as well as inlet and outlet effects. The solvent side is always of more interest and it is therefore appropriate to allocated it to the tube side where the flow is well defined.

The inner shell radius due to the Happel's free surface model[35], is given by[24] as

$$r_3 = \left(\frac{1}{1 - \epsilon} \right)^{\frac{1}{2}} r_2 \tag{A.1}$$

where, r_2 is the external tube radius, r_3 is the inner shell radius and ϵ is the volume fraction of the void. r_1 in Figure A.4 is the internal tube radius.

The dimensions of the membrane contactor used here are listed in Table A.3. Since a reasonable value for the diameter of a natural gas well is around $0.2-0.5\ m$, the value for the inner module diameter is taken as $0.3175\ m$, which is 10 times the value taken by Marzouqui et al[24].

The transport equations for the molar concentration of component C_i in the shell (superscript s), the membrane (m) and the tube side (t) using the Fick's law of diffusion are in a cylindrical coordinate system derived as

$$D_i^s \left(\frac{\partial^2 C_i^s(z,r)}{\partial z^2} + \frac{1}{r} \left(\frac{\partial}{\partial r} \left(r \frac{\partial C_i^s(z,r)}{\partial r} \right) \right) \right) = V_z^s(r) \frac{\partial C_i^s(z,r)}{\partial z}, \tag{A.2}$$

Figure A.4: *(a) Schematic representation of the membrane contactor module (top view) (b) A membrane tube used for modeling (c) Cross-section of a membrane tube (top view) (d) Cross-section of a membrane tube (side view)*

Table A.3: *Dimensions of the membrane contactor*

Parameter	Value
Inner tube diameter	0.22×10^{-3} m
Outer tube diameter	0.30×10^{-3} m
Inner module diameter	0.3175 m
Total number of tubes	360000
Inner shell diameter	0.529×10^{-3} m
Module length	0.2286 m

$$D_i^m \left(\frac{\partial^2 C_i^m(z,r)}{\partial z^2} + \frac{1}{r} \left(\frac{\partial}{\partial r} \left(r \frac{\partial C_i^m(z,r)}{\partial r} \right) \right) \right) = 0, \qquad \text{(A.3)}$$

$$D_i^t \left(\frac{\partial^2 C_i^t(z,r)}{\partial z^2} + \frac{1}{r} \left(\frac{\partial}{\partial r} \left(r \frac{\partial C_i^t(z,r)}{\partial r} \right) \right) \right) \nu_i R = V_z^t(r) \frac{\partial C_i^t(z,r)}{\partial z}, \qquad \text{(A.4)}$$
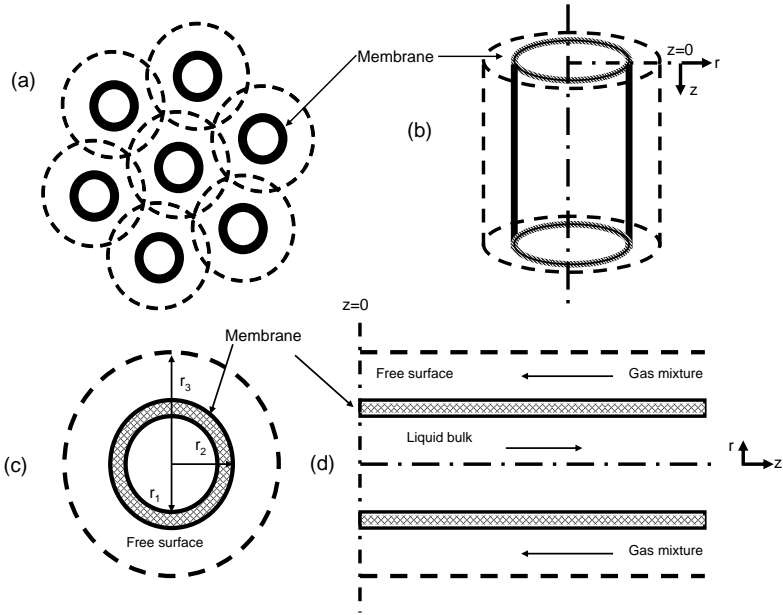
where D_i^s is the diffusion coefficient of species i in the shell in units $[m^2/s]$, D_i^m is the diffusion coefficient of species i in the membrane, D_i^t is the diffusion coefficient of species i in the tube, V_z^s is the velocity in the shell in units $[m/s]$, V_z^t is the velocity in the shell, and z is the length coordinate according to Figure A.4. For details on the boundary conditions to these equations we refer to the study of Al-Marzouqi et al.[24].

The method proposed by Raizi and Curtis [36] for dense fluids at reservoir conditions is used for calculating D_i^s. Table A.4 lists the correlations for other diffussion coefficients.

The mass transfer in the pores of membrane is assumed to be entirely controlled by molecular diffusion. The pores of the membranes are assumed to be large enough to prevent any contribution due to Knudsen diffusion and surface diffusion. On the other hand, convection in the pore is considered negligible. A fully developed parabolic velocity profile is assumed for the tube side. In this model, the liquid phase is assumed as incompressible, so that the pressure dependence is not resolved.

A.4.2   Reactions of CO_2 with an aqueous K_2CO_3 solutions

The enhancement in solubility due to reactions need to be properly accounted for in absorption of carbon dioxide by a reactive absorbent such as aqueous potassium carbonate solution. The dissolution of potassium carbonate in water yields potassium ions (K^+) and carbonate ions (CO_3^{2-}). The hydroxyl ions (OH^-) and bicarbonate ions (HCO_3^-) are then generated by the hydrolysis of the carbonate ions[28]. Carbon dioxide reacts with water to yield HCO_3^- (Reaction A.5),
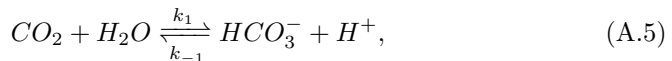
$$CO_2 + H_2O \underset{k_{-1}}{\overset{k_1}{\rightleftharpoons}} HCO_3^- + H^+, \qquad \text{(A.5)}$$

Table A.4: *Correlations for diffusion coefficients*

| Parameter	Unit	Value	Ref.
$D_{CO_2-K_2CO_3}$ [a,b]	m^2/s	$\left[\frac{2.35\times10^{-2}exp(\frac{-2119}{T})}{(1+0.354\times M_{K_2CO_3})^{0.82}}\right]\times 10^{-4}$	[28]
$D_{CO_3^{2-}}\approx D_{HCO3^-}$ [d]	m^2/s	$D_{CO_2-K_2CO_3}\times\left(\frac{M_{w,CO_2}}{M_{w,HCO_3}}\right)^{0.5}$	[37]
$D_{CO_2-membrane}$ [c]	m^2/s	$\frac{D_{CO_2-shell}\times\epsilon}{\tau}$	[24]

[a] : T is the temperature in K;

[b] : $M_{K_2CO_3}$ is the initial concentration of the potassium carbonate solution in mol/dm^3;

[c] : $\epsilon = 0.4$ and $\tau = 2$ represent the porosity and tortuosity respectively of the membrane;

[d] : M_{w,K_2CO_3} and M_{w,HCO_3^-} are molecular weight of carbon dioxide and bicarbonate ion respectively.

CO_2 at the same time reacts with the OH^- to give HCO_3^- as depicted in Reaction A.6,

$$CO_2 + OH^- \underset{k_{-2}}{\overset{k_2}{\rightleftharpoons}} HCO_3^-, \tag{A.6}$$
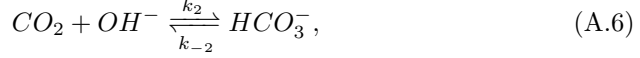
where k_1, k_{-1}, k_2 and k_{-2} are the reaction constants. K_1 and K_2 are the equilibrium constants of Reaction A.5 and Reaction A.6, respectively. These two reactions are slow, thus the rate controlling reactions in the system. In addition to the two reactions above, two other reactions, which are considered as very fast reactions and thus assumed to be in equilibrium, are also involved,

$$HCO_3^- \overset{K_3}{\rightleftharpoons} CO_3^{2-} + H^+ \tag{A.7}$$

$$H_2O \overset{K_4}{\rightleftharpoons} H^+ + OH^- \tag{A.8}$$

where K_3 and K_4 are the equilibrium constants of reaction A.7 and A.8 respectively. The reaction A.5, A.6, A.7 and A.8 can be added up to give an overall reaction, given as[38],

$$CO_2 + CO_3^{2-} + H_2O \Longleftrightarrow 2HCO_3^-. \tag{A.9}$$
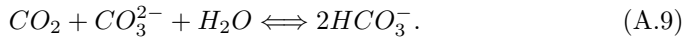
The initial bulk concentration of each species can be obtained from the equilibrium constraints in combination with the overall mass balance on carbon and the electro neutrality constraint[39, 40]. The equations used in estimating the equilibrium and rate constants are taken from Ref. [28]. Steady state conditions are assumed and the continuity equation for describing the transport of a component i in a chemical absorption process where there is simultaneous mass transfer and chemical reaction is given as

$$-\nabla N_i + \nu_i R = 0, \tag{A.10}$$

where N_i is the flux of component i and R is the reaction rate, ν_i is stoichimetric coefficient.

A.4.3   Solubility correlation of CO_2 in aqueous K_2CO_3-solution

An isothermal process is assumed in the development of the mathematical model. Moreover, the non-corrected Henry's law for CO_2, which is valid for low pressures

is extrapolated over the entire pressure range. The ideal gas law was used with Fick's law model for low and also high pressures (up to 10 MPa) which is a coarse approximation. The phase equilibrium condition applies to the interface of gas and liquid. A correlation for the solubility for the carbon dioxide - potassium carbonate system was proposed[28] as

$$[CO_2] = 10^{\left[\frac{-1140\ K}{T} - 5.3 - 0.125\frac{dm^3}{mol}M_{K_2CO_3}\right]} \times 10^3\ \frac{mol}{dm^3 atm} \tag{A.11}$$

where, $[CO_2]$ is solubility of CO_2 in aqueous K_2CO_3 solution and $M_{K_2CO_3}$ is the initial concentration of the potassium carbonate solution.

From this relation, one can estimate the Henry's constant $H_{CO_2,sol}$ with

$$y_{CO_2} \cdot p = x_{CO_2} \cdot H_{CO_2,sol} \tag{A.12}$$

as

$$H_{CO_2,sol} = \frac{c^{liq}}{[CO_2]} \tag{A.13}$$

where c^{liq} is the molar liquid density, y_{CO_2} and x_{CO_2} are the molar concentration of CO_2 in gas phase and liquid phase, respectively and p is the pressure of the gas phase.

A.4.4   Results and discussion

Figure A.5 depicts the dimensionless carbon dioxide concentration in the shell side ($r/r_3 = 0.567$ to $r/r_3 = 1.0$), the membrane side ($r/r_3 = 0.416$ to $r/r_3 = 0.567$) and the tube side ($r/r_3 = 0$ to $r/r_3 = 0.416$) at the middle ($z/L = 0.5$) of the membrane contactor for a carbon dioxide-potassium carbonate system at different CO_2 partial pressure (as well as total pressure). The dimensionless CO_2 concentration in shell side is decreasing with increasing CO_2 partial pressures (as with increasing the total system pressures), which means CO_2 sequestration process is more efficient at higher pressure systems. The changes of CO_2 concentration along the r direction in the shell side and membrane side at $P_{CO_2} = 0.01$ MPa ($P_{Total} = 0.1$ MPa), with the symbol of circle, is very small while a pronounced decrease of the CO_2 concentration along r direction occurs in the tube side. This is due to the fact that the reaction occurs in the liquid phase in tube side. For higher CO_2 partial pressures cases, 0.1 MPa, 0.5 MPa and 1.0 MPa (total

pressures 1 MPa, 5 MPa and 10 MPa), there are no obvious changes in carbon dioxide concentration along the r direction in the shell side. However perceptible concentration gradients are observed in the membrane side. These gradients in the membrane side are due to the fact that at higher pressure, diffusion coefficients in denser gases, which tend to behave like liquids, are much lower. The diffusion coefficients of gases decrease as the pressures increase[36].
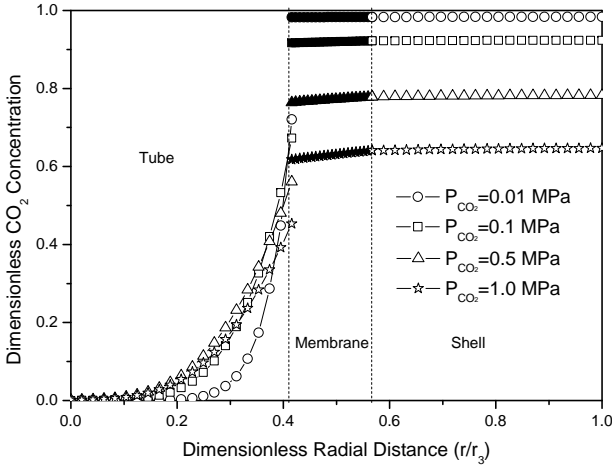

Figure A.5: *Concentration of carbon dioxide in the radial direction at the middle of the membrane contactor for $CO_2 - K_2CO_3$, $T = 298.15$ K, absorbent concentration= 0.373 mol/L, $F_{shell} = 1.0 \times 10^4$ L/min(standard condition: 298.15 K, 0.1 MPa), $F_{tube} = 1.0 \times 10^2$ L/min(298.15 K, 0.1 MPa).*

Figure A.6 gives the dimensionless carbon dioxide concentration along the axial distance (z direction) at the membrane-shell interface ($r/r_3 = 0.567$) for different CO_2 partial pressures. L represents the length of the membrane contactor and z stands for any position in the axial distance. The carbon dioxide concentration decreased from the inlet (at $z/L = 1$) to the outlet ($z/L = 0$) at the top of the shell side. Furthermore, when the pressure increases, CO_2 concentration at outlet decreases($z/L = 0$), which means the amount of carbon dioxide removed increases.

The effect of temperature on CO_2 removal in the three compartments of a hollow fiber membrane contactor is presented in Figure A.7 at the middle ($z/L = 0.5$) of the membrane contactor. The dimensionless CO_2 concentrations in the

Figure A.6: *Concentration of carbon dioxide in the axial direction at the membrane-shell interface for $CO_2 - K_2CO_3$, $T = 298.15$ K, absorbent concentration= 0.373 mol/L, $F_{shell} = 1.0 \times 10^4$ L/min(298.15 K, 0.1 MPa), $F_{tube} = 1.0 \times 10^2$ L/min(298.15 K, 0.1 MPa).*

Figure A.7: *Concentration of carbon dioxide in the radial direction at the middle of the membrane contactor for $CO_2 - K_2CO_3$, $T = 298.15$ K, 323.15 K, 353.15 K, $P(CO_2) = 0.5$ MPa, absorbent concentration= 0.373 mol/L, $F_{shell} = 1.0 \times 10^4$ L/min(298.15 K, 0.1 MPa), $F_{tube} = 1.0 \times 10^2$ L/min(298.15 K, 0.1 MPa).*
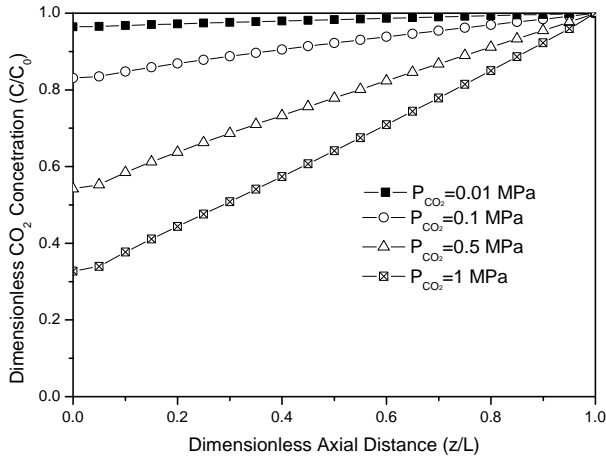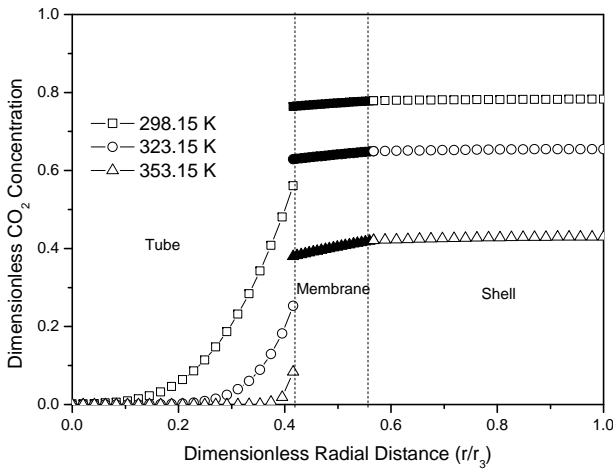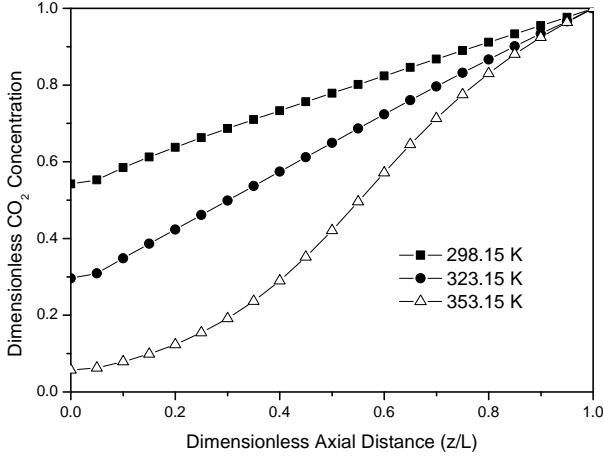
Figure A.8: *Concentration of carbon dioxide in the axial direction at the membrane-shell interface for CO_2 - K_2CO_3, $T = 298.15$ K, 323.15 K, 353.15 K, $P(CO_2) = 5$ MPa, absorbent concentration= 0.373 mol/L, $F_{shell} = 1.0 \times 10^4$ L/min(298.15 K, 0.1 MPa), $F_{tube} = 1.0 \times 10^2$ L/min(298.15 K, 0.1 MPa).*

shell side, membranes side and tube side at $P_{CO_2} = 0.5$ MPa decrease significantly with temperatures rise. This is due to the reaction rates in the liquid phase are increasing with increasing temperatures. Figure A.8 gives the dimensionless carbon dioxide concentration in the axial distance (z direction) at the membrane-shell interface ($r/r_3 = 0.567$) at three different temperatures cases in the system. With the temperature increasing, the outlet CO_2 concentration is decreasing, which means the amount of CO_2 removed is increasing.

Figure A.9 shows the percentage carbon dioxide removal with the changing liquid flow rates at 353.15 K for three different CO_2 partial pressures and total pressures. With the increasing liquid flow rate, CO_2 removal is increasing. With the increasing CO_2 partial pressures and total pressures, CO_2 removal is increasing. Figure A.10 shows the percentage CO_2 removal with the changing gas flow rate at 353.15 K for three different CO_2 partial pressures and total pressures. With the increasing gas flow rate, CO_2 removal is decreasing. But still with the increasing CO_2 partial pressures and total pressures, CO_2 removal is increasing. Figure A.11 shows the effect of absorbent concentration in CO_2 removal at different temperatures. Relative CO_2 removal increases mildly

Figure A.9: *Effect of liquid flow rate (at standard condition: 298.15 K, 0.1 MPa) on the percentage removal of carbon dioxide, absorbent concentration= 0.373 mol/L, $T = 353.15$ K, $F_{shell} = 1.0 \times 10^4$ L/min(298.15 K, 0.1 MPa).*
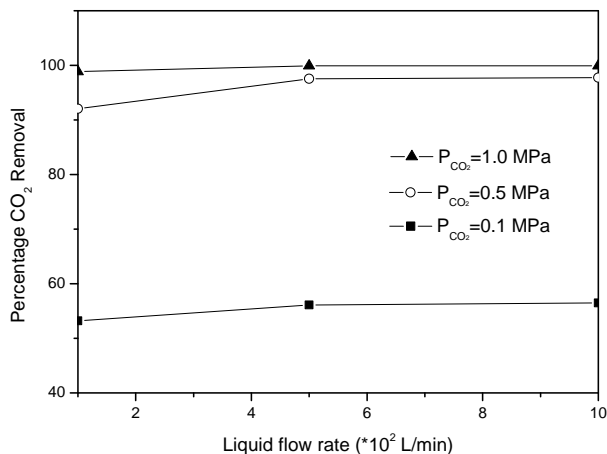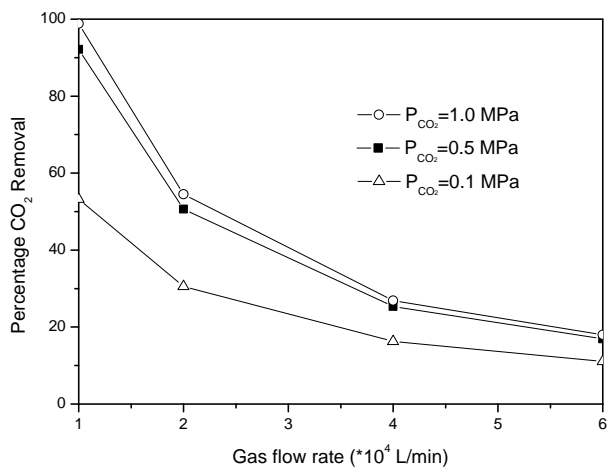

Figure A.10: *Effect of gas flow rate (at standard condition: 298.15 K, 0.1 MPa) on the percentage removal of carbon dioxide, absorbent concentration= 0.373 mol/L, $T = 353.15$ K, $F_{tube} = 1.0 \times 10^2$ L/min(298.15 K, 0.1 MPa).*
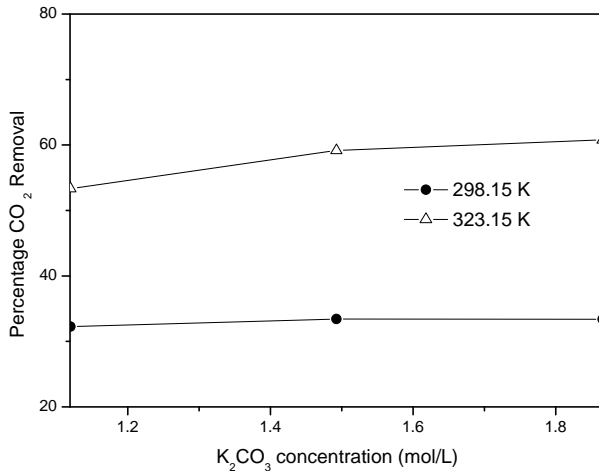
Figure A.11: *Effect of K_2CO_3 concentration in liquid phase on the percentage removal of carbon dioxide, $P(CO_2) = 0.5$ MPa, Fshell$= 1.0 \times 10^4$ L/min(298.15 K, 0.1 MPa), Ftube$= 20$ L/min(298.15 K, 0.1 MPa).*

with increasing K_2CO_3 concentration in liquid phase at 298.15 K. For the higher temperature case, percentage CO_2 removal increased more with the increasing K_2CO_3 concentration in liquid phase. This is still due to the higher reaction rate at higher temperature.

The results presented here confirm the expected trends with respect to CO_2 removal as function of temperature, pressure and absorbents concentration.

A.5   Survey on selective membranes for acid gas separation processes

Selective membrane technology is used in acid gas separation from gas/oil contaminants in industry. The advantages of membrane separation are: the pressure difference of feed side and sweep side can be used to aim at high gas permeability; membrane separation can be used for contaminants separation from oil. The disadvantages of membrane separation are: most selective membranes available now are vulnerable to high pressure/temperature, or to the presence of wa-

ter/impurities in gas/oil; maintenance and cleanness of membranes are a limiting factor. A large number of membrane materials are used in different areas, but most of them are applied in the lab without contacting the impurities in the feed and they were not tested at high pressure up to 30 MPa and temperature up to, say, 373 K. For membrane separation, it is important to test the stability of the selected membrane materials for reservoir conditions and impurities. Here, the selectivities and stabilities of different types of membranes are reviewed and evaluated in section A.5.1 and section A.5.2, respectively. The promising membrane candidates for downhole separation are screened for the separation of CO_2/CH_4 (and H_2S/CH_4).

A.5.1 Permeance and selectivity for various membrane materials

Table A.6 gives pure gas permeance of CO_2 and CH_4, and the ideal selectivity for CO_2/CH_4 of different membranes. The separation factors calculated from the binary fluxes and the so-called ideal separation factor, which is given by the ratio of the one-component flux, were compared with each other. It is found that the separation factor is a function of both the composition and the pressure. A reasonable description of the separation factor as a function of the pressure and composition is possible with the ideal adsorbed solution theory[41]. The permeance is calculated as $P_i = \frac{Q_i}{A \cdot \Delta p_i}$, Where P_i is permeance $[mol \cdot m^{-2} \cdot s^{-1} \cdot Pa^{-1}]$, Q_i is the molar flux in units $[mol \cdot s^{-1}]$, A is the membrane area, and Δp_i is partial pressure difference.

Table A.5: *Kinetic diameter for various molecules*

Molecule	Kinetic Diameter /	Ref.
CO_2	3.3	[42]
H_2S	3.6	[43]
CH_4	3.8	[42]

In Figure A.12, when $\Delta p < 0.25 MPa$, the ideal selectivity of CO_2/CH_4 system and the permeance of CO_2 for different membrane are shown. It is more unambiguous to compare membranes performance from different literature sources using the ideal selectivity, since different ratio of CO_2 and H_2S in the mixtures are used in different papers under different temperature and pressure. The real mixture selectivity certainly be different from the ideal selectivity, but the ideal

selectivity sufficiently serves as an indicator for the separating selectivity. For the membrane performance, a good membrane candidate should have both high selectivity and high permeance. From the figures, inorganic membranes are promising candidate materials comparing with polymeric membrane materials. In addition inorganic membranes are thermally more robust than polymer membranes. A more elaborate synthesis protocol, however, usually leads to higher production costs for inorganic membranes compared with polymeric materials. The performance of the DD3R which has a good chemical and thermal stability is one of the best as Figure A.12 indicates. Some polyimide membranes show a very high permeance of CO_2 and should be suitable for the separation of the acid contaminants from natural gas. Membranes like PDMS[44, 45, 46, 47], which has high permeance but low selectivities can be used for the separation process combined with selective membranes or with absorption processes (then moderate selectivities for CO_2/CH_4 are sufficient).
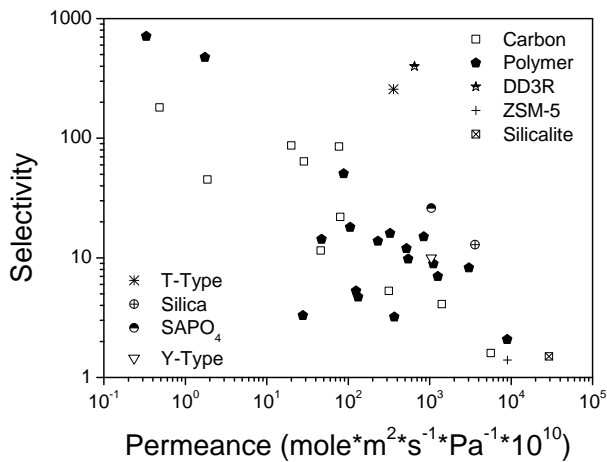

Figure A.12: *The performance of the different membranes $\Delta P < 0.25 MPa$: the ideal selectivity of CO_2/CH_4 system versus the pure component permeance of CO_2*

Table A.6: *Membranes performance: permeance of CO_2 and CH_4 $(mol * m^{-2} * s^{-1} * Pa^{-1} * 10^{10})$, ideal selectivity of CO_2 to CH_4.*

Membrane	$\Delta P_i/kPa$	T/K	P/kPa	P_{CO_2}	P_{CH_4}	ideal α	Pore size/	Ref.
Carbon	-	298	-	77	0.95	85	4.4	[48]
Carbon	59-160	298	160	0.48-316	0.09-0.76	5.3-180	4.3-5	[49]
Carbon	100	298-323	100	20-29	0.23-0.45	64-87	4.2	[50]
Carbon	-	296	187	1400-5600	860-1400	1.6-4.1	5.5	[51]
Silica	-	298	-	3600	280	13	-	[52]
ZSM5	138	300	276	9000	6400	1.4	5.5	[53]
Silicalite	138	300	270	29200	19200	1.5	5.5	[53]
DD3R	101	300	202	700	1.45	483	3.6*4.4	[54]
DD3R	299	300	400	500	1.4	357	3.6*4.4	[54]
T-Zeolite	101	308	101	360	1.4	257	3.6*5.1	[55]
Y-Zeolite	99	300	101	1050	105	10	0.74	[56, 57]
SAPO-34	138	295	222	1050	40	26	0.38	[58, 59]
Polyimide	-	308	202-607	4700-5540	137-189	29-33	-	[60, 61]
polymer	-	308	101	0.33-1.7	0.0005-0.004	475-712	-	[45]
polymer	-	308	101	47-546	3.3-56	9.8-14	-	[62]
Ethyl cellulose	-	308	1013	1450-2400	143-230	10	-	[63]
Composite	-	303	-	30-170	0.81-0.87	8.2-83	-	[64]
Polymer	101	308	101	328-521	28-248	12-16	-	[65]
Cellulose acetate	206	298	-	232	17	13.8	-	[66]

Table A.6: *Continued*

PDMS	729.5	308	831	47600	14423	3.3	-	[67]
MEM-101	206	298	-	368	115	3.2	-	[66]
Silastic	206	298	-	28	8.6	3.3	-	[66]
MEM-213	206	298	-	133	28	4.7	-	[66]
polyimide	276	298	377	3040-8940	367-4351	2.1-8.3	-	[68]
polysulfone	783	298	790	54	12	4.3	-	[69]
PPO	152-172	298	152-172	848	55.7	15	-	[44]
Polysulfone	152-172	298	152-172	106	5.9	18	-	[44]
PVTMS	152-172	298	152-172	1110-1262	125-177	7.0-8.9	-	[44]
Composite	-	293	202-813	88-405	0.36-6.7	27-51	7-400	[70]
Matrix	730	298	790	73-148	3.9-12	19-24	10	[69]

A.5.2 Stability of membranes

The selective membranes considered for subsurface separation processes need to be stable enough under elevated pressure and temperature conditions (5-30 MPa, 323 K - 373 K) and be resistant to impurities, for example H_2O[71], and higher hydrocarbons[59].

Inorganic membranes like carbon membranes[72, 73], SAPO-34 membranes[59], Zeolite membranes were investigated for the stabilities under reservoir conditions. There is a decrease in performance of carbon membranes when they are exposed to water[74]. It has been reported that the selectivity of a typical membrane decreases as the amount of sorbed water increases[75]. The material stability of silica membranes can also be a problem, it was found that exposure to water[71, 76] at high activities, even for low temperatures, results in irreversible changes in the silica membrane pore structure. Natural gas impurities are known to cause drastic selectivity loss for carbon membranes, silica membrane and SAPO-34 membranes. For most inorganic membranes, it was found that with increasing pressure the solubility of methane increases in the membrane, which means that the selectivity decreases.

Zeolite membranes, especially DD3R[77] is specifically suited for the CO_2/CH_4 separation because of its specific window opening that facilitates molecular sieving of CH_4. DD3R is an all silica zeolite and therefore has a good chemical and thermal stability and is hydrophobic of nature. This hydrophobicity leads to low water adsorption and increase the zeolite stability in humid conditions[78, 79]. But a decrease of CO_2-permeance was found when feed pressure increases[80].

Polymer membranes showed plasticization at elevated pressure thus lost their selectivities of CO_2 to CH_4. The polymer matrix[81] swells upon sorption of CO_2 which accelerates the permeation of CH_4. And there are a few articles[82, 83, 84, 85] reporting how to prevent or decrease the plasticization of polymer membranes. Mixed-matrix membranes[86] that consist of zeolite particles dispersed in a polymer matrix[61, 87, 70] could combine the selectivity of zeolite membranes with the low cost and ease of manufacturing polymeric membranes.

REFERENCES

[1] A. P. S. Kamps, E. Meyer, B. Rumpf, and G. Maurer. Solubility of CO_2 in aqueous solutions of KCl and in aqueous solutions of K_2CO_3. *J. Chem.*

Eng. Data, 52(3):817–832, 2007.

[2] B. Rumpf, J. Xia, and G. Maurer. An experimental investigation of the solubility of carbon dioxide in aqueous solutions containing sodium nitrate or ammonium nitrate at temperatures from 313 K to 433 K and pressures up to 10 MPa. *J. Chem. Thermodyn.*, 29:1101–1111, 1997.

[3] J. S. Tosh, J. H. Field, H. E. Benson, and W. P. Haynes. Equilibriun study of the system potassium carbonate potassium bicarbonate, carbon dioxide, and water. *Bur. Mines Rep. Invest.*, page 5484, 1959.

[4] S. B. Park, C. S. Shim, H. Lee, and K. H. Lee. Solubilities of carbon dioxide in the aqueous potassium carbonate and potassium carbonate-poly(ethylene glycol) solutions. *Fluid Phase Equilib.*, 134:141–149, 1997.

[5] S. B. Park, H. Lee, and K. H. Lee. Solubilities of carbon dioxide in aqueous potassium carbonate solutions mixed with physical solvents. *Int. J. Thermophys.*, 19(5):1421–1428, 1998.

[6] Z. Duan and R. Sun. An improved model calculating CO_2 solubility in pure water and aqueous $NaCl$ solutions from 273 to 533 K and from 0 to 2000 bar. *Chem. Geol.*, 193:257–271, 2003.

[7] J. Kiepe, S. Horstmann, K. Fischer, and J. Gmehling. Experimental determination and prediction of gas solubility data for $CO_2 + H_2O$ mixtures containing $NaCl$ or KCl at temperatures between 313 and 393 k and pressures up to 10 MPa. *Ind. Eng. Chem. Res.*, 41:4393–4398, 2002.

[8] J. A. Nighswander, N. Kalogerakis, and A. K. Mehrotra. Solubilities of carbon dioxide in water and 1 wt % $NaCl$ solution at pressures up to 10 MPa and temperatures from 80 to 200 C. *J. Chem. Eng. Data*, 34:355–360, 1989.

[9] B. Rumpf, H. Nicolaisen, C. Ocal, and G. Maurer. Solubility of carbon dioxide in aqueous solutions of sodium chloride: experimental results and correlation. *J. Solution Chem.*, 23(3):431–448, 1994.

[10] O. M. Suleimenov and R. E. Krupp. Solubility of hydrogen sulfide in pure water and in $NaCl$ solutions from 20 to 320 C and at saturation pressures. *Geochim. Cosmochim. Acta*, 58(11):2433–2444, 1994.

[11] J. Gao, D.-Q. Zheng, and T.-M. Guo. Solubilities of methane, nitrogen, carbon dioxide, and a natural gas mixture in aqueous sodium bicarbonate solutions under high pressure and elevated temperature. *J. Chem. Eng. Data*, 42:69–73, 1997.

[12] J. Z. Xia, A. P. S. Kamps, B. Rumpf, and G. Maurer. Solubility of hydrogen sulfide in aqueous solutions of the single salts sodium sulfate, ammonium sulfate, sodium chloride, and ammonium chloride at temperatures from 313 to 393 K and total pressures up to 10 MPa. *Ind. Eng. Chem. Res.*, 39(4):1064–1073, 2000.

[13] M. D. Bermejo, A. Martin, L. J. Florusse, C. J. Peters, and M. J. Cocero. The influence of Na_2SO_4 on the CO_2 solubility in water at high presure. *Fluid Phase Equilib.*, 238:220–228, 2005.

[14] B. Rumpf and G. Maurer. An experimental and theoretical investigation on the solubility of carbon dioxide in aqueous solutions of strong electrolytes. *Ber. Bunsenges Phys. Chem.*, 97(1):85–97, 1993.

[15] F. Kurz, B. Rumpf, R. Sing, and G. Maurer. Vapor-liquid and vapor-liquid-solid equilibria in the system ammonia-carbon dioxide-sodium chloride-water at temperatures from 313 to 393 K and pressures up to 3 MPa. *Ind. Eng. Chem. Res.*, 35(10):3795–3802, 1996.

[16] J. Z. Xia, A. P. S. Kamps, B. Rumpf, and G. Maurer. Solubility of hydrogen sulfide in aqueous solutions of single strong electrolytes sodium nitrate, ammonium nitrate, and sodium hydroxide at temperatures from 313 to 393 K and total pressures up to 10 MPa. *Fluid Phase Equilib.*, 167(2):263–284, 2000.

[17] F. Y. Jou, F. D. Otto, and A. E. Mather. Solubility of H_2S and CO_2 in diethylene glycol at elevated pressures. *Fluid Phase Equilib.*, 175(1-2):53–61, 2000.

[18] W. Weber, S. Zeck, and H. Knapp. Gas solubilities in liquid solvents at high pressures: apparatus and results for binary and ternary systems of N_2, CO_2 and CH_3OH. *Fluid Phase Equilib.*, 18:253–278, 1984.

[19] A. Henni and A. E. Mather. The solubility of CO_2 in triethylene glycol monomethyl ether. *Can. J. Chem. Eng.*, 73:156–159, 1995.

[20] C. J. Chang, C. Y. Day, C. M. Ko, and K. L. Chiu. Densities and P-x-y diagrams for carbon dioxide dissolution in methanol, ethanol, and acetone mixtures. *Fluid Phase Equilib.*, 131(1-2):243–258, 1997.

[21] Q. Zhang and E. L. Cussler. Microporous hollow fibers for gas absorption: I. Mass transfer in the liquid. *J. Membr. Sci.*, 23(3):321–332, 1985.

[22] M. C. Yang and E. L. Cussler. Designing hollow-fiber contactors. *AIChE*, 32(11):1910–1916, 1986.

[23] K. L. Wang and E. L. Cussler. Baffled membrane modules made with hollow-fiber fabric. *J. Membr. Sci.*, 85(3):265–278, 1993.

[24] M. H. Al-Marzouqi, M. H. El-Naas, S. A. M. Marzouk, M. A. Al-Zarooni, N. Abdullatif, and R. Faiz. Modeling of CO_2 absorption in membrane contactors. *Sep. Purif. Technol.*, 59(3):286–293, 2008.

[25] S. Shirazian, A. Moghadassi, and S. Moradi. Numerical simulation of mass transfer in gas-liquid hollow fiber membrane contactors for laminar flow conditions. *Simul. Modell. Pract. Theory*, 17(4):708–718, 2009.

[26] H. Y. Zhang, R. Wang, D. T. Liang, and J. H. Tay. Modeling and experimental study of CO_2 absorption in a hollow fiber membrane contactor. *J. Membr. Sci.*, 279(1-2):301–310, 2006.

[27] S. Karoor and K. K. Sirkar. Gas-absorption studies in microporous hollow fiber membrane modules. *Ind. Eng. Chem. Res.*, 32(4):674–684, 1993.

[28] Y. Lee, R. D. Noble, B.-Y. Yeom, Y.-I. Park, and K.-H. Lee. Analysis of CO_2 removal by hollow fiber membrane contactors. *J. Membr. Sci.*, 194(1):57–67, 2001.

[29] S. Atchariyawut, R. Jiraratananon, and R. Wang. Separation of CO_2 from CH_4 by using gas-liquid membrane contacting process. *J. Membr. Sci.*, 304(1-2):163–172, 2007.

[30] Y. S. Kim and S. M. Yang. Absorption of carbon dioxide through hollow fiber membranes using various aqueous absorbents. *Sep. Purif. Technol.*, 21(1-2):101–109, 2000.

[31] J. L. Li and B. H. Chen. Review of CO_2 absorption using chemical solvents in hollow fiber membrane contactors. *Sep. Purif. Technol.*, 41(2):109–122, 2005.

[32] J. M. Zheng, Y. Y. Xu, and Z. K. Xu. Shell side mass transfer characteristics in a parallel flow hollow fiber membrane module. *Sep. Sci. Technol.*, 38(6):1247–1267, 2003.

[33] S. R. Wickramasinghe, M. J. Semmens, and E. L. Cussler. Mass-transfer in various hollow fiber geometries. *J. Membr. Sci.*, 69(3):235–250, 1992.

[34] J. Wu and V. Chen. Shell-side mass transfer performance of randomly packed hollow fiber modules. *J. Membr. Sci.*, 172(1-2):59–74, 2000.

[35] J. Happel. Viscous flow relative to arrays of cylinders. *AIChE*, 5(2):174–177, 1959.

[36] M. R. Riazi and C. H. Whitson. Estimating diffusion-coefficients of dense fluids. *Ind. Eng. Chem. Res.*, 32(12):3081–3088, 1993.

[37] M. G. Shalygin, D. Roizard, E. Favre, and V. V. Teplyakov. CO_2 transfer in an aqueous potassium carbonate liquid membrane module with dense polymeric supporting layers: influence of concentration, circulation flow rate and temperature. *J. Membr. Sci.*, 318(1-2):317–326, 2008.

[38] S. R. Suchdeo and J. S. Schultz. Permeability of gases through reacting solutions: carbon dioxide - bicarbonate membrane system. *Chem. Eng. Sci.*, 29(1):13–23, 1974.

[39] A. H. G. Cents, D. W. F. Brilman, and G. F. Versteeg. CO_2 absorption in carbonate/bicarbonate solutions: the danckwerts - criterion revisited. *Chem. Eng. Sci.*, 60(21):5830–5835, 2005.

[40] V. Y. Dindore, D. W. F. Brilman, and G. F. Versteeg. Modelling of crossflow membrane contactors: physical mass transfer processes. *J. Membr. Sci.*, 251(1-2):209–222, 2005.

[41] A. L. Myers and J. M. Pransnitz. Thermodynamics of mixed-gas adsorption. *AIChE*, 11:121–126, 1965.

[42] S. Kulprathipanja. Mixed matrix membrane development. *Ann. N.Y. Acad. Sci.*, 984:361–369, 2003.

[43] A. Nijmeijer. *Hydrogen-selective silica membranes for use in membrane steam reforming.* Twente University Press, Enschede, the Netherlands, 1999.

[44] J. D. L. Roux, V. V. Teplyakov, and D. R. Paul. Gas transport properties of surface fluorinated poly (vinyltrimethylsilane) films and composite membranes. *J. Membr. Sci.*, 90:55–68, 1994.

[45] A. J. Ashworth, B. J. Brisdon, R. England, A. G. W. Hodson, and A. R. Watts. The permeability of carbon dioxide and methane in poly(organosiloxane) membranes containing mono- and di-ester functionalities. *J. Membr. Sci.*, 101:109–115, 1995.

[46] T. C. Merkel, R. P. Gupta, B. S. Turk, and B. D. Freeman. Mixed-gas permeation of syngas components in poly(dimethylsiloxane) and poly(1-trimethylsilyl- 1- propyne) at elevated temperatures. *J. Membr. Sci.*, 191:85–94, 2001.

[47] B. Wilks and M. E. Rezac. Properties of rubbery polymers for the recovery of hydrogen sulfide from gasification gases. *J. Appl. Polym. Sci.*, 85:2436–2444, 2002.

[48] T. A. Centeno and A. B. Fuertes. Carbon molecular sieve membranes derived from a phenolic resin supported on porous ceramic tubes. *Sep. Purif. Technol.*, 25:379–384, 2001.

[49] M. Ogawa and Y. Nakano. Separation of CO_2/CH_4 mixture through carbonized membrane prepared by gel modification. *J. Membr. Sci.*, 173:123–132, 2000.

[50] T. A. Centeno and A. B. Fuertes. Supported carbon molecular sieve membranes based on a phenolic resin. *J. Membr. Sci.*, 160:201–211, 1999.

[51] M. B. Rao and S. Sircar. Nanoporous carbon membrane for gas separation. *Gas Sep. Purif.*, 7(4):279, 1993.

[52] R. S. A. de Lange, J. H. A. Hekkink, K. Keizer, and A. J. Burggraaf. Permeation and separation studies on microporous sol-gel modified ceramic membranes. *Microporous Mater.*, 4:169–186, 1995.

[53] J. C. Poshusta, R. D. Noble, and J. L. Falconer. Temperature and pressre effects on CO_2 and CH_4 permeation through MFI zieolite membranes. *J. Membr. Sci.*, 160:115–125, 1999.

[54] J. v. d. Bergh, W. Zhu, J. C. Groen, F. Kapteijn, J. A. Moulijn, K. Yajima, K. Nakayama, T. Tomita, and S. Yoshida. Nautral gas purification with a DDR zeolite membrane; permeation modelling with maxwell-stefan equations. *Stud. Surf. Sci. Catal.*, 170:1021–1027, 2007.

[55] Y. Cui, H. Kita, and K. Okamoto. Preparation and gas separation performance of zeolite T membrane. *J. Master. Chem.*, 14:924–932, 2004.

[56] K. Kusakabe, T. Kuroda, A. Murata, and S. Morooka. Formation of a Y-type zeolite membrane on a porous α-alumina tube for gas separation. *Ind. Eng. Chem. Res.*, 36:649–655, 1997.

[57] Y. Hasegawa, T. Tanaka, K. Watanabe, B. H. Jeong, K. Kusakabe, and S. Morooka. Separation of $CO_2 - CH_4$ and $CO_2 - N_2$ systems using ion-exchanged FAU-type zeolite membranes with different Si/Al ratios. *Korean J. Chem. Eng.*, 19(2):309–313, 2002.

[58] S. Li, J. L. Falconer, and R. D. Noble. SAPO-34 membranes for CO_2/CH_4 separation. *J. Membr. Sci.*, 241:121–135, 2004.

[59] S. Li, J. G. Martinek, J. L. Falconer, R. D. Noble, and T. Q. Gardner. High-pressure CO_2/CH_4 separation using SAPO-34 membranes. *Ind. Eng. Chem. Res.*, 44:3220–3228, 2005.

[60] Y. Li, M. Ding, and J. Xu. Gas permeation properties of copolyimides from 1,4-bis(3,4-dicarboxphenoxy)benzene dianhydride and 2,2-bis(3,4-dicarboxyphenyl)hexafluoroisopropane dianhydride. *Polym. Int.*, pages 121–126, 1997.

[61] Q. Hu, E. Marand, S. Dhingra, D. Fritsch, J. Wen, and G. Wilkes. Poly(amide-imide)/TiO_2 nano-composite gas separation membranes: fabrication and characterization. *J. Membr. Sci.*, 135:65–79, 1997.

[62] G. Perego, A. Roggero, R. Sisto, and C. Valentini. Membranes for gas separation polyphenylene oxide based on silylated. *J. Membr. Sci.*, 55:325–331, 1991.

[63] A. Y. Houde and S. A. Stem. Solubility and diffusivity of light gases in ethyl cellulose at elevated pressures effects of ethoxy content. *J. Membr. Sci.*, 127:171–183, 1997.

[64] T.-S. Chung, J.-J. Shieh, W. W. Y. Lau, M. P. Srinivasan, and D. R. Paul. Fabrication of multi-layer composite hollow fiber membranes for gas separation. *J. Membr. Sci.*, 152:211–225, 1999.

[65] Z.-K. Xu, C. Dannenberg, J. Springer, S. Banerjee, and G. Maier. Novel poly(arylene ether) as membranes for gas separation. *J. Membr. Sci.*, 205:23–31, 2002.

[66] M. Kayhanian and D. J. Hills. Membrane purification of anaerobic digester gas. *Biol. Waste*, 23:1–15, 1987.

[67] S. A. Stern and R. Vaidyanathan. Structure/permeability relationships of siliconcontaining polyimides. *J. Membr. Sci.*, 49:1–14, 1990.

[68] T.-S. Chung, W.-H. Lin, and R. H. Vora. The effect of shear rates on gas separation performance of 6FDA-durene polyimide hollow fibers. *J. Membr. Sci.*, 167:55–66, 2000.

[69] T. M. Gur. Permselectivity of zeolite filled polysulfone gas separation membranes. *J. Membr. Sci.*, 93:283–289, 1994.

[70] M. Anson, J. Marchese, E. Garis, N. Ochoa, and C. Pagliero. ABS copolymer-activated carbon mixed matrix membranes for CO_2/CH_4 separation. *J. Membr. Sci.*, 243:19–28, 2004.

[71] D. C. Calabro, S. E. Jakubowicz, C. J. Yoon, T. E. Clark, H. W. Deckman, R. R. Chance, B.C. Bonekamp, and P. P. A. C. Pex. Intrinsic gas transport and water stability of silica membranes for CO_2/CH_4 separations. *ECN-RX-04-083 (the ICIM 8 conference in Cincinati, Ohio, USA)*, 2004.

[72] F. K. Katsaros, T. A. Steriotis, A. K. Stubos, A. Mitropoulos, N. K. Kanellopoulos, and S. Tennison. High pressure gas permeability of microporous carbon membranes. *Microporous Mater.*, 8:171–176, 1997.

[73] D. Q. Vu and W. J. Koros. High pressure CO_2/CH_4 separation using carbon molecular sieve hollow fiber membranes. *Ind. Eng. Chem. Res.*, 41:367–380, 2002.

[74] S. M. Saufi and A. F. Ismail. Fraction of carbon membranes for gas separation - a review. *Carbon*, 42:241–259, 2004.

[75] C. W. Jones and W. J. Koros. Characterization of ultramicroporous carbon membranes with humidified feeds. *Ind. Eng. Chem. Res.*, 34:15863, 1995.

[76] J. Kuhn, S. Sutanto, J. Gascon, S. Calero, J. Gross, and F. Kapteijn. Performance and stability of multi-channel MFI zeolite membranes detempled by calcination and ozonication in ethanol/water pervaporation. *J. Membr. Sci.*, 339:261–274, 2009.

[77] T. Tomita, K. Nakayama, and H. Sakai. Gas separation characteristics of DDR type zeolite membrane. *Microporous Mesoporous Mater.*, 68:71–75, 2004.

[78] J. Kuhn, K. Yajima, T. Tomita, J. Gross, and F. Kapteijn. Dehydration performance of a hydrophobic DD3R zeolite membrane. *J. Membr. Sci.*, 321:344–349, 2008.

[79] J. Kuhn, J. M. Castillo-Sanchez, J. Gascon, S. Calero, D. Dubbeldam, T. J. H. Vlugt, F. Kapteijn, and J. Gross. Adsorption and diffusion of water, methanol, and ethanol in all-silica dd3r: Experiments and simulation. *J. Phys. Chem. C*, 113:14290–14301, 2009.

[80] J. van den Bergh, A. Tihaya, and F. Kapteijn. High temperature permeation and separation characteristics of an all-silica DDR zeolite membrane. *Microporous and Mesoporous Materials*, 132:137147, 2010.

[81] X. Xu and M. R. Coleman. Preliminary investigation of gas transport mechanism in a H^+ irradiated polyimide-ceramic composite membrane. *Nucl. Instrum. Methods Phys. Res., Sect. B*, 152:325–334, 1999.

[82] A. Bos, I. G. M. Punt, M. Wessling, and H. Strathaan. Suppression of CO_2 - plasticization by semiinterpenetrating polymer network formation. *J. Polym. Sci., Part B: Polym. Phys.*, 36:1547–1556, 1998.

[83] A. F. Ismail and W. Lorna. Suppression of plasticization in polysulfone membranes for gas separations by heat-treatment technique. *Sep. Purif. Technol.*, 30:37–46, 2003.

[84] S. M. Jordan and W. J. Koros. Characterization of CO_2 - induced conditioning of substituted polycarbonates using various 'exchange' penetrants. *J. Membr. Sci.,*, 51:233–247, 1990.

[85] J. D. Wind, S. M. Sirard, D. R. Paul, P. F. Green, K. P. Johnston, and W. J. Koros. Carbon dioxide-induced plasticization of polyimide membranes: pseudo-equilibrium relationships of diffusion, sorption and swelling. *Macromolecules*, 36:6433–6441, 2003.

[86] R. W. Baker, editor. *Membrane Technology and Applications*. John Wiley & Son, Ltd, London, UK, 2 edition, 2004.

[87] D. Q. Vu, W. J. Koros, and S. J. Miller. Mixed matrix membranes using carbon molecular sieves i. preparation and experimental results. *J. Membr. Sci.*, 211:311334, 2003.

Appendix B

Second asymmetric binary parameter l_{ij} for the PC-SAFT equation of state

A second asymmetric binary parameter l_{ij} can be introduced for dispersive energy, according to

$$\overline{m^2\epsilon\sigma^3} = \sum_i\sum_j x_i x_j m_i m_j \epsilon_{ij}\sigma_{ij}^3 + \sum_i x_i m_i(\sum_j x_j m_j \sigma_{ij}(\sqrt{\epsilon_{ii}\epsilon_{jj}}l_{ij})^{\frac{1}{3}})^3 \quad \text{(B.1)}$$

This formulation follows a suggestion of Mathias et al.[1] and does not suffer from deficiencies pointed out by Michelsen and Kistenmacher[2] for several alternative asymmetric mixing rules. Eq. B.1 substitutes Eq. (A.12) of Ref. [3]. For compatibility, the energy-parameter ϵ_{ij} on the right-hand side of Eq. B.1 then has to be made dimensionless, by division of kT.

REFERENCES

[1] P. M. Mathias, H. C. Klotz, and J. M. Prausnitz. Equation-of-state mixing rules for multicomponent mixtures - the problem of invariance. *Fluid Phase Equilib.*, 67:31–44, 1991.

[2] M. L. Michelsen and H. Kistenmacher. On composition dependent interaction coefficients. *Fluid Phase Equilib.*, 58(1-2):229–230, 1990.

[3] J. Gross and G. Sadowski. Perturbed-chain SAFT: an equation of state based

on a perturbation theory for chain molecules. *Ind. Eng. Chem. Res.*, 40:1244–1260, 2001.

Curriculum Vitae

Xiaohua Tang was born in Nanjing, China on October 27, 1980. She studied at Nanjing University of Technology in China from September 1997 to July 2001, where she received her Bachelor of Science degree (BSc.) in Chemical Engneering. She continued in the Masters program at the Nanjing University of Technology, focuing on synthesis of molecular sieves on honeycomb and on the formation of pelleted catalysts without bonds. After having completed the Master of Science curriculum including the graduation thesis, she recieved a certificate of graduataion. In October 2003, she moved to the Netherlands and started her Master study in Chemistry at the Leiden University. With the graduation thesis: Characterization and catalytic activity of unpromoted and alkali (earth)-promoted Au/Al_2O_3 catalysts for low-temperature CO oxidation, she received her Master of Science degree (MSc.) in Chemistry in August 2005. In Feburary 2006, she joined the Process & Energy Department at Delft University of Technology as a PhD student. Her PhD project concerned the development of a thermodynamic model for CO_2/H_2S capture from natural gas at elevated pressures and this book is her thesis.

Selected Publications

B.1   Papers

- Xiaohua Tang and Joachim Gross, Density functional theory modeling of surface tension for pure fluids near the critical region, Journal of Supercritical Fluids , Volume 55(2), 2010, 735-742

- Xiaohua Tang and Joachim Gross, Renormalization-Group Corrections to the Perturbed-Chain Statistical Associating Fluid Theory for Binary Mixtures Near to and Far from the Critical Region, Industrial & Engineering Chemistry Research , Volume 49, 2010, 9436-9444

- Xiaohua Tang and Joachim Gross, Modeling the phase equilibria of hydrogen sulfide and carbon dioxide in mixture with hydrocarbons and water using the PCP-SAFT equation of state, Fluid Phase Equilibria, Volume 293, 2010, 11-21

- Xiaohua Tang, Ruben Spoek and Joachim Gross, Modeling the phase equilibria of CO_2 and H_2S in aqueous electrolyte systems at elevated pressure, Energy Procedia, Volume 1, 2009, 1807-1814

- Palanisamy Uma Maheswari, Xiaohua Tang, Ronald Hage, Patrick Gamez, and Jan Reedijk, The role of carboxylic acids on a Na_2WO_4/H_2WO_4-based biphasic homogeneous alkene epoxidation, using H_2O_2 as oxidant, Journal

of Molecular Catalysis A: Chemical, Volume 258, Issues 1-2 , 2 October 2006, Pages 295-301

- A. C. Gluhoi, X. Tang, P. Marginean and B. E. Nieuwenhuys, Characterization and catalytic activity of unpromoted and alkali (earth)-promoted Au/Al_2O_3 catalysts for low-temperature CO oxidation, Topics in Catalysis, Volume 39, Numbers 1-2/ September, 2006, Pages 101-110

B.2   Oral/ Poster presentations

- X. Tang, P.J. Jansens, A. Bardow, J. Gross Evaluation of membrane absorption process for underground separation of sour gases from natural gas Conference Proceedings of NPS8, Veldhoven, The Netherlands, October 2008

- X. Tang, J. Gross Density functional theory for calculating surface tensions with a simple renormalization formalism for the critical point Thermodynamik-Kolloquium und Ingenieurdaten 2010

- X. Tang, J. Gross Renormalization-Group Corrections to a Perturbed-Chain Statistical Associating Fluid Theory for Binary Mixtures Near to and Far from the Critical Region Proceedings of NPS9 Conference, Veldhoven, The Netherlands, October 2009

- X. Tang, J. Gross Modeling the phase equilibria of CO_2 and H_2S in aqueous electrolyte systems at elevated pressure Conference Proceedings of GHGT9, Washington D.C., US, November 2008

- X. Tang, J. Gross, P.J. Jansens Absorption of CO_2 and H_2S from gas within the well Proceedings of NPS7 Conference, Veldhoven, The Netherlands, October 2007

- X. Tang, J. Gross, P.J. Jansens Technologies Comparison for Separation of CO_2 and H_2S from Oil/Gas within the Reservoir Conference Proceedings of ECCE6, Copenhagen, Denmark, September 2007

- X. Tang, J. Gross, P.J. Jansens Separation of CO_2 and H_2S from oil / gas within the reservoir Proceedings of NPS6 Conference, Veldhoven, The Netherlands, October 2006

Acknowledgements

Looking back on these five years, it has been a memorable journey, during which I have learned a lot, and during which I have met a lot of wonderful people to whom I feel so grateful.

First, I would like to thank Prof. Joachim Gross, my promoter and daily supervisor. Dear Joachim, thank you sincerely for giving me the opportunity to carry out this research as a PhD candidate in P&E. This thesis would not have been possible without your support, guidance and encouragement from the initial to the final level, enabling me to develop an understanding of the subject.

I would like to thank Prof. Peter Jansens for your efforts, fruitful advice and attention and the care to this PhD project I was conducting. To Prof. Andre Bardow, I would like to thank you for your fruitful scientific discussions and always creative ideas for my work. I want to thank Theo de Loos and Eugene Straver for your guidance with the experimental work, which was conducted for Chapter 5. I would like to thank Teus van der Stelt and Piero Colonna for helpful discussions on the cubic equation of state in Chapter 5. To Prof. Thijs Vlugt: thanks for the support and the encouragement especially during the last months.

I would also like to thank people in the user-group for the subsurface separation project: Annermieke Runstraat, Erik Meuleman, Esther van Soest, Joris IJzermans, Marta Kozlowska, Nadja Muller, Rick van der Vaart. Annermieke: thank you for all your support, your guidance, you kindness and your time.

To Prof. Jan de Graauw, thank you for the great guidance and discussions

for traditional/ membrane column calculations when I was really in need of it. To Zarko Olujic, thank you for spending time with me to discuss subsurface separations. To the colleague in TNO, Eva Sanchez Fernandez, thank you for the fruitful discussions on membrane contactor calculations. I would like to thank my Master students, Ruben Spoek and Okpanachi Onuche, who contributed their work to this thesis, and helped deepen my understanding of the project.

My gratitude goes to our wonderful managerial support: Eveline, Helma, Ilona, Judith and Leslie. Thank you for being always kind and helpful. A special thanks to dear Judith for taking care of people in the ETh group.

I would like to thank my officemates who built a scientific and active atmosphere in the office: Aylin, Ernesto, Guido, Kedar, Magda, Marta K., Martijn, Michal, Stephanie, Tomek. We shared a lot together and discussed various things together: PhD life, history and culture of different countries, learning Dutch, job searching and so on. I am indebted to you for supporting me during these years. Magda and Tomek, I am so thankful to be your officemate (and friend), thank you for your kindness and providing me with all the necessary assistance in my work and life. Guido, it is always enjoyable to exchange thoughts during our discussions, and thank you so much for your help with translating the summary of my thesis into Dutch.

Widya, looking back 5 years , I still remember the first time you came to my office and introduced yourself in a very soft voice: "my name is Widya" I didn't know at that moment that I would feel so lucky to have a friend like you. Thank you so much for all these years of friendship, especially during the difficult time I had. You have made your support available in multitude of ways. Many thanks to you and Arief.

Somnath, thanks for the comments and suggestions to my work, my thesis and propositions, which were very helpful for me. Xin L., thanks for your kindness during my PhD, you are such a nice girl, quiet but always so helpful and so open whenever I need your help. Dennis and Mahinder, thanks for translating the propositions in my thesis into Dutch. Lawien, thanks for your fruitful comments on the membrane absorption part of my thesis. Erin, thanks for correcting the English in the acknowledgement section in my thesis. Atif, Bowen, Elif, Ryan, Shanfeng and Xiangmei, thank you for the discussions and suggestions in different aspects of my work and my life.

It is a pleasure to work in this department meeting a lot of the international

colleagues by, exam correction committee (Bernado, Christian, Henry, JuanMa, Sondre, Theo...), OSPT course (Eleonora, Marta L., Jacopo, Jelan, Helene, Richard...), girl parties (Alondra, Martina, Sara, Stevia, Somayeh...), dinners (Albert, Ali, Almudena, Ana, Casten, Cristi, Giorgos, John, Joop, Mahsa, Norbert, Orchidea, Sander, Sergio, Thijs...). It is also great to share life abroad with a bunch of Chinese colleagues (Huaiyu, Jie, Liyuan, Ming, Xiaoqian, Yuan, Zuopeng...). It was a good experience to work in ITT, Stuttgart University with the colleagues there for sevaral months. All these made my life more colorful and enjoyable.

I would like to thank my friends in the Netherlands: Juanjuan, Fengju, Elim, Kachun, Zan and others, my cousins far away from Nanjing, China: Xiaoyan and Xiaowen and my uncle in France: Wei Xu and his family. Thank you for your caring words and support.

I want to give my deepest gratitude to my mother, Min Huang. Mama, thank you for your support and encouragement along the way through your love.

To my late father, Baba, I miss you so much and believe you are always here with me and have never left, supporting me with your strength.

Xiaohua Tang

Delft, March 2011